Dipl.-Ing. Christoph Grimmer, BSc, B.A. (Econ.)

Energy and Hydrogen Storage in Borohydride based Ionic Liquids

DOCTORAL THESIS

to achieve the university degree of

Doktor der technischen Wissenschaften

submitted to

Graz University of Technology

Supervisor

Assoc.Prof. Dipl.-Ing. Dr.techn.
Viktor Hacker

Institute of Chemical Engineering and
Environmental Technology

Graz, February 2016

AFFIDAVIT

I declare that I have authored this thesis independently, that I have not used other than the declared sources/resources, and that I have explicitly indicated all material which has been quoted either literally or by content from the sources used. The text document uploaded to TUGRAZonline is identical to the present doctoral thesis.

Date

Signature

to my girl Ilena
and
my family

Acknowledgement

Dear Viktor, I would like to thank you for the opportunity to write my PhD thesis in the Fuel Cell Systems Group at Graz University of Technology. Your guidance and supervision during my master thesis and during the time of my PhD from 2013-2016 made this thesis possible.

I am also very grateful for the support of the Institute of Chemical Engineering and Environmental Technology, especially of our head of the institute Prof. Matthäus Siebenhofer. Furthermore, thanks go to my industrial partner proionic GmbH and VTU engineering, especially to Dr. Michael Koncar and Roland Kalb, who were great supporters of my research.

I would like to thank my colleagues and friends from the Fuel Cell Systems Group and the Institute of Chemical Engineering and Environmental Technology for the great time, their assistance, their collaboration and their friendship during these three years. Schnecki (Stephan Weinberger) was there as well.

Most of all, I want to express my gratitude to the love of my life Ilena, to my parents and my sister for their support during my time at Graz University of Technology. Their support and back-up have been essential for my success so far.

Financial support by the Austrian Research Promotion Agency (FFG) through the program “Mobilität der Zukunft” and our industrial partners, VTU engineering and proionic GmbH, is gratefully acknowledged.

Abstract

Efficient and long-term storage of energy is a crucial issue for future energy scenarios that are based on renewable energy sources. Energy storage in chemical compounds is assumed to be a key technology in this regard. Among various storage compounds borohydride is a promising candidate, which is able to act as hydrogen and energy carrier.

The aim of this thesis is the investigation of novel organic borohydride compounds with ionic liquid behavior acting as hydrogen carrier compound and as fuel for direct borohydride fuel cells. The anionic compound borohydride is combined with various organic cations resulting in ionic liquids with high hydrogen/energy storage densities and excellent long-term stability.

These ionic liquids can be dehydrogenated by a hydrolysis reaction that is catalyzed by various noble and non-noble metals. A catalyst based on the inexpensive metal cobalt on nickel foam is developed and characterized comprehensively concerning long-term stability, hydrogen release kinetics and purity of the released hydrogen. Based on this non-noble metal catalyst a prototype of a complete self-regulating hydrogen release unit is designed, manufactured and tested successfully.

Alternatively the borohydride based ionic liquid can be used as fuel for direct borohydride fuel cells. This type of fuel cell is able to convert the chemical energy of borohydride directly into electrical energy without any intermediate steps. Anodes based on various noble metal catalysts, a manganese oxide based oxygen cathode and two different fuel cell approaches are designed and developed. These electrodes were combined with an organic borohydride in a direct liquid fuel cell with a peak power density of 27 mW cm^{-2} and the ability to block the hydrolysis side reaction.

Kurzfassung

Effiziente Speicherung von Energie über längere Zeitperioden ist eine technologische Kernfrage für zukünftige Energieszenarien basierend auf erneuerbaren Energieträgern. Die Speicherung von Energie in chemischen Verbindungen wird in diesem Zusammenhang als Schlüsseltechnologie gesehen. Borhydrid ist eine der vielversprechendsten Verbindungen, welche im Stande ist als Wasserstoff- oder als Energieträger zu fungieren.

Ziel dieser Doktorarbeit ist die Untersuchung neuer organischer Borhydride, welche die Eigenschaften von ionischen Flüssigkeiten aufweisen, als Wasserstoffspeicher und als Treibstoff für Direkt-Borhydrid-Brennstoffzellen. Die anionische Verbindung Borhydrid wird mit diversen organischen Kationen kombiniert, resultierend in ionischen Flüssigkeiten mit hohen Energie- und Wasserstoffspeicherdichten und ausgezeichneter Langzeitstabilität.

Diese ionische Flüssigkeiten werden durch eine Hydrolysereaktion, welche durch verschiedene edle und unedle Metalle katalysiert wird, dehydratisiert. Ein kostengünstiger Cobalt basierter Katalysator auf Nickelschaum wurde entwickelt und auf Langzeitstabilität, Wasserstoff-Freisetzungs-Kinetik und Reinheit des Wasserstoffs untersucht. Basierend auf diesem Katalysator wurde ein Prototyp einer komplett selbstregulierenden Wasserstoffzelle designt, hergestellt und erfolgreich getestet.

Alternativ wird die Borhydrid-basierte ionische Flüssigkeit als Treibstoff in Direkt-Borhydrid-Brennstoffzellen verwendet. Diese Brennstoffzelle ist in der Lage die chemisch gespeicherte Energie ohne Zwischenschritte direkt in elektrische Energie umzuwandeln. Anoden basierend auf diversen Edelmetallen, Manganoxid-basierte Kathoden und zwei verschiedene Brennstoffzellentypen wurden entwickelt. Darauf aufbauend und durch Verwendung von organischen Borhydriden wurde eine Direkt-Brennstoffzelle mit einer Leistungsdichte von 27 mW cm^{-2} realisiert, die in der Lage ist die Hydrolyse-Nebenreaktion vollständig zu unterdrücken.

1 INTRODUCTION

1.1 Energy demand and global warming

Industrialization and development of modern societies have ever been associated to the demand and utilization of energy of any kind. One of the first major steps in the history of humanity is the usage of fire and the associated possibility of working with metallic materials. Today the access to basic energy services and a power grid for everyone is still not achieved, lacking billions of humans [1].

"Lack of access to modern energy services is a serious hindrance to economic and social development and must be overcome if the UN Millennium Development Goals are to be achieved." [1]

Modern civilization as we know began with the industrial revolution and the heavy use of fossil fuels, mainly coal (see Fig. 1). In this respect humanity faces massive local emissions and the accompanying smog problem in urban areas, the finiteness of fossil resources and substantial climate changes. There is scientific consensus concerning the correlation of CO_2 emissions and global warming [2]. Ever increasing demand for primary energy would also require extensive exploitation of non-conventional sources, such as oil sands and offshore wells.

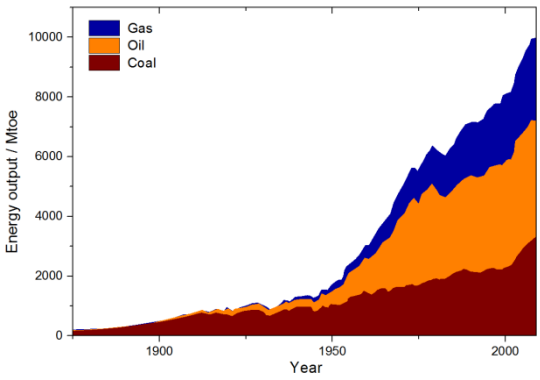

Figure 1: Global production of fossil fuels 1800-2009 [3].

Fig. 2 shows a possible pathway that allows the stabilization of the CO_2 concentration at 450 ppm, referred as the 450 scenario [1]. Without policy changes the emissions of CO_2 will increase steadily until 2035. In the next five years a reversal trend is necessary in order to achieve the goal of 450 ppm CO_2 in the atmosphere. There is a 50% chance that the global warming can be stabilized at 2 °C with a carbon dioxide concentration of 450 ppm.

As can be seen from the abatement "wedges", about half of the emission savings come from efficiency gains. It is also assumed that 19% of the final abatement is done by carbon capture and storage in 2035. This is only possible if fossil fuels are used centralized; producing for example hydrogen by steam reforming that can be further distributed and combusted without local emissions. However, high effort and new technological approaches are necessary in order to achieve these goals. Due to high converting efficiencies and the absence of local emissions, hydrogen technology and fuel cells are considered to play a major role on the roadway towards the 450 scenario.

The second biggest abatement wedge is referred as "Renewables". Increasing the share of primary renewable energy sources also increases the need for reliable large-scale energy storage systems. In general, tertiary electrochemical cells are considered as most suitable because the size of the energy storage and the cell itself is independent.

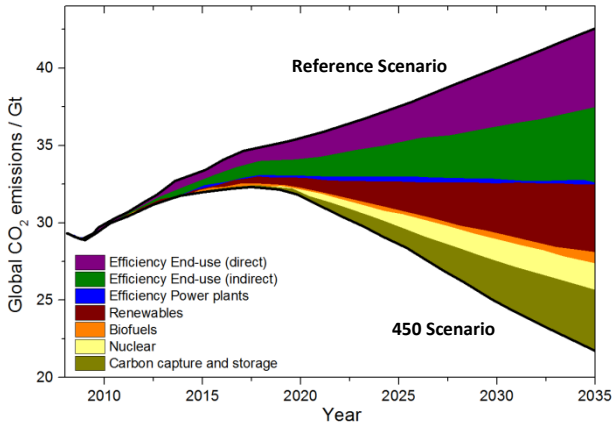

Figure 2: Global annual carbon dioxide emissions forecast and possible abatement strategies [1].

1.2 The aim of this thesis

Storing energy efficiently and over long periods of time is a crucial issue for all sustainable energy scenarios. Energy storage in chemical compounds by electrochemical processes is one of the most promising approaches. A compound that is able to perform this task is the anion borohydride BH_4^-.

In this dissertation the possibilities of using borohydride (BH_4^-) for hydrogen and energy storage applications are investigated comprehensively. The results of four international journal articles are presented, embedded in some unpublished results. My research effort of the last three years can be divided into two major topics, namely the hydrogen storage application and the direct borohydride fuel cell.

First, borohydride acts as hydrogen carrier compound. This hydrogen storage technology enables a liquid state approach with excellent long-term stability and optimal hydrogen release thermodynamics and kinetics at ambient conditions. Furthermore the liquid storage medium is not burnable and exhibits low toxicity. Compared to gaseous energy carriers the borohydride based technology allows the usage of the current energy infrastructure without massive investments.

Second, borohydride is used as fuel for the so-called direct borohydride fuel cell (DBFC). Direct liquid fuel cells have the potential of converting chemical energy to electric energy very efficiently with a simple and save fuel storage. The DBFC itself outstands by high cell voltages, good electrode kinetics and high energy densities.

2 THEORY

2.1 Hydrogen

Hydrogen is the lightest and most ambient element in the universe. At standard conditions it is a non-smelling and burnable gas with a density of 0.0899 g l^{-1} making it approx. 14 times lighter than air. Hydrogen molecules consist of two hydrogen atoms, each consisting of one proton and one electron. Molecular hydrogen is not found in nature, it is present in compounds, mainly combined with oxygen in water and carbon in fossil resources and biomass.

Hydrogen is considered to play a major role as energy carrier in a future society based on renewable energy resources [4,5]. It can be produced by various ways utilizing completely different energy sources. Today about 95% of the global production is done via the steam reforming process of natural gas. Alternative routes for the future are the usage of biomass via reforming or the usage of electrical energy via water electrolysis.

Besides the issue of non-renewable production and CO_2 emissions, one of the main challenges to overcome is the safe and easy storage of hydrogen. State-of-the-art storage is done as pressurized gaseous hydrogen at pressures between 30 and 700 bar (depending on application; stationary or mobile). Main drawbacks are the energy demand of pressurizing hydrogen, remaining safety issues and the usage of pressurized gaseous fuels requires massive investments in new infrastructure.

Alternative ways of storing hydrogen are investigated extensively in the last decades. The most important technological approaches are [6–9]:

- Metal hydrides
- Liquid organic compounds (LOCs)
- Chemical hydrides

Metal hydrides are metallic compounds, mainly alloys of non-noble transition metals that are capable of inserting hydrogen into the atomic lattice at elevated pressures and releasing it at decreased pressures. Major drawbacks are the storage density of approx. 1 wt.%, the limited release rates and the relatively high costs [6].

LOCs are organic compounds that can be easily hydrogenated and dehydrogenated, mainly including aromatic substances. Most interesting examples are the compounds toluene-methylcyclohexane and carbazoles (illustrated in Figure 3) [10]. Major drawback of these compounds is the sluggish kinetics and the efficiency losses thereof.

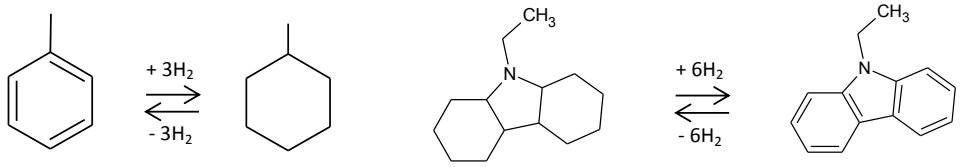

Figure 3: Hydrogenation and dehydrogenation of toluene (C_7H_8) and methylcyclohexane (C_7H_{14}) and N-ethylcarbazole ($C_{14}H_{13}N$ and $C_{14}H_{25}N$).

Chemical hydrides are substances with hydrogen that exhibits a formal oxidation state -1. The most promising candidates are amino borane (NH_3BH_3) and sodium borohydride ($NaBH_4$). In general these compounds show high volumetric and gravimetric storage densities and good hydrogen release kinetics. Major challenges to overcome are the purity of the released hydrogen and effective, inexpensive recycling processes [7].

2.2 Fuel Cells

Fuel cells are an energy transforming technology, which enables highly efficient power generation with very little local emissions [11]. A fuel cell is a so-called tertiary electrochemical cell meaning the energy carrier (the fuel) is not stored within the cell but continuously supplied. The principle of fuel cells was first published by Sir William Robert Grove in 1838 and by Christian Friedrich Schönbein in 1939 demonstrating an acidic hydrogen fuel cell [12,13].

Today there are various types of fuel cells divided by means of the electrolyte and/or the fuel. The differentiation by electrolyte gives five major types of fuel cells [14]:

- Alkaline fuel cells (AFCs)
- Proton-exchange membrane fuel cells (PEMFCs)
- Solid oxide fuel cells (SOFCs)
- Phosphoric acid fuel cells (PACFs)
- Molten carbonate fuel cells (MCFCs)

After the Nasa Gemini project, that employed alkaline fuel cell technology for the first time and the successful demonstration of an AFC driven vehicle by Prof. Kordesch, the alkaline approach fell behind the acidic one due to the development of proton conductive electrolyte membranes [15,16]. Today, the most developed fuel cell is the acidic polymer electrolyte membrane (PEM) fuel cell using e.g. Nafion® membranes (perfluorinated carbon backbone polymer with acidic sulfonate ending groups). More than 130,000 PEM fuel cell units are installed so far in Japan for residential use as micro combined heat and power units (μCHP) [5]. However, recent developments of anion conductive membranes increased scientific interest in alkaline fuel cells in the last decade significantly [14]. Main advantages of alkaline conditions are the possibility of using non-noble and inexpensive transition metal catalysts and the faster cathode reaction kinetics (electrode reactions are given below) [17,18].

	acidic	alkaline
Anode	$H_2 \rightarrow 2H^+ + 2e^-$	$H_2 + 2OH^- \rightarrow 2H_2O + 2e^-$
Cathode	$½O_2 + 2H^+ + 2e^- \rightarrow H_2O$	$½O_2 + H_2O + 2e^- \rightarrow 2OH^-$
Cell	$H_2 + ½O_2 \rightarrow H_2O$	

As mentioned above, an alternative way of subdividing fuel cells is the fuel. Conventional fuel cells are operated with gaseous hydrogen. However, in general a fuel cell can be operated with any substance that is exothermically oxidizable with oxygen. Besides one commercialized direct fuel cell, namely the direct methanol fuel cell, there are several interesting and promising oxidizable liquids like alcohols, or-

ganic acids, ammonia, hydrazine or borohydride [19–22]. The main advantage of these alternative fuels (or their derivatives) is their property of being in liquid state at standard conditions.

2.2.1 Thermodynamics

In general thermodynamic considerations are expressed in terms of the Gibbs energy, which consists of the reaction enthalpy and the entropy (see Equ. 1).

$$\Delta G^0 = \Delta H^0 - T\Delta S^0 \qquad \textbf{Equ. 1}$$

ΔG^0	Gibbs free energy	J mol^{-1}
ΔH^0	Reaction enthalpy	J mol^{-1}
T	Absolute temperature	K
ΔS^0	Change of entropy	J mol^{-1} K^{-1}

The reaction enthalpy of the combustion of hydrogen can be given by means of lower and higher heating value (LVH and HHV). While the reaction product water is considered to be in gaseous state for the LHV it is liquid for the HHV (both at 25 °C). Therefore, the difference of these values equals the energy of evaporation [23,24]. In fuel cell science the higher heating value is considered for efficiency considerations.

Thermodynamic values		
HHV $\Delta H^0_{H2O\ liquid}$	**-285.8**	**kJ mol^{-1}**
LHV $\Delta H^0_{H2O\ gas}$	**-241.8**	**kJ mol^{-1}**
$S^0_{H2O\ liquid}$	**69.9**	**J K^{-1} mol^{-1}**
$S^0_{H2O\ gas}$	**188.8**	**J K^{-1} mol^{-1}**
S^0_{H2}	**130.7**	**J K^{-1} mol^{-1}**
S^0_{O2}	**205.1**	**J K^{-1} mol^{-1}**
$T\Delta S^0_{H2O\ liquid}$	**-48.7**	**kJ mol^{-1}**
$\Delta G^0_{H2O\ liquid}$	**-237.1**	**kJ mol^{-1}**
$\Delta G^0_{H2O\ gas}$	**-228.6**	**kJ mol^{-1}**

The entropy of the hydrogen fuel cell reaction depends on the assumed state of the product water. However, in both cases the change of entropy (ΔS) during the combustion is negative, meaning that the maximum usable energy, the Gibbs free energy, decreases with increasing temperature. The theoretic maximum efficiency can be described as a ratio between the Gibbs Energy and the HHV giving 83% assuming liquid water at 25 °C (see Equ. 2) and 95% for steam at 25 °C.

$$\eta_{th} = \frac{\Delta G^0}{\Delta H^0} \; (= 83\%) \qquad \textbf{Equ. 2}$$

η_{th} Theoretic maximum efficiency

The Gibbs free energy can be transformed to a reversible cell voltage according to Equ. 3. For the hydrogen/oxygen fuel cell the reversible cell voltage is 1.229 V at standard conditions assuming liquid product water.

$$E^0 = \frac{-\Delta G^0}{n \cdot F} \qquad \textbf{Equ. 3}$$

E^0	Reversible cell voltage	V
n	Number of exchanged electrons	
F	Faraday constant	96485 C mol^{-1}

Due to various loss mechanisms the actual cell voltage is always below this theoretical value. Therefore the actual efficiency is a ratio of the cell voltage to the theoretical voltage (see Equ. 4). The difference of these values is lost in form of heat during the operation.

$$\eta_{eff} = \frac{E}{E^0} \qquad \textbf{Equ. 4}$$

η_{eff}	Effective efficiency	
E	Actual cell voltage	V

The efficiency of hydrogen fuel cells is in general in the range of 40-60% at voltages of approx. 0.5-0.7 V, depending on the type of fuel cell and the operating point.

2.3 Hydrogen storage in ionic liquids

The chemical storage of hydrogen in the form of the borohydride anion (BH_4^-) is a promising technological approach for future applications. The most disseminated compound is sodium borohydride ($NaBH_4$)

[25–49]. Since the sodium cation (Na^+) is passive during all reactions it can be replaced by any other stable cation.

Our industrial partner, proionic GmbH, holds two patents for organic cation borohydride compounds that are used as hydrogen storage materials [50,51]. Replacing sodium with large organic cations exhibits several advantages:

- Higher storage densities in liquid state
- Enhanced long-term stability
- Possibility of melting the compound

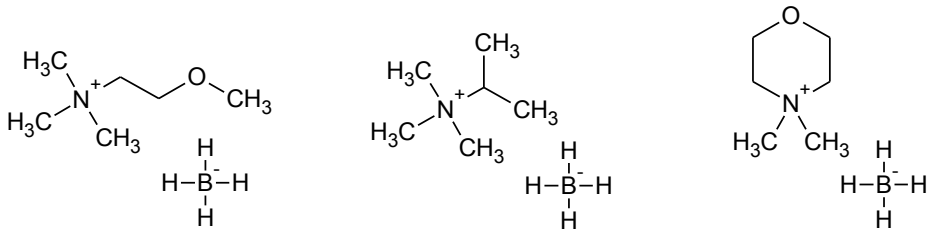

Figure 4: Examples of ionic liquid type borohydrides proposed by Kalb (left: METMA BH_4 – 2-methoxy-N,N,N-trimethylethan-ammonium borohydride; middle: TMPA BH_4 – N,N,N-trimethylpropan-2-ammonium borohydride; right: DMMor BH_4 - 4,4-dimetyl-morpholin-4-ium borohydride [50,51].

The hydrogen storage density of borohydride based storage systems is always limited by the solubility of the byproduct metaborate BO_2^-. The organic borohydrides exhibit between 3.5 and 4.5 wt.% hydrogen in aqueous solution while $NaBH_4$ is limited to 2.1 wt.%. Although the compound itself exhibits a higher molecular mass the storage density is increased due to the excellent solubility properties [50,51].

Borohydride undergoes spontaneous hydrolysis reaction dissolved in water, resulting in the loss of stored hydrogen. The hydrogen loss rate strongly depends on the pH of the solution (see Table 1) [52]. Replacing sodium with steric hindered organic cations shows a massive change in long-term behavior of the borohydride anion, even at decreased hydroxide concentrations. The US Department of Energy (DOE) defined the ultimate target of hydrogen loss rates for onboard hydrogen storage devices at 0.05 g H_2/h/kg $_{H2\ stored}$. The stability of the compounds shown in Fig. 5 meets this target of the US DOE.

Table 1: Half-life of $NaBH_4$ in dependence of pH value.

pH	Half-life	
4.0	**0.0037**	**sec**
5.0	**0.037**	**sec**
6.0	**0.37**	**sec**
7.0	**3.7**	**sec**
8.0	**36.8**	**sec**
9.0	**6.1**	**min**
10.0	**61.4**	**min**
11.0	**10.2**	**h**
12.0	**4.3**	**d**
13.0	**42.6**	**d**
14.0	**426.2**	**d**

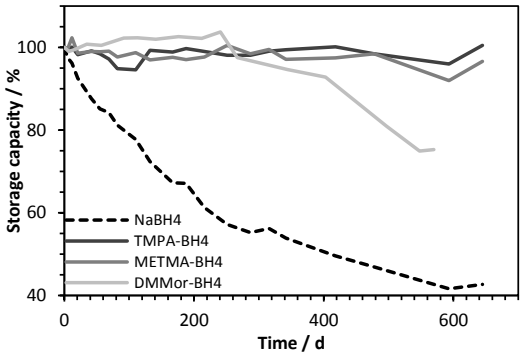

Figure 5: Long-term stability of various borohydrides in alkaline solution (pH 14), data provided by proionic GmbH.

Sodium borohydride cannot be molten, in air it decomposes at approx. 300 °C, in vacuum at above 400 °C [53]. Organic borohydrides on the other hand show ionic liquid behavior with melting points below 100 °C. The possibility of producing an ionic melting offers the opportunity of using non-aqueous electrochemical methods. For an electrochemical recycling process of borohydride non-aqueous approaches are absolutely necessary [54–56].

2.3.1 Hydrogen release reaction

Borohydride is a water splitting agent that delivers as much as four hydrogen molecules per molecule of borohydride. Thermodynamic details of the reaction are given below [57–59].

$$BH_4^- + 2H_2O \rightarrow BO_2^- + 4H_2 \quad (1)$$

Thermodynamic values		
ΔH^0	-210 ± 11	kJ mol^{-1}
S^0_{NaBH4}	101.3	J K^{-1} mol^{-1}
S^0_{NaBO2}	73.4	J K^{-1} mol^{-1}
S^0_{H2}	130.7	J K^{-1} mol^{-1}
$S^0_{H2O\ liquid}$	69.9	J K^{-1} mol^{-1}
$T\Delta S^0$	104.8	kJ mol^{-1}
ΔG^0	-315 ± 11	kJ mol^{-1}

The thermodynamics as well as the kinetics of this reaction exhibits optimal properties for the application as hydrogen storage system. The release reaction does not occur without a catalyst, hence the storage media is stable at ambient conditions. By establishing contact to a catalyst, the reaction starts even at temperatures below 0 °C (as long as the storage medium is liquid) and at pressures up to several hundred bars [50,51].

The cation does not participate in any reaction, therefore it does not influence the thermodynamics. The kinetics on the other hand is influenced massively. Due to the formation of ion pairs the concentration of free borohydride anions in solution is changed. The formation of ion pairs can be experimentally confirmed by the electrolytic conductivity at various concentrations [60]. As confirmed the electrolytic conductivity and the hydrogen release kinetics follow the same trend and confirm the influence of the cation due to ion pair formation (see Fig. 10, experimental section).

2.3.2 Catalysts

As mentioned above, the reaction needs to be catalyzed; the activation energy of the reaction has to be lowered accordingly. The reaction is catalyzed by a long list of noble and non-noble metals, such as Pt, Ru, Rh, Ni, Co etc. In general, noble metals do exhibit higher catalytic activity than non-noble metals [39].

Holbrook and Twist suggested a mechanism based on their experiments with isotope marked water and borohydride [61]. The reaction undergoes several steps starting with the donation of one hydride to the catalyst surface while the remaining BH_3 species is bound. BH_3 leaves the surface and reacts with a hy-

droxide, which is omnipresent in alkaline media. The remaining negative charge on the catalyst splits one molecule of water. The third step is the reaction of two hydrogen atoms from the surface (one from borohydride and one from water) forming gaseous hydrogen. This step is repeated four times resulting in the reaction byproduct metaborate BO_2^- [43,61].

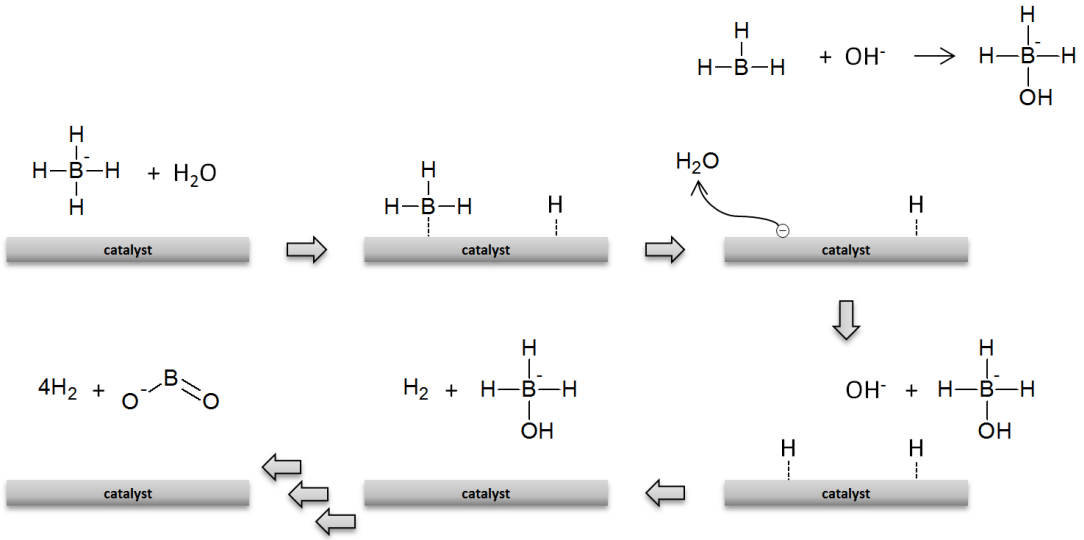

Figure 6: Proposed mechanism of catalytic borohydride hydrolysis [43,61].

A list of the most important catalysts and their activities are given in Table 2.

Table 2: Comparison of various borohydride hydrolysis catalysts.

Catalyst	Activity	Temperature	Reference
	ml H_2 min^{-1} g_{metal}^{-1}	°C	
$Pt/LiCoO_2$	**206,500**	**22**	[62]
$Ru/LiCoO_2$	**270,000**	**25**	[63]
Rh/TiO_2	**360,000**	**40**	[64]
Ni nanoclusters	**4,250**	**25**	[38]
CoW/Ni-foam	**15,000**	**20**	[65]

2.3.3 Recycling process

The recycling of metaborate BO_2^- to borohydride BH_4^- is probably the main challange of this technology. The state-of-the-art chemical process (Schlesing process) exhibits high energy intensity resulting in a price of hydrogen as high as 50 US$ per kg.

An alternative route is the electrochemical reduction. There are several relevant studies attempting electrochemical synthesis of BH_4^- in aqueous electrolyte. However, most authors agree that the electroreduction is not possible in presence of water [54–56]. Using ionic liquid based borohydrides offer the possibility to apply electrochemical methods in the pure molten substance. Since a simple reverse oxidation reaction would yield two molecules of water, other electrochemical routes with an oxygen acceptor have to be developed (see reactions 2 and 3).

$$BO_2^- + 4H_2 \rightarrow BH_4^- + 2H_2O \quad (2)$$

$$BO_2^- + 2H_2 + A \rightarrow BH_4^- + AO_2 \quad (3)$$

A … oxygen acceptor

2.4 The direct borohydride fuel cell

The direct borohydride fuel cell (DBFC) is an electrochemical device, which is capable of converting the chemical stored energy in borohydride to electric energy. Theoretically, the borohydride anion delivers eight electrons at an anode potential of -1.24 V vs. SHE [66,67]. Many studies of DBFC systems run with hydrogen peroxide cathodes although employing air in an oxygen electrode is the most practical approach. The combination borohydride-oxygen gives a reversible cell voltage of 1.64 V (electrode reactions are given below).

$$BH_4^- + 8OH^- \rightarrow BO_2^- + 6H_2O + 8e^- \qquad E^0 = -1.24 \text{ V vs. SHE} \quad (4)$$

$$O_2 + 2H_2O + 4e^- \rightarrow 4OH^- \qquad E^0 = 0.40 \text{ V vs. SHE} \quad (5)$$

$$BH_4^- + 2O_2 \rightarrow BO_2^- + 2H_2O \qquad E^0 = 1.64 \text{ V} \quad (6)$$

Sodium borohydride as pure solid compound exhibits the highest energy density of 9.3 Wh g^{-1} $NaBH_4$ [68]. However, as mentioned before the more suitable solubility properties of organic borohydrides in-

crease the energy density in liquid state significantly (comparison in Table 3). The energy density in liquid state is more than doubled compared to sodium borohydride.

Table 3: Theoretical energy densities of pure borohydride compounds.

Compound	Energy density Pure compound Wh g^{-1}	Energy density Liquid state Wh g^{-1}
$NaBH_4$	9.80	3.89
TMPA BH_4	3.17	6.49
METMA BH_4	2.79	7.79
DMMor BH_4	2.83	8.34

One of the biggest challenges to overcome is the major side reaction of the borohydride oxidation reaction (BOR), namely the hydrolysis reaction. This competing reaction (1) causes a drop of coulombic efficiency due to loss of gaseous hydrogen and mechanical stress on the electrode. So far there is no final solution to this problem.

By comparing the competing reactions (1) and (4) it is obvious that the reaction pathway strongly depends on the pH, or more precisely the local hydroxide concentration at the active site of the electrode. According to a study by Liu et al. the ratio $[OH^-]/[BH_4^-]$ has to be at least 4.4 in order to reach a complete eight electron oxidation of BH_4^- [69]. Mechanistic studies showed that after donating the hydride to the catalyst surface there are two possible steps: firstly the electrochemical reduction of the hydride with one molecule of hydroxide or secondly the splitting of a water molecule (as described for the hydrolysis mechanism) and the chemical formation of one molecule of hydrogen [70].

$$H_{ad} + OH^- \rightarrow H_2O + e^- \quad (7)$$

$$H_{ad} + H_{ad} \rightarrow H_2 \quad (8)$$

Besides the pH the catalyst has major influence on the reaction pathway. In general electrocatalysts can be divided into hydrolyzing and non-hydrolyzing materials. There is major agreement that gold is inactive for hydrolysis while platinum and palladium do show activity.

2.4.1 Thermodynamics of the DBFC

Thermodynamic considerations of the DBFC follow the approach of the hydrogen fuel cell. Because we are not dealing with elemental substances here and the heat of formation of elemental substances is always zero, these expressions are slightly more complex. The standard enthalpy of a reaction (ΔH^0) is a function of the standard enthalpy of formation (ΔH_f) (given in Equ. 5). The entropy term can be treated in a similar manner, although these values have a complete different foundation compared to the enthalpy terms.

$$\Delta H^0 = \Delta H_{f\ products} - \Delta H_{f\ reactants} \qquad \textbf{Equ. 5}$$

$$\Delta S^0 = S_{products} - S_{reactants} \qquad \textbf{Equ. 6}$$

These standard thermodynamic values (of formation) of solid sodium borohydride and the solvated borohydride anion are:

Thermodynamic values		
$\Delta H_{f\ NaBH4}$	-190.5	kJ mol^{-1}
S^0_{NaBH4}	101.5	J K^{-1} mol^{-1}
$\Delta G_f{}^0_{NaBH4}$	-125.9	kJ mol^{-1}
$\Delta H_{f\ BH4-\ (aq)}$	51.9	kJ mol^{-1}
$S^0_{BH4-\ (aq)}$	106.7	J K^{-1} mol^{-1}
$\Delta G_{f\ BH4-\ (aq)}$	119.7	kJ mol^{-1}

Continuously the Gibbs free reaction energy of the DBFC reaction (6) can be calculated and is given below. For the DBFC the product water is considered to be in liquid state because it is produced at the anode and the anode is flooded with aqueous fuel. Borohydride BH_4^- and metaborate BO_2^- should be con-

sidered as solvated anions. However, since entropy data of dissolved metaborate is not available and solvation energies are assumed to be similar for both substances, entropy data from crystals is used [57–59].

Thermodynamic values*		
ΔH^0	-1355	kJ mol^{-1}
S^0_{NaBH4}	101.3	J K^{-1} mol^{-1}
S^0_{NaBO2}	73.4	J K^{-1} mol^{-1}
S^0_{O2}	205.1	J K^{-1} mol^{-1}
$S^0_{H2O, liquid}$	69.9	J K^{-1} mol^{-1}
$T\Delta S^0$	-88.0	kJ mol^{-1}
ΔG^0_{cell}	-1265.9	kJ mol^{-1}

*Missing consistency of the values originates from various literature sources.

Based on these fundamental values the theoretic efficiency and the reversible cell voltage can be calculated.

$$\eta_{th} = 93.4\ \%$$

$$E^0 = 1.64\ V$$

The consistence of thermodynamics can be shown by connecting the DBFC to the hydrolysis reaction and the hydrogen fuel cell (see Fig. 7). The Gibbs free energy of reaction (6) is -1265.9 kJ mol^{-1} borohydride and of the combustion of hydrogen -237 kJ mol^{-1} giving -948 kJ mol^{-1} for four molecules of hydrogen. The difference of these values is exactly the Gibbs free energy of the hydrogen release reaction, namely -315 kJ mol^{-1}. As mentioned above, slight deviations of the thermodynamic values originate from experimental uncertainties; the values are from different literature resources.

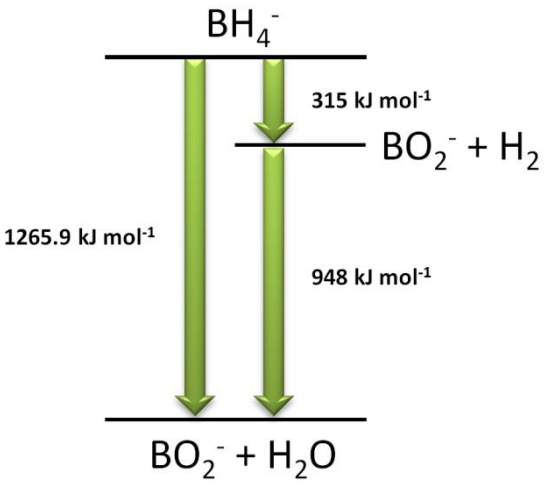

Figure 7: Gibbs free energy of the conversion of borohydride to metaborate via two routes.

2.4.2 DBFC approaches

The fuel cell approaches can be generally divided into membrane based and non-membrane based systems. For membrane based approaches anion as well as cation exchange membranes are discussed (illustrations shown in Fig. 8). The usage of cation exchange membranes show unpractical drawbacks, namely the excessive need of hydroxide at the anode (at least eight equivalents to borohydride), the drop of pH in the fuel during operation and the formation of sodium hydroxide at the cathode [71]. The anion exchange membrane does not show any of these disadvantages. Therefore the usage of an anion exchange membrane is indispensable for a practicable application.

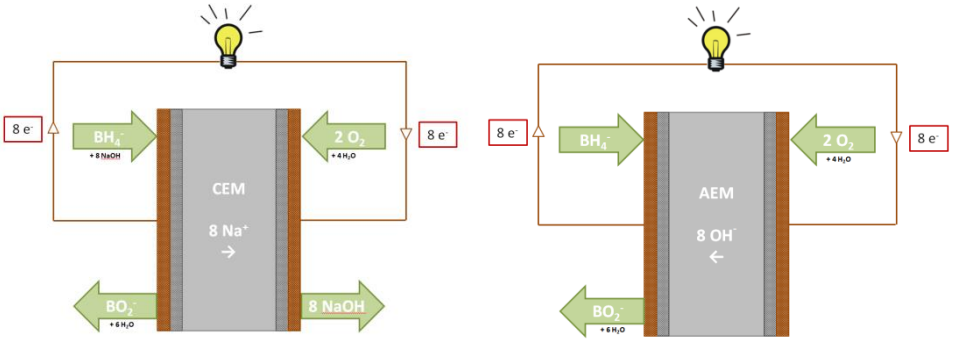

Figure 8: Cation and anion exchange membrane based DBFC approaches.

Membrane-less systems show several advantages but also require catalysts with high selectivity. The so-called mixed reagent DBFC employs the fuel combined with oxygen to the cell and requires highly selective anode as well as cathode catalysts [72,73]. In this approach the electrodes and a separator are rolled, similar to a conventional primary or secondary battery.

A compromise of these approaches is the mixed electrolyte fuel cell. Since borohydride has to be stored in high alkaline aqueous media, it is able to act as electrolyte at the same time. Anode and cathode are sandwiched with a simple polyethylene separator that is soaked with fuel. The fuel is pumped through the porous structure of the anode also ensuring proper mass transport. The main advantage of this approach is that only the cathode catalyst has to show high selectivity because there is no oxygen present at the anode.

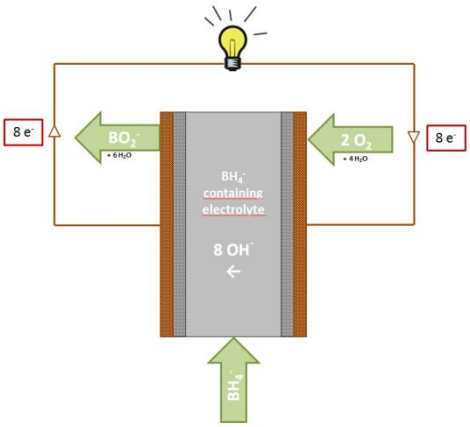

Figure 9: Non-membrane based mixed electrolyte DBFC approach.

3 EXPERIMENTAL

3.1 Hydrogen storage

For comprehensive investigations of the ionic liquid based hydrogen storage system the hydrogen release kinetics, the recharging of the liquid by ion exchange, a self-regulating hydrogen release unit and the purity of the released hydrogen are studied accordingly.

A reliable method for the quantification of hydrogen, especially in mixtures of gases, is a key issue in all research projects concerning hydrogen technologies. An electrochemical method is developed and validated by employing a mass flow controller, the borohydride hydrolysis and the steam-iron process [74,75]. Experimental details are described in my paper added to this dissertation **(C. Grimmer et al., *Selective real-time quantification of hydrogen within mixtures of gases via an electrochemical method*, Int. J. Hydrogen Energy, 40 (2015) 2055-2061)**.

Hydrogen storage in borohydride based ionic liquids is not published in a peer-reviewed journal so far. Still, the sections 3.1.1-3.1.4 are originally published in my conference proceedings of the European Fuel Cell Forum 2015 **(C. Grimmer et al., *Borohydride based Ionic Liquids as novel Hydrogen Storage*, Proceedings of the 8th European Fuel Cell Forum 2015, B0503 1-8, ISBN 978-3-905592-19-1)**.

3.1.1 Catalyst preparation

Cobalt based catalysts on nickel foam are prepared by a previously published method using deposition of metal precursors with $NaBH_4$ as reducing agent [65]. In short, Ni-foam is cut in in appropriate pieces of 1x1 cm^2, cleaned with acetone in an ultrasonic bath, hydrochloric acid and rinsed with ultrapure water right before the deposition step. A solution containing $CoCl_2$, $NaWO_4$, NH_4Cl and NH_3 as well as a reducing solution containing $NaBH_4$ and NaOH are prepared. The cleaned and etched Ni-foam is immersed in

the metal salt containing solution before the same amount of the reducing solution is added. In order to achieve the desired metal loading this step is repeated twice. The as-prepared catalyst samples are tempered in nitrogen atmosphere at 250 °C with a heating ramp of 1 °C min^{-1}.

Scanning electron microscopy (SEM) images are taken with a Zeiss Ultra 55 at an acceleration voltage of 5 kV by Dr. Julian Wagner (FELMI Graz).

3.1.2 Testing of catalyst performance

The catalytic performance for the hydrogen release reaction (HRR) is tested with $NaBH_4$ for benchmarking the catalysts with literature values as well as with organic borohydrides. All solution concentrations are given with respect to hydrogen storage density for easier comparability. The catalyst is placed in a temperature controlled reaction chamber and after flushing the whole system with nitrogen a defined amount of borohydride solution is added via a septum. The quantification of hydrogen is done with our previously published electrochemical method that is capable of detecting hydrogen selectively and in real-time [75]. With a carrier gas the released hydrogen is transported to an electrochemical cell where hydrogen is oxidized selectively at a set potential of 430 mV vs. RHE. The corresponding current is analyzed considering Faraday's Law and ideal gas behavior at standard conditions.

3.1.3 Long-term stability

In order to evaluate the long-term stability and durability of the catalyst system the catalytic performance is tested after its synthesis and after 720 hours of performing hydrogen release. The catalyst is placed in a 2 liter container containing $NaBH_4$ with a concentration of 1 wt.% H_2 in 1M NaOH (equals 47.3 g $NaBH_4$/kg). After 720 hours the catalytic performance is tested and compared to the begin of lifetime (BOL) performance.

3.1.4 Purity of hydrogen

Gas purity of the released hydrogen is measured by mass spectrometry employing a Netzsch MS 403C Aëolos with a heated capillary and a quadrupole mass separation unit. In order to evaluate the detection limit a model amine is evaporated in a sealed container ending up with a concentration of 10 ppm in the gas phase. After gaining the expected signal from the MS, released hydrogen from borohydride ionic liquids is evaluated.

3.2 Direct borohydride fuel cell

The utilization of the chemical energy of borohydride in a direct fuel cell is investigated extensively in two different fuel cell approaches, namely an anion exchange membrane based and a mixed electrolyte based approach (schematically shown in Fig. 18). Anode as well as cathode catalysts are developed and studied by ex-situ methods and in-situ in single test cells. In order to ensure proper in-situ measurements two new test cells are designed and manufactured.

The most relevant results are published in three peer-reviewed journal articles [76–78]. DBFC results that are not published so far are presented in section 4.2.

A direct comparison of five noble metal catalysts (platinum, palladium, ruthenium, gold and rhodium) by rotating disk electrode measurements shows the catalytic performance of each metal. The preparation of the catalyst samples is done by the so-called instant method and is described in my publications.

In arrangement with our industrial partners the usage of organic borohydrides in DBFCs is not published so far. Therefore, ex-situ as well as in-situ results are presented in section 4.2. For proper comparisons with $NaBH_4$ the same experimental conditions are used for all experiments (details are described in the respective publications).

4 RESULTS AND DISCUSSION

The most relevant results are published and discussed in my articles. However, some relevant observations and discussions are not published yet – they are described in the following section.

4.1 Hydrogen storage

For a practicable hydrogen release system a long-term stable and inexpensive catalyst with a stable form and structure is necessary. For this purpose a catalyst is developed based on non-nobel transition metals on a support material with an optimal trade-off between catalytic surface and porosity for proper mass transfer. Chemically deposited cobalt and tungsten on commercially available nickel foam was developed [29,33,35,39,65].

In order to ensure proper hydrogen release measurements for the catalyst development, hydrogen has to be quantified accordingly. An electrochemical quantification method was developed that is capable of quantifying hydrogen in real-time within mixtures of gases even at very low flow rates. It is shown that this method outperforms state-of-the-art methods like gas chromatography, mass spectrometry, gas flow meters and volumetric methods (**C. Grimmer et al., *Selective real-time quantification of hydrogen within mixtures of gases via an electrochemical method*, Int. J. Hydrogen Energy, 40 (2015) 2055-2061**).

As mentioned above organic borohydrides exhibit significant enhanced long-term stability. This big advantage entails the disadvantage of suffering hydrogen release kinetics. Hence there is a clear and obvious trade-off between the factors long-term stability and release kinetics.

In this context a strong relationship between borohydride stability and the availability of free anions is assumed, which is associated to the formation of ion pairs in aqueous solution. The influence of concentration on electrolytic conductivity strongly supports this assumption. In general the conductivity of an

electrolyte increases with concentration up to a certain point, where ion pair formation lowers the availability of free ions [60]. With increasing concentration of sodium borohydride the electrolytic conductivity also increases as expected (see Fig. 10). Organic borohydrides show exact opposite behavior: increased concentration leads to decreased conductivity (conductivity measurements are conducted by Theo Friedrich).

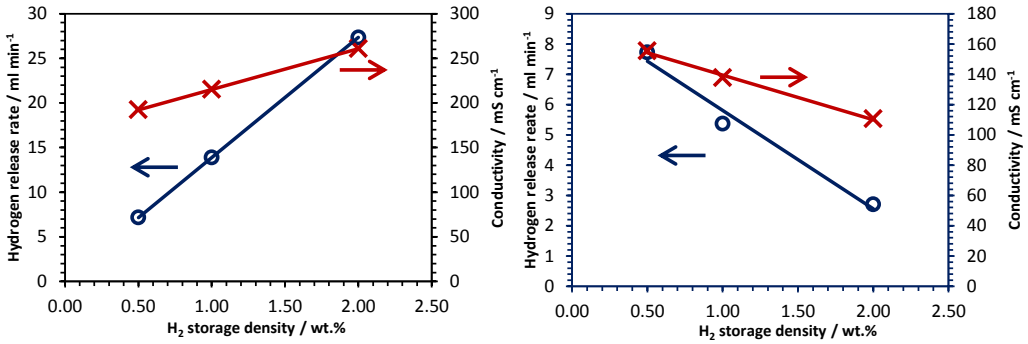

Figure 10: Electrolyte conductivity compared to hydrogen release rate of $NaBH_4$ (left) and METMA BH_4 (right).

Concerning organic borohydrides the hydrogen release, the purity of the released hydrogen and the long-term behavior of the non-noble metal catalyst were investigated, published in a conference proceedings and reprinted in the following sections (**C. Grimmer et al., *Borohydride based Ionic Liquids as novel Hydrogen Storage*, Proceedings of the 8th European Fuel Cell Forum 2015, B0503 1-8, ISBN 978-3-905592-19-1)**.

4.1.1 Catalyst preparation

After two deposition steps the catalyst loading on the substrate is approx. 50 mg cm^{-2}. SEM images (see Fig. 11) show the as-received nickel foam (supplied by Alantum, pore size: 800 µm, thickness: 2.5 mm) and the prepared catalyst after tempering and before first hydrolysis reaction.

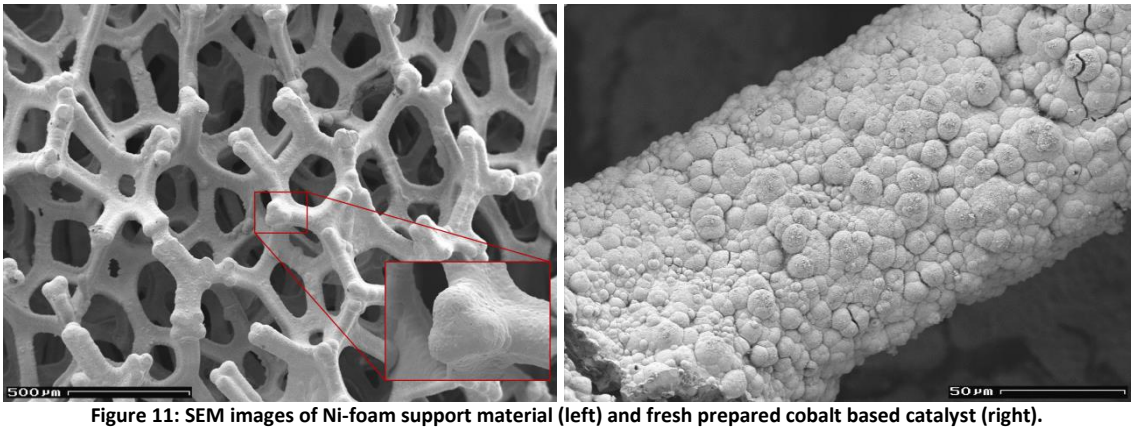

Figure 11: SEM images of Ni-foam support material (left) and fresh prepared cobalt based catalyst (right).

4.1.2 HRR performance testing

All catalysts are tested by hydrolyzing a solution of $NaBH_4$ in 1 M NaOH with a concentration of 1 wt.% H_2 at 30 °C as internal benchmark. The hydrolysis activity has a maximum of approx. 2000 ml H_2 min^{-1} g^{-1} catalyst which is comparable to literature data. In Fig. 12 the results are shown in two types of diagrams, first the hydrogen release rate in terms of ml H_2 min^{-1} g^{-1} catalyst (left) and second the remaining hydrogen concentration in solution. The hydrogen is released within approx. 5 minutes starting immediately after the solution is added. The remaining hydrogen content that cannot be released in a non-stirred experiment is 0.12 wt.% for $NaBH_4$.

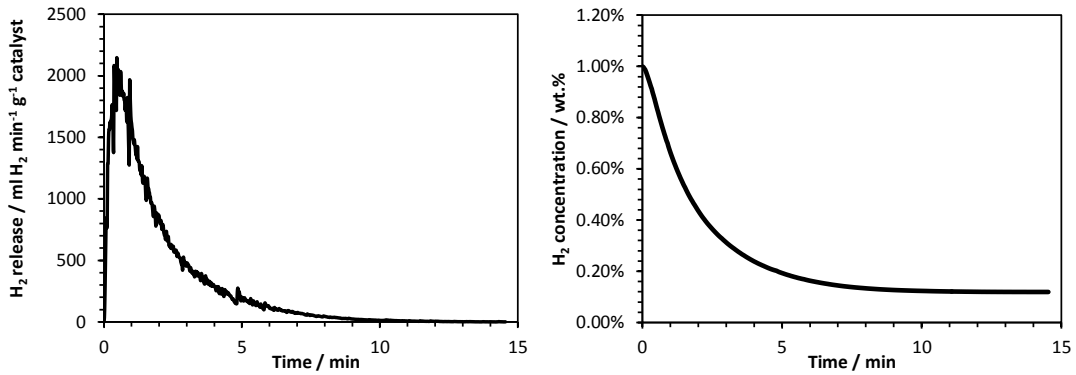

Figure 12: Hydrogen release from $NaBH_4$ solution (1 wt.% H_2) at 30 °C with Co/Ni-foam catalyst, analyzed by electrochemical approach.

Hydrogen release from ionic liquids behaves slightly different compared to sodium borohydride. Due to increased long-term stability of the organic compounds the hydrogen release rate is influenced in a similar way. Fig. 13 shows a typical HRR reaction of TMPA BH_4 in 1 M NaOH with the non-noble metal cata-

lyst. The HRR rate is approx. 600 ml min^{-1} g^{-1} catalyst. Due to decreased reaction rate the reaction time is approx. three times higher until the same amount of hydrogen remains in solution in unstirred condition.

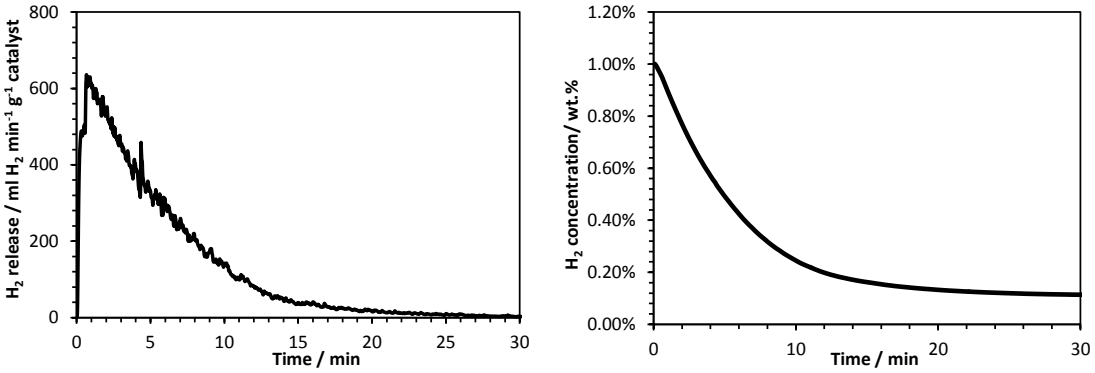

Figure 13: Hydrogen release from TMAP BH_4 solution (1 wt.% H_2) at 30 °C with Co/Ni-foam catalyst, analyzed by electrochemical approach.

4.1.3 Long-term stability

Fig. 14 shows the result of a hydrogen release experiment from $NaBH_4$ at BOL and after 720 hours of operation. The highest reaction rate observed for this sample is approx. 1900 ml H_2 min^{-1} g^{-1} catalyst at BOL. After 720 hours of non-stop operation the activity drops to about 45 % of its initial value.

This result fits previously published experiments quite well. By employing various degradation tests for various catalyst systems and support materials the retained activity was found to be between 25 and 80% [34,35,79]. While complete hydrogen release is achieved after only 20 minutes with a fresh catalyst, it takes about 50 minutes after long-term operation. Kim et al. conducted 200 cycles of HRR experiments and observed the loss of active surface area of 37% by BET analysis [80]. Unfortunately the procedure of cycling the catalyst is not described in detail.

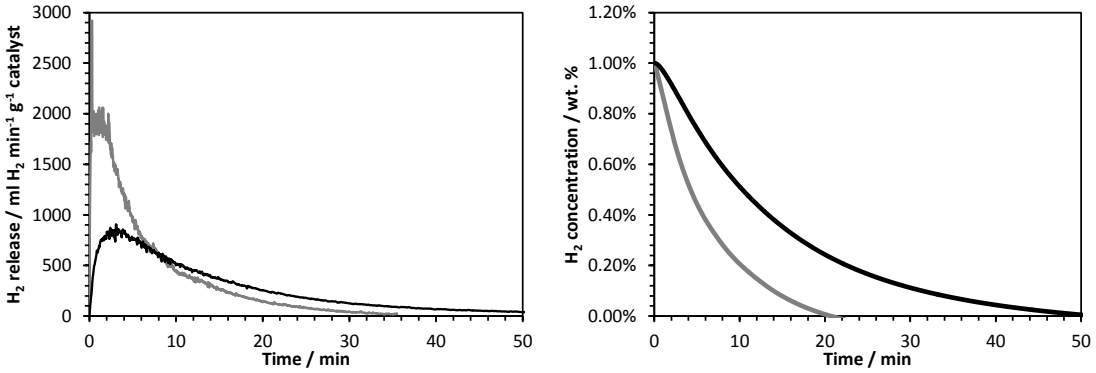

Figure 14: Hydrogen release from $NaBH_4$ solution (1 wt.% H_2) at 30 °C, Co/Ni-foam catalyst BOL (gray) and after 720 hours of operation (black).

SEM experiments of both catalysts (Fig. 15) show small cracks all over the catalysts' surface. A loss of active material was not observed during the long-term operation which is also confirmed by the SEM images. The only obvious change of the catalyst is the formation of small depositions in the size range of several hundred nanometers. According to EDX analysis (not shown) these depositions consist of iron enriched cobalt.

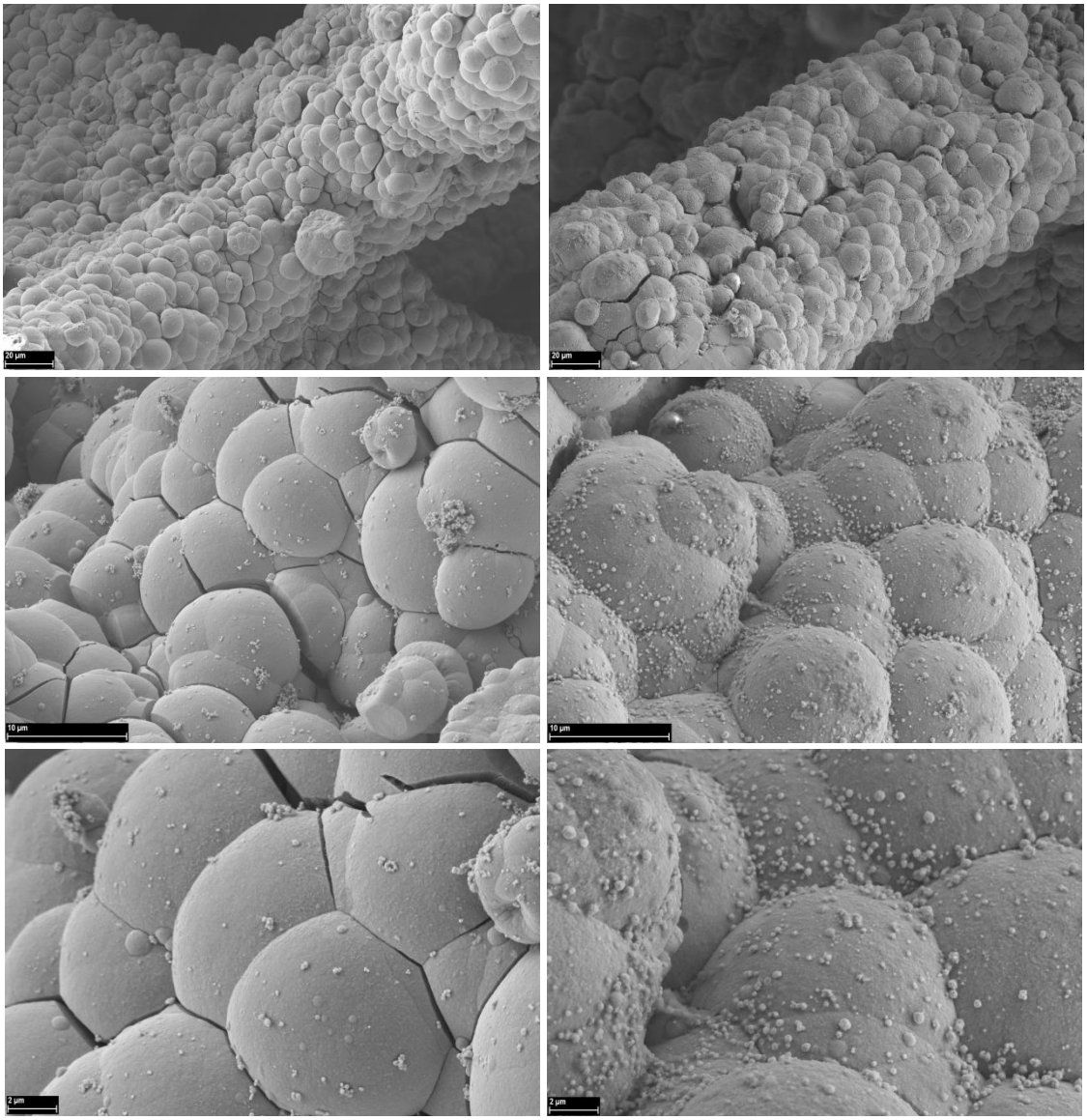

Figure 15: SEM images of fresh catalyst (left) and after 720 hours of operation (right).

4.1.4 Purity of hydrogen

An aqueous solution of N,N-dimethyl-isopropyl-amine as model amine and potential degradation product of the TMPA cation is added to a sealed and temperature controlled chamber. After heating the reaction chamber to 100 °C gas samples with an amine concentration of 10 ppm are taken via a heated capillary (160 °C). The result of a typical scan in the m/z range of 50-90 is shown in Fig. 16. A concentration of

10 ppm can be detected in this experimental approach. Because no corresponding and no other peaks are detected within the released hydrogen from an organic borohydride the hydrogen purity is at least 99.999% (humidity not considered).

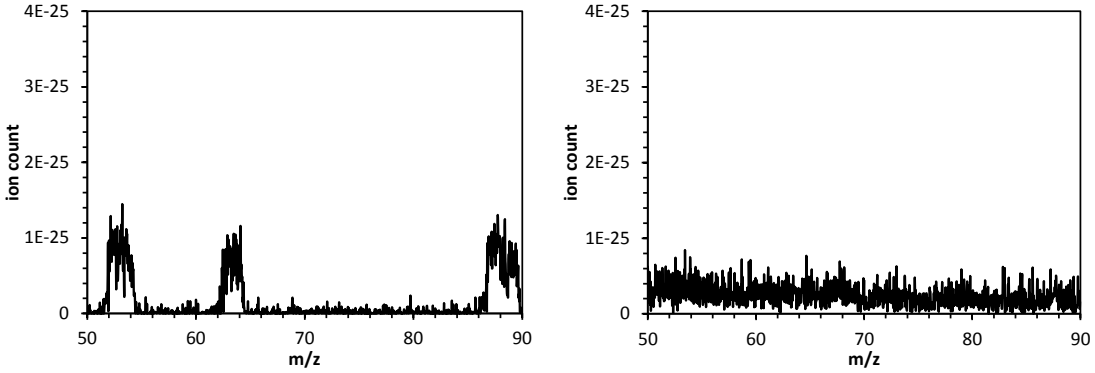

Figure 16: MS spectra of calibration cell with an amine concentration of 10 ppm (left), results of hydrogen released from ionic liquid in corresponding m/z range.

4.1.5 Self-regulating hydrogen release

A complete self-regulating hydrogen release unit was designed and manufactured for an on-site hydrogen supply system. This unit is capable of releasing pressurized hydrogen at the moment of need, sleeping during non-using periods and ensuring proper convection in order to exploit the complete stored hydrogen.

In general this system works in two cycles demonstrated in Fig. 17 (left sleeping and right hydrogen releasing). During cycle one there is no contact to the catalyst, therefore no release reaction occurs. When hydrogen is removed, the pressure in chamber 1 decreases until valve A breaks and the storage medium is flushed into chamber 1. At this moment cycle 2 starts; the catalyst that is capable of releasing twice the amount of hydrogen that is taken, starts to release hydrogen. The pressure in chamber 2 builds up again until valve B breaks and the liquid is flushed back. As long as hydrogen is released from the system these cycles ensure convection. This simple system employs the volumetric work of the reaction, resulting in a system that is independent of any external power source. As such it is comparable to the self-regulating system patented by Millenium Cell in 2000 with the additional capability of inducing convection [25].

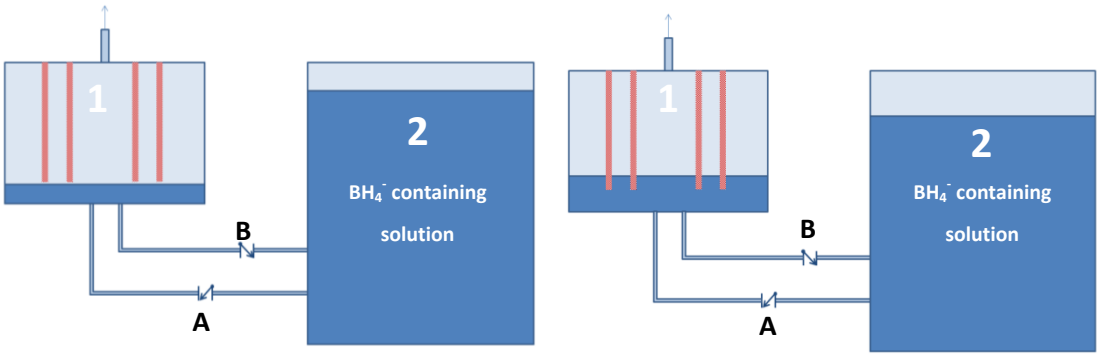

Figure 17: Self-regulating hydrogen release unit in both states - sleeping (left) and releasing (right), catalyst is illustrated in red.

4.2 Direct borohydride fuel cell

The possibility of using the chemically stored energy of borohydride directly without the formation of hydrogen offers certain advantages, most importantly:

- Only 1 system unit (instead of a hydrogen release unit and a hydrogen fuel cell; hence easier cooling of the system)
- The theoretic possibility of higher efficiencies (reaction enthalpy of hydrolysis is not lost)
- No pressures in the system, no gaseous compounds

The development of the DBFC system is done in two steps; first the catalyst development and ex-situ characterization and second, the electrode and single cell development and in-situ characterization. All system components are tested with sodium borohydride as model substance ensuring comparability to literature, and with organic borohydrides. Ex-situ characterizations are done employing standard electrochemical methods in three electrode configuration with rotating disk electrodes (RDE) [81–84].

4.2.1 Fuel cell approaches

In-situ measurements are conducted with two kinds of fuel cell approaches, namely the anion membrane based FC and the mixed electrolyte approach (see Fig. 18).

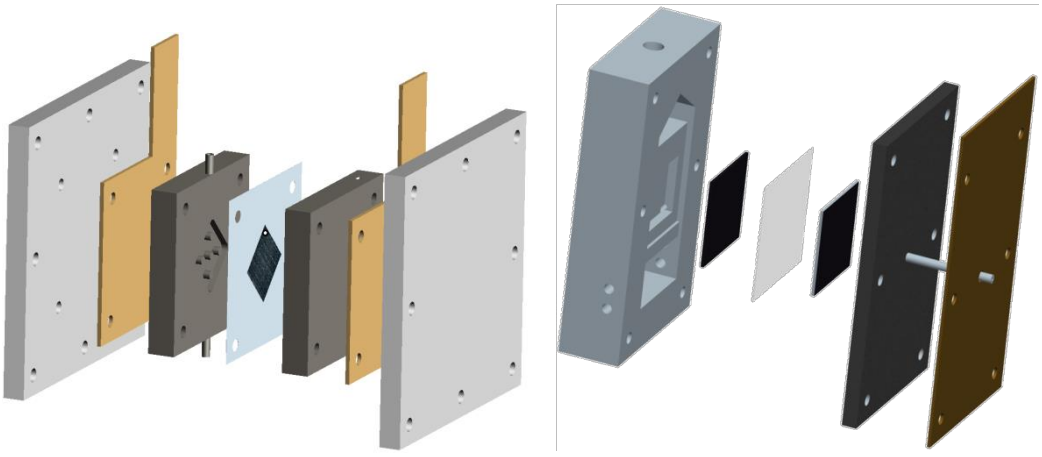

Figure 18: Design of membrane based single test cell (left) and mixed electrolyte single test cell (right).

In general it is indispensable being able to follow the electrode potentials in direct fuel cells in order to gain further insight. However, mounting a Luggin capillary can be quite challenging especially in fuel cells with solid electrolytes. For the DBFC approaches the circumstance that the fuel is an electrolyte at the same time is exploited. A Luggin capillary that is mounted from the backside to the anode was developed. All polariziation curves are measured galvanostatically while measuring the cell voltage and the anode potential versus a reversible hydrogen electrode (RHE) at the same time (using a Gamry Reference 600).

4.2.2 Anode catalysts

The noble metal catalysts platinum, gold, palladium, ruthenium and rhodium were investigated ex-situ for borohydride electrooxidation. All catalysts were prepared using the so-called instant method on high surface area carbon (commercial Vulcan XC72R) [85,86]. While platinum and gold are comprehensively investigated and published, only little literature concerning palladium, ruthenium and rhodium is available.

To the author's knowledge, these catalysts are compared directly for the first time in Fig. 19. RDE experiments were conducted in 1 M NaOH with 5 mM of $NaBH_4$ [7,66–71,87–131]. The only difference is the metal loading on the electrode. The loading on a rotating disk electrode differs for every catalytic system and has to be determined experimentally to fit the following criteria published by Mayrhofer et al. [82]:

- Reaching the assumed number of electrons from the Levich equation in diffusion limited regimes
- Independence of the normalized activity of the metal loading
- Activity parameters should be calculated at approx. half of diffusion limitation

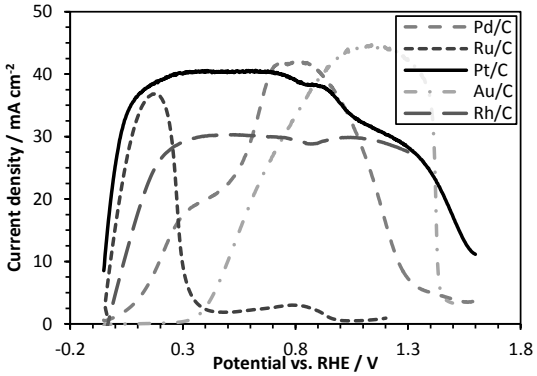

Figure 19: Rotating disk electrode measurements of various noble metals at 1600 rpm with 5 mM $NaBH_4$.

Best catalytic performance is shown by platinum followed by ruthenium. However, the activity towards the main side reaction, the hydrogen release reaction, has to be considered as well. In this respect ruthenium and palladium in combination with organic borohydrides are the most promising candidates.

4.2.3 Organic borohydrides in DBFCs

In ex-situ measurements no significant differences between sodium and various organic cations were observed due to their low concentrations in the electrolyte. As shown in Fig. 20 the onset potential is similar while the diffusion limited current is lower due to poisoning effects of the ammonium compound. In this context in-situ characterizations are necessary for experimental evidence.

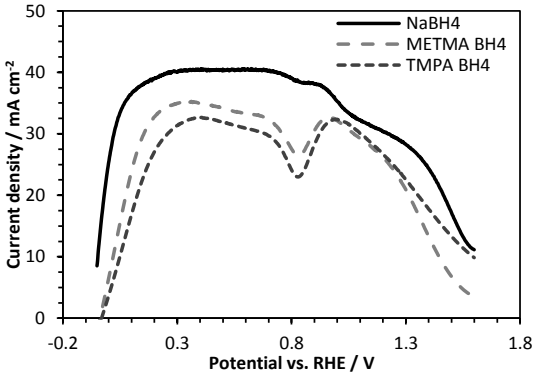

Figure 20: Rotating disk electrode measurements of various borohydrides at 1600 rpm with 5 mM BH_4^-.

In-situ fuel cell tests with ionic liquid borohydrides show significantly decreased performance. In Fig. 21 the polarization curve of the mixed electrolyte DBFC with Ru/C anode catalyst and $La_{0.6}Ca_{0.4}CoO_3$ perovskite catalyst driven with METMA BH_4 is presented. Although the anode performance suffers due to the organic cation, there is one major advantage of these new fuels, namely the complete inhibition of the hydrolysis side reaction. The current state of development suggests that this approach might overcome one of the main challenges of DBFC systems.

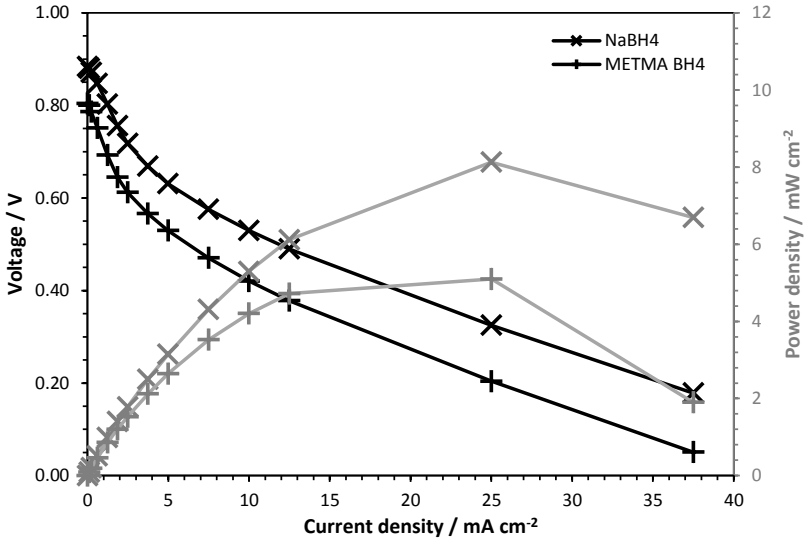

Figure 21: Polarization curves of $NaBH_4$ and METMA BH_4 fueled DBFCs with Ru/C at the anode and $La_{0.6}Ca_{0.4}CoO_3$ perovskite cathode.

4.2.4 Summary of publications

In order to improve the DBFC performance considerable catalyst development was done during the course of this PhD thesis. In three international publications the anode and cathode catalyst developments are presented.

Amongst the noble metal catalysts, palladium is investigated extensively employing various electrochemical methods as well as ^{11}B-NMR (nuclear magnetic resonance spectroscopy) and in in-situ FTIR (infrared spectroscopy) (**C. Grimmer et al., *The electrooxidation of borohydride: A mechanistic study on palladium (Pd/C) applying RRDE, 11B-NMR and FTIR*, Appl. Catal. B Environ. 180 (2016) 614-621**).

An additional study on the performance of the anode with alternative catalysts is published with a ruthenium catalyst. Ru/C is directly compared to Pt/C by means of ex-situ measurements as well as in-situ tests using the anion exchange membrane approach. The cathode catalyst consisted of an inexpensive perovskite catalyst with the composition $La_{0.6}Ca_{0.4}CoO_3$ (**C. Grimmer et al.,** ***Carbon Supported Ruthenium as Anode Catalyst for Alkaline Direct Borohydride Fuel Cells*****, J. Phys. Chem. C 119 (2015) 23839-23844**).

Due to the omnipresence of borohydride at the cathode, the tolerance of the cathode catalyst is essential for the cell performance. By employing a tolerant catalyst the complete abandonment of the membrane offers a simple and practical DBFC approach. Ag-Mn_3O_4/C based cathodes instead of the state-of-the-art catalyst Pt/C is used resulting in a power density of approx. 17 mW cm^{-2} **(C. Grimmer et al.,** ***A membrane-free and practical mixed electrolyte direct borohydride fuel cell*****, J. Electrochem. Soc. 163 (3) (2016) F278-F283).**

5 CONCLUSION

Sustainable energy scenarios identify the need for large-scale energy storage. This encourages scientists in the field of electrochemistry all over to world to search for suitable chemical compounds. Borohydride is selected as a promising chemical compound to store energy over long periods of time.

Borohydride is an anionic compound that is capable of storing chemical energy at very high densities and possesses good long-term stability properties in its pure, solid form. The proper combination of borohydride with organic cations allows high storage densities even in liquid states and further increased long-term stability properties. The stored energy can be utilized in two ways, namely as hydrogen carrier compound and as anodic fuel for direct borohydride fuel cells.

Hydrogen is released by the borohydride hydrolysis reaction delivering 4 molecules of hydrogen by splitting two molecules of water. Various materials including inexpensive transition metals like cobalt catalyze this reaction. In order to supply hydrogen for a 100 kW fuel cell a total amount of approx. 2 kg of cobalt and a release cell with a volume of approx. 2 l is necessary. Catalytic properties, the purity of the released hydrogen and long-term behavior of the catalyst have been proven to be sufficient. Additionally, a self-regulating hydrogen release unit for pressurized hydrogen and fuel convection is developed. The system storage density for mobile applications is estimated and shown in Fig. 22.

In the course of the catalyst development a reliable, selective and robust hydrogen quantification method in real-time is established [74].

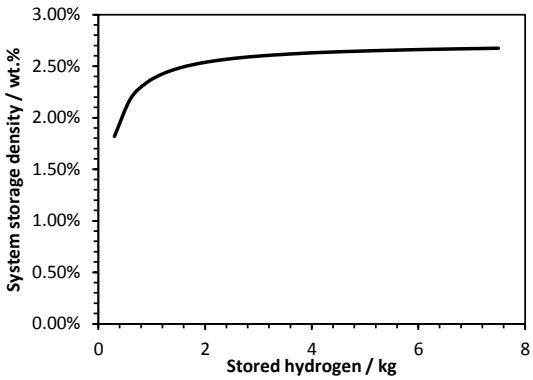

Figure 22: Estimated system storage density in dependence of system size.

The direct borohydride fuel cell offers the possibility of utilizing the stored energy more efficiently while enabling a simpler system design and showing very high energy densities (see Fig. 23). Anode catalysts, cathode catalysts, an anion exchange membrane based fuel cell and a mixed electrolyte DBFC are developed, characterized extensively and published.

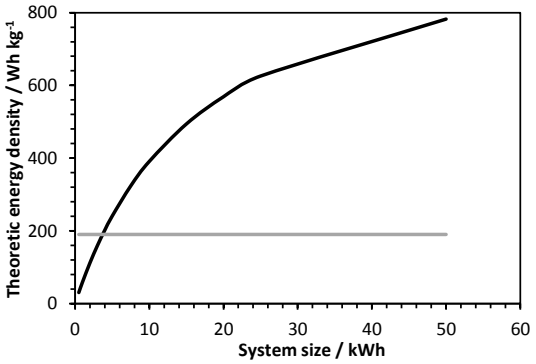

Figure 23: Estimated energy density of a 1 kW system compared to a Li-ion battery (gray).

Among all tested catalysts the ruthenium based catalyst possesses most promising properties with the organic borohydride METMA BH_4 while palladium shows good results in combination with DMMor BH_4. The major drawback of DBFC systems, namely the hydrolysis side reaction, can be resolved by this approach.

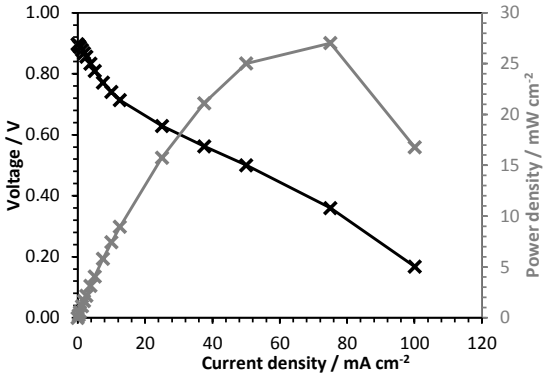

Figure 24: Polarization curve of mixed electrolyte DBFC with Pd/C anode catalyst and MnO_2/C cathode catalyst (iR 0.186 Ω), fueled with DMMor BH_4.

At current status of research and development the maximum power density of this approach is 27 mW cm^{-2} at 40 °C (polarization curve shown in Fig. 24). During the complete operation of the DBFC with the organic borohydride DBFC the hydrogen production due to the hydrolysis side reaction was below the limit of quantification of 0.01 ml H_2 min^{-1}.

6.1.1 Borohydride hybrid-cell

Borohydride based hydrogen storage systems are a promising technological approach. A significant simplification of such a system could be achieved by combining the hydrogen release cell and the fuel cell, to a so-called borohydride hybrid cell (see illustration in Fig. 25). The borohydride containing solution is fed to a hydrogen releasing layer and the formed gaseous hydrogen is transported through a semipermeable membrane to the anode. Smart design and engineering of the hybrid cell could enable a self-regulating mechanism depending on the hydrogen pressure in the anode flow field.

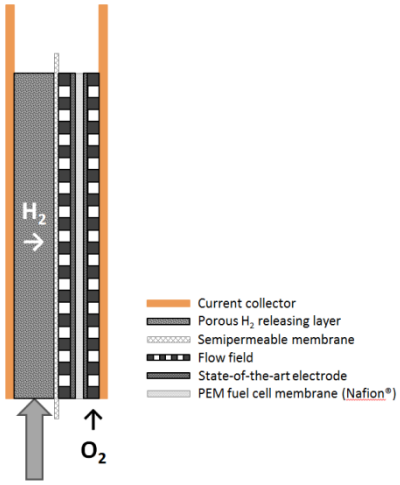

Figure 25: Illustration of borohydride hybrid fuel cell.

6.1.2 Direct biomass fuel cell

In a long-term future perspective, high efficient fuel cells of natural products are highly desirable. One example is the herein proposed direct biomass fuel cell. The anodic fuel for this kind of fuel cell is dissolved cellulose and/or lignin in ionic liquids combined with a standard oxygen cathode. Fig. 26 shows the principle of this kind of fuel cell approach. A future generation of electrocatalyst, for example an inorganic mimic of an enzymatic active site, could be the key for these technologies.

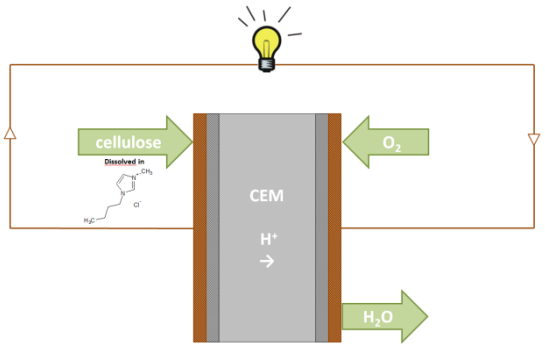

Figure 26: Proposed electrochemical cell that is capable of converting biomass directly.

6.1.3 High temperature anion exchange membrane fuel cell

Another promising approach for future investigations might be a type of high temperature anion exchange membrane fuel cell. One kind of anion exchange membrane is polybenzimidazole doped with KOH, which has a strong dependence on humidification of the membrane. If KOH could be replaced by a stable ionic liquid based hydroxide with a melting point below the operation temperature (e.g. 160 °C), a HTAEM is feasible. With this approach the reaction kinetics could be enhanced and the challenging water management could be simplified significantly at operating temperatures above 100 °C.

6.1.4 Non-aqueous flow cells

Non-aqueous electrochemical flow cells that allow high cell voltages will be a key for grid-scale energy storage in a long-term perspective. Ionic liquids might be a key compound on the road toward these next generation cell applications. A flow cell employing either the anion or the cation itself as reversible storage compound is proposed. The example illustrated in Fig. 27 shows the redox pair ClO_2^- and ClO^- in one

cell compartment and PO_4^{3-}/PO_3^{3-} in the second compartment (see reactions below). The reduction of ClO_2^- as well as the oxidation of PO_3^{3-} are highly exothermic, promising high cell voltages. In this context the combination of any other ion pair is possible. Again, a future generation of catalysts and membranes will be necessary in order to establish these kinds of flow cell applications.

$$ClO_2^- + 2e^- \rightarrow ClO^- + O^{2-}$$

$$PO_3^{3-} + O^{2-} \rightarrow PO_4^{3-} + 2e^-$$

$$ClO_2^- + PO_3^{3-} \rightarrow ClO^- + PO_4^{3-}$$

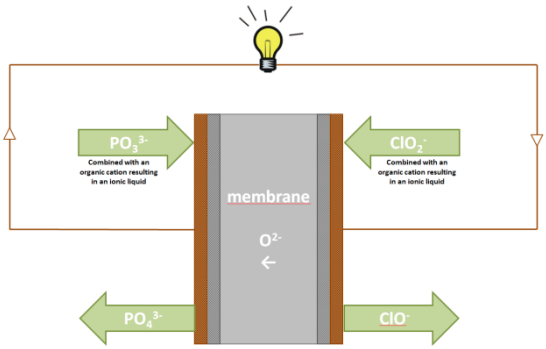

Figure 27: Proposed electrochemical cell using ionic liquids as reversible fuel for grid scale energy storage.

Unfortunately the time of my PhD thesis under supervision of Prof. Viktor Hacker at the Institute of Chemical Engineering and Environmental Technology did not allow proper investigations on these topics.

7 PUBLICATIONS

7.1 Journals

C. Grimmer, M. Grandi, R. Zacharias, B. Cermenek, H. Weber, C. Morais, et al., The electrooxidation of borohydride: A mechanistic study on palladium (Pd/C) applying RRDE , 11B-NMR and FTIR, Appl. Catal. B Environ. 180 (2016) 614–621.

C. Grimmer, R. Zacharias, M. Grandi, B. Pichler, I. Kaltenboeck, F. Gebetsroither, J. Wagner, B. Cermenek, S. Weinberger, A. Schenk, V. Hacker, A membrane-free and practical mixed electrolyte direct borohydride fuel cell, J. Electrochem. Soc. 163 (3) (2016) F278-F283.

C. Grimmer, R. Zacharias, M. Grandi, B. Cermenek, A. Schenk, S. Weinberger, et al., Carbon Supported Ruthenium as Anode Catalyst for Alkaline Direct Borohydride Fuel Cells, J. Phys. Chem. C. 119 (2015) 23839–23844.

C. Grimmer, S. Nestl, J. Senn, V. Hacker, Selective real-time quantification of hydrogen within mixtures of gases via an electrochemical method, Int. J. Hydrogen Energy. 40 (2015) 2055–2061.

C. Grimmer, T. Friedrich, D. Woisetschläger, N. Mayer, R. Kalb, V. Hacker, Novel Borohydride-Based Ionic Liquids as Hydrogen Carrier, Chemie Ing. Tech. 86 (2014) 1443–1443.

A. Schenk, **C. Grimmer**, M. Perchthaler, S. Weinberger, B. Pichler, C. Heinzl, et al., Platinum–cobalt catalysts for the oxygen reduction reaction in high temperature proton exchange membrane fuel cells – Long term behavior under ex-situ and in-situ conditions, J. Power Sources. 266 (2014) 313–322.

T. Friedrich, **C. Grimmer**, D. Woisetschläger, N. Mayer, M. Koncar, V. Hacker, Borhydride mit Ionic-Liquid-Kation als Wasserstoffspeicher – Rezyklierung des Speichermediums, Chemie Ing. Tech. 86 (2014) 1429–1430.

C. Grimmer, A. Schenk, B.E. Pichler, M. Perchthaler, V. Hacker, Manufacturing and Stabilization of PtCo/C Cocatalysts for PEM Fuel Cells, ECS Trans. 58 (2013) 753–759.

7.2 Conference proceedings

C. Grimmer, J. Senn, T. Friedrich, D. Woisetschläger, N. Mayer, R. Kalb, M. Koncar, J. Wagner, V. Hacker, Borohydride based Ionic Liquids as novel Hydrogen Storage. 5th European PEFC & H2 Forum - Proceedings (2015), S. B0305/1-B0305/8.

C. Grimmer, M. Grandi, J. Senn, R. Zacharias, T. Friedrich, V. Hacker, Liquid Hydrogen Carrier Technology based on Ionic Liquids. 11. Minisymposium Verfahrenstechnik - Proceedings (2015), S. 40–43.

C. Grimmer, R. Zacharias, M. Grandi, V. Hacker, The benefits of a mixed electrolyte approach for direct borohydride fuel cells. 1st International Workshop on Hydrogen and Fuel Cells (2015), S. 36–37.

J. Senn, **C. Grimmer**, S. Nestl, V. Hacker, Real-time quantification method for hydrogen. 1st International Workshop on Hydrogen and Fuel Cells (2015), S. 32–33.

M. Grandi, **C. Grimmer**, R. Zacharias, J. Senn, V. Hacker, Synthesis and characterisation of carbon supported bimetallic Platinum-Gold-Nanoparticles for Borohydride Direct Oxidation. 1st International Workshop on Hydrogen and Fuel Cells (2015), S. 30–31.

I. Kaltenböck, A. Schenk, **C. Grimmer**, B. E. Pichler, V. Hacker, Active and stable oxygen reduction catalysts for the high temperature Polymer electrolyte fuel cell. 1st International Workshop on Hydrogen and Fuel Cells (2015), S. 18–19.

R. Zacharias, **C. Grimmer**, M. Grandi, J. Senn, V. Hacker, Hydrolysis in direct borohydride fuel cells. 1st International Workshop on Hydrogen and Fuel Cells (2015), S. 34–35.

B. Cermenek, R. Zacharias, M. Grandi, **C. Grimmer**, A. Schenk, V. Hacker, Palladium based electrocatalysts for ethanol oxidation reaction in alkaline medium. 1st International Workshop on Hydrogen and Fuel Cells (2015), S. 28–29.

C. Grimmer, T. Friedrich, D. Woisetschläger, N. Mayer, M. Koncar, R. Kalb. V. Hacker, Borohydride based Ionic Liquids as Hydrogen and Energy Carrier. Proceedings of the 10th Minisymposium Verfahrenstechnik (2014), S. 95–98.

C. Grimmer, M. Grandi, J. Senn, T. Friedrich, V. Hacker, Novel ionic liquids based on borohydrides for hydrogen and energy storage. 7th International Summer School on Advanced Studies of Polymer Electrolyte Fuel Cells (2014), S. 155–156.

T. Friedrich, **C. Grimmer**, D. Woisetschläger, N. Mayer, M. Koncar, R. Kalb, V. Hacker, Ionic Liquid Borohydrides - A Liquid Phase Chemical Hydrogen Storage Material. MH2014 Programme and Abstracts (2014), S. 191.

J. Senn, **C. Grimmer**, M. Grandi, T. Friedrich, V. Hacker, Comparison of different nickel foams as catalyst support for hydrogen release of borohydride based liquid storage systems. 7th International Summer School on Advanced Studies of Polymer Electrolyte Fuel Cells (2014), S. 161-162.

A. Schenk, **C. Grimmer**, M. Perchthaler, B. E. Pichler, V. Hacker, Platinum Cobalt Catalysts for the High Temperature PEFC. Advanced Studies on Polymer Electrolyte Fuel Cells (2014), S. 147-148.

T. Friedrich, **C. Grimmer**, D. Woisetschläger, N. Mayer, M. Koncar, R. Kalb, V. Hacker, Borhydrid basierte flüssige Wasserstoffspeicher - Rezyklierung des Speichermediums. - in: Proceedings of the 10th Minisymposium Verfahrenstechnik (2014), S. 91–94.

T. Friedrich, **C. Grimmer**, D. Woisetschläger, N. Mayer, M. Koncar, R. Kalb, V. Hacker, Ionic liquid borohydrides - recycling of the storage medium. 7th International Summer School on Advanced Studies of Polymer Electrolyte Fuel Cells (2014), S. 151-152.

C. Grimmer, A. Schenk, B. E. Pichler, M. Perchthaler, V. Hacker, Activity of Platinum First Row Transition Metal PtM/C Cocatalysts. Advanced Studies of Polymer Electrolyte Fuel Cells (2013), S. 148–149.

A. Schenk, **C. Grimmer**, M. Perchthaler, B. E. Pichler, V. Hacker, Development of Platinum Cobalt Co-Catalysts for HT-PEM Fuel Cells. Advanced Studies of Polymer Electrolyte Fuel Cells (2013), S. 152–153.

B. E. Pichler, A. Schenk, **C. Grimmer**, M. Perchthaler, V. Hacker, Manufacture and Stability Enhancement of Platinum Nickel Co-Catalysts for HT-PEM Fuel Cells. Advanced Studies of Polymer Electrolyte Fuel Cells (2013), S. 144–145.

C. Grimmer, A. Schenk, M. Perchthaler, A. Stadlhofer, V. Hacker, Platinum-Cobalt Catalysts for the Oxygen Reduction Reaction in HT PEMFCs. Advanced Studies of Polymer Electrolyte Fuel Cells - 5th International Summer School (2012), S. 162–163.

A. Schenk, M. Perchthaler, A. Stadlhofer, **C. Grimmer**, V. Hacker, Platinum-Cobalt Catalysts for the Oxygen Reduction Reaction in HT PEMFCs. CARISMA (2012), S. 86–86.

7.3 Presentations

C. Grimmer, R. Zacharias, M. Grandi, V. Hacker, Electrochemical Oxidation of Borohydride for Direct Fuel Cells. 228th Meeting of the Electrochemical Society, Phoenix, USA, 11.10.2015.

C. Grimmer, T. Friedrich, D. Woisetschläger, N. Mayer, R. Kalb, M. Koncar, V. Hacker, Borohydride based Ionic Liquids as novel Hydrogen Storage Technology. European Fuel Cell Forum, Lucerne, Switzerland, 30.06.2015.

C. Grimmer, M. Grandi, J. Senn, R. Zacharias, T. Friedrich, V. Hacker, Liquid Hydrogen Carrier Technology based on Ionic Liquids. Minisymposium Verfahrenstechnik, Vienna, Austria, 14.04.2015.

T. Friedrich, **C. Grimmer**, V. Hacker, CEET research Activities on Portable FC Applications. IEA AFC Implementing Agreemnet Annex 35 Meeting, Oldenburg, Germany, 16.09.2015.

T. Friedrich, **C. Grimmer**, V. Hacker, CEET Research Activities on Portable Applications - Borohydride H2 Storage System. IEA AFC Annex 27 Meeting, Messina, Italy, 11.09.2014.

T. Friedrich, **C. Grimmer**, D. Woisetschläger, N. Mayer, M. Koncar, V. Hacker, Organische Borhydride als Wasserstoffspeicher - Rezyklierung des Speichermediums. ProcessNet Jahrestagung, Aachen, Germany, 01.10.2014.

T. Friedrich, **C. Grimmer**, D. Woisetschläger, N. Mayer, M. Koncar, R. Kalb, V. Hacker, V. Ionic Liquid Borohydrides - A Liquid Phase Chemical Hydrogen Storage Material. 14th International Symposium on Metal-Hydrogen Systems, Manchester, England, 23.07.2014.

C. Grimmer, A. Schenk, V. Hacker, PtCo Cocatalysts for HT PEM Fuel Cells. IEA Annex 22 Spring Meeting 2013, Stockholm, Sweden, 16.05.2013.

C. Grimmer, A. Schenk, V. Hacker, Manufacturing and Stabilization of PtCo/C Cocatalysts for PEM Fuel Cells. 15th Austrian Chemistry Days, Graz, Austria, 23.09.2013.

C. Grimmer, A. Schenk, V. Hacker, Manufacturing and Stabilization of PtCo/C Cocatalysts for PEM Fuel Cells. 224th Meeting of the Electrochemical Society, San Francisco, USA, 27.10.2013.

V. Hacker, S. Weinberger, **C. Grimmer**, Stack online monitoring and development of hydrogen storage material. IEA AFC, Annex 22 Meeting, Tokyo, Japan, 11.12.2013.

V. Hacker, A. Hofer, M. Bodner, **C. Grimmer**, A. Schenk, Pt-free Direct Ethanol Fuel Cells. 8th A3PS Conference Eco-Mobility 2013, Vienna, Austria, 03.10.2013.

A. Schenk, **C. Grimmer**, V. Hacker, Developement of Catalysts for the HT PEM Fuel Cell. IEA Annex 22 Fall Workshop 2012. Espoo, Finland, 29.11.2012.

C. Grimmer, T. Wrodnigg, A. Stütz, A Novel Glycosidaseinhibitor: N-(Dansylamino)hexylaminocarbonylpentyl-1,5-dideoxy-1,5-imino-l-iditol. 15th Glycoworkshop, Graz, Austria, 15.02.2011.

7.4 Poster

C. Grimmer, A. Schenk, B. E. Pichler, M. Perchthaler, V. Hacker, Development of a PtCo/C catalyst manufacturing and stabilization method. European Fuel Cell Forum, Lucerne, Switzerland, 30.06.2015.

C. Grimmer, R. Zacharias, M. Grandi, V. Hacker, A mechanistic Study of Palladium as Anode Catalyst for Direct Borohydride Fuel Cells. 8th International Summer School on Advanced Studies of Polymer Electrolyte Fuel Cells, Yokohama, Japan, 30.08.2015.

J. Senn, **C. Grimmer**, S. Nestl, V. Hacker, Real-time quantification method for hydrogen. 8th International Summer School on Advanced Studies of Polymer Electrolyte Fuel Cells. Yokohama, Japan, 31.08.2015.

R. Zacharias, **C. Grimmer**, M. Grandi, J. Senn, V. Hacker, Hydrolysis in direct borohydride fuel cells. 8th International Summer School on Advanced Studies of Polymer Electrolyte Fuel Cells, Yokohama, Japan, 30.08.2015.

M. Grandi, **C. Grimmer**, R. Zacharias, J. Senn, V. Hacker, Synthesis and characterisation of carbon supported bimetallic Platinum-Gold-Nanoparticles for Borohydride Direct Oxidation. 8th International Summer School on advanced studies of Polymer Electrolyte Fuel Cells. Yokohama, Japan, 31.08.2015.

I. Kaltenböck, A. Schenk, **C. Grimmer**, B. E. Pichler, V. Hacker, Active and stable oxygen reduction catalysts for the high temperature Polymer electrolyte fuel cell. 8th International Summer School on Advanced Studies of Polymer Electrolyte Fuel Cells, Yokohama, Japan, 30.08.2015.

B. Cermenek, R. Zacharias, M. Grandi, **C. Grimmer**, A. Schenk, V. Hacker, Palladium based electrocatalysts for ethanol oxidation reaction in alkaline medium. 8th International Summer School on Advanced Studies of Polymer Electrolyte Fuel Cells, Yokohama, Japan, 02.09.2015.

C. Grimmer, T. Friedrich, D. Woisetschläger, N. Mayer, R. Kalb, M. Koncar, V. Hacker, Novel Borohydride based Ionic Liquids as Hydrogen Carrier. ProcessNet Jahrestagung, Aachen, Germany, 30.09.2014.

C. Grimmer, T. Friedrich, D. Woisetschläger, N. Mayer, M. Koncar, R. Kalb, V. Hacker, Borohydride based Ionic Liquids as Hydrogen and Energy Carrier. 10. Minisymposium Verfahrenstechnik, Vienna, Austria, 17.06.2014.

C. Grimmer, M. Grandi, J. Senn, T. Friedrich, V. Hacker, Novel ionic liquids based on borohydrides for hydrogen and energy storage. 7th International Summer School on Advanced Studies of Polymer Electrolyte Fuel Cells, Graz, Austria, 09.09.2014.

J. Senn, **C. Grimmer**, M. Grandi, T. Friedrich, V. Hacker, Comparison of different nickel foams as catalyst support for hydrogen release of borohydride based liquid storage systems. 7th International Summer School on Advanced Studies of Polymer Electrolyte Fuel Cells, Graz, Austria, 08.09.2014.

A. Schenk, **C. Grimmer**, M. Perchthaler, B.E. Pichler, V. Hacker, Platinum Cobalt Catalysts for the High Temperature PEFC. 7th International Summer School on Advanced Studies on Polymer Electrolyte Fuel Cells, Graz, Austria, 08.09.2014.

T. Friedrich, **C. Grimmer**, D. Woisetschläger, N. Mayer, M. Koncar, R. Kalb, V. Hacker, Ionic Liquid Borohydrides - A Liquid Phase Hydrogen Carrier. 10. Minisymposium Verfahrenstechnik, Vienna, Austria, 17.06.2014.

T. Friedrich, **C. Grimmer**, D. Woisetschläger, N. Mayer, M. Koncar, R. Kalb, V. Hacker, Ionic liquid borohydrides - Recycling of the storage medium. 7th International Summer School on Advanced Studies of Polymer Electrolyte Fuel Cells, Graz, Austria, 09.09.2014.

B.E. Pichler, A. Schenk, **C. Grimmer**, M. Perchthaler, V. Hacker, Synthesis of Platinum-Iron/Carbon Catalysts for the Oxygen Reduction Reaction in High-Temperature PEFC. 7th International Summer School on Advanced Studies on Polymer Electrolyte Fuel Cells, Graz, Austria, 08.09.2014.

C. Grimmer, A. Schenk, B.E. Pichler, M. Perchthaler, V. Hacker, Activity of Platinum First Row Transition Metal PtM/C Cocatalysts. 6th International Summer School on Advanced Studies of Polymer Electrolyte Fuel Cells, Yokohama, Japan, 28.08.2013.

A. Schenk, **C. Grimmer**, M. Perchthaler, B.E. Pichler, A. Stadlhofer, V. Hacker, Influences on the Stability of Platinum Cobalt Catalysts for the High Temperature PEM Fuel Cells. 6th International Conference on Polymer Batteries and Fuel Cells, Ulm, Germany, 02.06.2013

A. Schenk, **C. Grimmer**, B.E. Pichler, M. Perchthaler, V. Hacker, Platinum Cobalt Co-Catalysts for the High Temperature Proton Exchange Membrane Fuel Cell. 15th Austrian Chemistry Days, Graz, Austria, 23.09.2013.

A. Schenk, **C. Grimmer**, M. Perchthaler, B.E. Pichler, V. Hacker, Developement of Platinum Cobalt Co-Catalysts for HT-PEM Fuel Cells. 6th International Summer School on Advanced Studies of Polymer Electrolyte Fuel Cells, Yokohama, Japan, 28.08.2013.

A. Schenk, **C. Grimmer**, M. Perchthaler, A. Stadlhofer, V. Hacker, Activity and Stability Enhancement of Platinum- Cobalt Catalysts for High Temperature PEM Fuel Cells. 9. Minisymposium der Verfahrenstechnik, Leoben, Austria, 17.04.2013.

B.E. Pichler, A. Schenk, **C. Grimmer**, M. Perchthaler, V. Hacker, Manufacture and Stability Enhancement of Platinum Nickel Co-Catalysts for HT-PEM Fuel Cells. 6th International Summer School on Advanced Studies of Polymer Electrolyte Fuel Cells, Yokohama, Japan, 25.08.2013.

B.E. Pichler, A. Schenk, **C. Grimmer**, M. Perchthaler, V. Hacker, Platinum Nickel Co-Catalysts for the Oxygen Reduction Reaction on PEM Fuel Cells. 15th Austrian Chemistry Days, Graz, Austria, 23.09.2013

C. Grimmer, A. Schenk, M. Perchthaler, A. Stadlhofer, V. Hacker, Platinum-Cobalt Catalysts for the Oxygen Reduction Reaction in HT PEMFCs. 5th International Summer School on Advanced Studies of Polymer Electrolyte Fuel Cells, Graz, Austria, 03.09.2012.

A. Schenk, **C. Grimmer**, M. Perchthaler, A. Stadlhofer, V. Hacker, Platinum-Cobalt Catalysts for the Oxygen Reduction Reaction in HT PEMFCs. 3rd CARISMA International Conference on Medium and High Temperature Proton Exchange Membrane Fuel Cells, Copenhagen, Denmark, 03.09.2012.

A. Schenk, **C. Grimmer**, M. Perchthaler, A. Stadlhofer, V. Hacker, Stable and Active ORR Catalysts for HT PEMFCs. 63rd Annual Meeting of the International Society of Electrochemistry, Prague, Czech Republic, 21.08.2012.

A. Schenk, **C. Grimmer**, A. Stadlhofer, V. Hacker, Katalysatorentwicklung für Hochtemperatur-Polymerelektrolytmembran-Brennstoffzellen. 7th A3PS Conference - ECO-MOBILITY 2012. Vienna, Austria 11.12.2012.

C. Grimmer, T. Wrodnigg, Synthesis of N-(Dansylamino)hexyl-aminocarbonylpentyl-1,5-dideoxy-1,5-imino-L-iditol. 14th Austrian Chemistry Days, Linz, Austria, 26.09.2011.

C. Grimmer, A. Stütz, T. Wrodnigg, A novel glycosidase inhibitor: N-(dansylamino)hexylamino-carbonylpentyl-1,5-didesoxy-1,5-imino-L-iditol. Einsteins in the City 2011. New York City, USA, 13.04.2011.

8 ABBREVIATIONS

AFC	Alkaline fuel cell
BOL	Begin of lifetime
BOR	Borohydride oxidation reaction
DBFC	Direct borohydride fuel cell
DMMor	4,4-dimetyl-morpholin-4-ium
HHV	Higher heating value
HTAEM	High temperature anion exchange membrane
HRR	Hydrogen release reaction
LHV	Lower heating value
LOC	Liquid organic compound
MCFC	Molton carbonate fuel cell
METMA	2-methoxy-N,N,N-trimethylethan-ammonium
PAFC	Phosphoric acid fuel cell
PEMFC	Polymer electrolyte membrane fuel cell Or: Proton exchange membrane fuel cell
RHE	Reversible hydrogen electrode
rpm	Revolutions per minute
SEM	Scanning electron microscopy
SHE	Standard hydrogen electrode
SOFC	Solid oxide fuel cell
TMPA	N,N,N-trimethylpropan-2-ammonium

9 REFERENCES

[1] I.E. Agency, World Energy Outlook 2010, 2010.

[2] IPCC, Climate Change 2013 - The Physical Science Basis, Fifth Asse, Cambrigde University Press, 2013.

[3] M. Höök, in:, J. Blanco (Ed.), Clim. Chang. - Res. Technol. Adapt. Mitig., 2011.

[4] K. Ota, A. Ishihara, K. Matsuzawa, S. Mitsushima, Electrochemistry 78 (2010) 970.

[5] S. Mitsushima, T. Araki, K. Ota, V. Hacker, M. Siebenhofer, Advanced Studies of Polymer Electrolyte Fuel Cells - 8th International Summer School 2015, 2015.

[6] M. V. Lototskyy, M.W. Davids, I. Tolj, Y. V. Klochko, B.S. Sekhar, S. Chidziva, F. Smith, D. Swanepoel, B.G. Pollet, Int. J. Hydrogen Energy 40 (2015) 11491.

[7] U.B. Demirci, P. Miele, Energy Environ. Sci. 2 (2009) 627.

[8] J.K. Ali, A. Baiker, Appl. Catal. A Gen. 155 (1997) 41.

[9] Y. Okada, E. Sasaki, E. Watanabe, S. Hyodo, H. Nishijima, Int. J. Hydrogen Energy 31 (2006) 1348.

[10] B. Müller, K. Müller, D. Teichmann, W. Arlt, Chemie-Ingenieur-Technik 83 (2011) 2002.

[11] Y. Wang, K.S. Chen, J. Mishler, S.C. Cho, X.C. Adroher, Appl. Energy 88 (2011) 981.

[12] W.R. Grove, London Edinburgh Philos. Mag. J. Sci. (1838).

[13] W.R. Grove, Philos. Mag. J. Sci. XIV (1839) 127.

[14] G. Merle, M. Wessling, K. Nijmeijer, J. Memb. Sci. 377 (2011) 1.

[15] E. Gülzow, J. Power Sources 61 (1996) 99.

[16] K. Kordesch, in:, W. Mitchell (Ed.), Chem. Technol., 1963, pp. 329–370.

[17] G. McLean, Int. J. Hydrogen Energy 27 (2002) 507.

[18] R. Bashyam, P. Zelenay, Nature 443 (2006) 63.

[19] K.V. Kordesch, Hydrazine Fuel Cell with Acrylic Acid Polymer Membrane, US3595698 A, 1971.

[20] M.Z.F. Kamarudin, S.K. Kamarudin, M.S. Masdar, W.R.W. Daud, Int. J. Hydrogen Energy 38 (2013) 9438.

[21] J.C.M. Silva, S.G. da Silva, R.F.B. De Souza, G.S. Buzzo, E. V. Spinacé, A.O. Neto, M.H.M.T. Assumpção, Appl. Catal. A Gen. 490 (2015) 133.

[22] J. Ma, N.A. Choudhury, Y. Sahai, Renew. Sustain. Energy Rev. 14 (2010) 183.

[23] V. Hacker, S. Mitsushima, in:, Adv. Stud. Polym. Electrolyte Fuel Cells - 5th Int. Summer Sch., 2012, pp. 20–24.

[24] P. Atkins, J. de Paula, Physical Chemistry, Oxford University Press, New York, 2002.

[25] S.C. Amendola, M. Binder, S.L. Sharp-Goldman, M.T. Kelly, P.J. Petillo, System for Hydrogen Generation, US 6,534,033 B1, 2003.

[26] Y. Bai, C. Wu, F. Wu, B. Yi, Mater. Lett. 60 (2006) 2236.

[27] Ç. Çakanyıldırım, M. Gürü, Int. J. Hydrogen Energy 33 (2008) 4634.

[28] C. Cento, P. Gislon, P.P. Prosini, Int. J. Hydrogen Energy 34 (2009) 4551.

[29] H.-B. Dai, Y. Liang, P. Wang, H.-M. Cheng, J. Power Sources 177 (2008) 17.

[30] J.C. Ingersoll, N. Mani, J.C. Thenmozhiyal, a. Muthaiah, J. Power Sources 173 (2007) 450.

[31] S.U. Jeong, E. a. Cho, S.W. Nam, I.H. Oh, U.H. Jung, S.H. Kim, Int. J. Hydrogen Energy 32 (2007) 1749.

[32] P. Krishnan, S. Advani, a Prasad, Int. J. Hydrogen Energy 33 (2008) 7095.

[33] J. Lee, K.Y. Kong, C.R. Jung, E. Cho, S.P. Yoon, J. Han, T.-G. Lee, S.W. Nam, Catal. Today 120 (2007) 305.

[34] J. Liang, Y. Li, Y. Huang, J. Yang, H. Tang, Z. Wei, P.K. Shen, Int. J. Hydrogen Energy 33 (2008) 4048.

[35] Y. Liang, P. Wang, H.-B. Dai, J. Alloys Compd. 491 (2010) 359.

[36] B. Liu, Q. Li, Int. J. Hydrogen Energy 33 (2008) 7385.

[37] N. Malvadkar, S. Park, M. Urquidi-MacDonald, H. Wang, M.C. Demirel, J. Power Sources 182 (2008) 323.

[38] Ö. Metin, S. Özkar, J. Mol. Catal. A Chem. 295 (2008) 39.

[39] S.S. Muir, X. Yao, Int. J. Hydrogen Energy 36 (2011) 5983.

[40] R. Retnamma, A.Q. Novais, C.M. Rangel, Int. J. Hydrogen Energy 36 (2011) 9772.

[41] S. Suda, Y.-M. Sun, B.-H. Liu, Y. Zhou, S. Morimitsu, K. Arai, N. Tsukamoto, M. Uchida, Y. Candra, Z.-P. Li, Appl. Phys. A Mater. Sci. Process. 72 (2001) 209.

[42] H. Tian, Q. Guo, D. Xu, J. Power Sources 195 (2010) 2136.

[43] J.C. Walter, A. Zurawski, D. Montgomery, M. Thornburg, S. Revankar, J. Power Sources 179 (2008) 335.

[44] C. Wu, F. Wu, Y. Bai, B. Yi, H. Zhang, Mater. Lett. 59 (2005) 1748.

[45] C. Wu, H. Zhang, B. Yi, Catal. Today 93-95 (2004) 477.

[46] D. Xu, P. Dai, Q. Guo, X. Yue, Int. J. Hydrogen Energy 33 (2008) 7371.

[47] D. Xu, P. Dai, X. Liu, C. Cao, Q. Guo, J. Power Sources 182 (2008) 616.

[48] D. Xu, H. Zhang, W. Ye, Catal. Commun. 8 (2007) 1767.

[49] J. Zhao, H. Ma, J. Chen, Int. J. Hydrogen Energy 32 (2007) 4711.

[50] R. Kalb, Method of Use of an Ionic Liquid for Storing Hydrogen, WO 2010/081657 A1, 2010.

[51] R. Kalb, A. Kraynov, Use of an Ionic Liquid for Storing Hydrogen, WO 2013/113452 A1, 2013.

[52] Prokopcikas, A. Salkauskiene, Russ. J. Phys. Chem. A 44 (1970) 2941.

[53] J. Yamamoto, The Sodium Borohydride Digest, 2003.

[54] E.L. Gyenge, C.W. Oloman, J. Appl. Electrochem. 28 (1998) 1147.

[55] J. McLafferty, S. Colominas, D.D. Macdonald, Electrochim. Acta 56 (2010) 108.

[56] D.M.F. Santos, C. a. C. Sequeira, Int. J. Hydrogen Energy 35 (2010) 9851.

[57] J. Zhang, T. Fisher, J. Gore, D. Hazra, P. Ramachandran, Int. J. Hydrogen Energy 31 (2006) 2292.

[58] L. V Gurvich, I. V Veyts, C.B. Alcock, Thermodynamic Properties of Individual Substances, Vol. 3, Fourth Edi, 1994.

[59] W.M. Haynes, CRC Handbook of Chemistry & Physics, 91st ed., 2010.

[60] C.H. Hamann, V. Wolf, Elektrochemie, 2005.

[61] K.A. Holbrook, J. Twist, J. Chem. Soc. (1971) 890.

[62] Y. Kojima, K. Suzuki, K. Fukumoto, M. Sasaki, T. Yamamoto, Y. Kawai, H. Hayashi, Int. J. Hydrogen Energy 27 (2002) 1029.

[63] Z. Liu, B. Guo, S.H. Chan, E.H. Tang, L. Hong, J. Power Sources 176 (2008) 306.

[64] V.I. Simagina, P.A. Storozhenko, O. V. Netskina, O. V. Komova, G. V. Odegova, T.Y. Samoilenko, G.A. Gentsler, Kinet. Catal. 48 (2007) 168.

[65] H. Dai, Y. Liang, P. Wang, X. Yao, T. Rufford, M. Lu, H. Cheng, Int. J. Hydrogen Energy 33 (2008) 4405.

[66] D.A. Finkelstein, N.D. Mota, J.L. Cohen, H.D. Abruna, J. Phys. Chem. C 113 (2009) 19700.

[67] E. Gyenge, Electrochim. Acta 49 (2004) 965.

[68] Z.P. Li, B.H. Liu, K. Arai, S. Suda, J. Alloys Compd. 404-406 (2005) 648.

[69] B.H. Liu, J.Q. Yang, Z.P. Li, Int. J. Hydrogen Energy 34 (2009) 9436.

[70] J.Q. Yang, B.H. Liu, S. Wu, J. Power Sources 194 (2009) 824.

[71] I. Merino-Jiménez, C. Ponce de León, A.A. Shah, F.C. Walsh, J. Power Sources 219 (2012) 339.

[72] A. Aziznia, C.W. Oloman, E.L. Gyenge, J. Power Sources 212 (2012) 154.

[73] A. Serov, A. Aziznia, P.H. Benhangi, K. Artyushkova, P. Atanassov, E. Gyenge, J. Mater. Chem. A 1 (2013) 14384.

[74] S. Nestl, G. Voitic, M. Lammer, B. Marius, J. Wagner, V. Hacker, J. Power Sources 280 (2015) 57.

[75] C. Grimmer, S. Nestl, J. Senn, V. Hacker, Int. J. Hydrogen Energy 40 (2015) 2055.

[76] C. Grimmer, R. Zacharias, M. Grandi, B. Cermenek, A. Schenk, S. Weinberger, F. Mautner, B. Bitschnau, V. Hacker, J. Phys. Chem. C 119 (2015) 23839.

[77] C. Grimmer, M. Grandi, R. Zacharias, B. Cermenek, H. Weber, C. Morais, T.W. Napporn, S. Weinberger, A. Schenk, V. Hacker, Appl. Catal. B Environ. 180 (2016) 614.

[78] C. Grimmer, R. Zacharias, M. Grandi, B. Pichler, I. Kaltenboeck, F. Gebetsroither, J. Wagner, B. Cermenek, S. Weinberger, A. Schenk, V. Hacker, J. Electrochem. Soc. 163 (2016) F278.

[79] D.R. Kim, K.W. Cho, Y. Il Choi, C.J. Park, Int. J. Hydrogen Energy 34 (2009) 2622.

[80] J.H. Kim, K.T. Kim, Y.M. Kang, H.S. Kim, M.S. Song, Y.J. Lee, P.S. Lee, J.Y. Lee, J. Alloys Compd. 379 (2004) 222.

[81] A.J. Bard, L.R. Faulkner, Electrochemical Methods - Fundamentals and Applications, 2000.

[82] K.J.J. Mayrhofer, D. Strmcnik, B.B. Blizanac, V. Stamenkovic, M. Arenz, N.M. Markovic, Electrochim. Acta 53 (2008) 3181.

[83] Y. Garsany, I.L. Singer, K.E. Swider-Lyons, J. Electroanal. Chem. 662 (2011) 396.

[84] Y. Garsany, O. a Baturina, K.E. Swider-Lyons, S.S. Kocha, Anal. Chem. 82 (2010) 6321.

[85] M.T. Reetz, M. Lopez, Method for in Situ Immobilization of Water-Soluble Nanodispersed Metal Oxide Colloids, WO2003078056, 2003.

[86] R.M. Piasentin, E.V. Spinacé, M.M. Tusi, A.O. Neto, Int. J. Electrochem. Sci. 6 (2011) 2255.

[87] G. Behmenyar, A.N. Akın, J. Power Sources 249 (2014) 239.

[88] M. Chatenet, M.B. Molina-Concha, N. El-Kissi, G. Parrour, J.-P. Diard, Electrochim. Acta 54 (2009) 4426.

[89] M. Chatenet, F.H.B. Lima, E.A. Ticianelli, J. Electrochem. Soc. 157 (2010) B697.

[90] M. Chatenet, F. Micoud, I. Roche, E. Chainet, Electrochim. Acta 51 (2006) 5459.

[91] B.M. Concha, M. Chatenet, Electrochim. Acta 54 (2009) 6119.

[92] B.M. Concha, M. Chatenet, Electrochim. Acta 54 (2009) 6130.

[93] B.M. Concha, M. Chatenet, F. Maillard, E.A. Ticianelli, F.H.B. Lima, R.B. de Lima, Phys. Chem. Chem. Phys. 12 (2010) 11507.

[94] B.M. Concha, M. Chatenet, C. Coutanceau, F. Hahn, Electrochem. Commun. 11 (2009) 223.

[95] B.M. Concha, M. Chatenet, E.A. Ticianelli, F.H.B. Lima, J. Phys. Chem. C 115 (2011) 12439.

[96] J. Datta, A. Dutta, S. Mukherjee, J. Phys. Chem. C 115 (2011) 15324.

[97] U.B. Demirci, J. Power Sources 172 (2007) 676.

[98] H. Dong, R. Feng, X. Ai, Y. Cao, H. Yang, C. Cha, J. Phys. Chem. B 109 (2005) 10896.

[99] D. Duan, S. Liu, Y. Sun, J. Power Sources 210 (2012) 198.

[100] R.X. Feng, H. Dong, Y.D. Wang, X.P. Ai, Y.L. Cao, H.X. Yang, Electrochem. Commun. 7 (2005) 449.

[101] K.S. Freitas, B.M. Concha, E.A. Ticianelli, M. Chatenet, Catal. Today 170 (2011) 110.

[102] X. Geng, H. Zhang, W. Ye, Y. Ma, H. Zhong, J. Power Sources 185 (2008) 627.

[103] E. Gyenge, V. Lam, Osmium Anode for Direct Borohydride Fuel Cells and Batteries, CA 2778688, 2013.

[104] P. He, X. Wang, Y. Liu, X. Liu, L. Yi, Int. J. Hydrogen Energy 37 (2012) 11984.

[105] P. He, Y. Wang, X. Wang, F. Pei, H. Wang, L. Liu, L. Yi, J. Power Sources 196 (2011) 1042.

[106] M. Indig, R. Snyder, J. Electrochem. Soc. 109 (1962) 1104.

[107] P.I. Iotov, S. V. Kalcheva, A.M. Bond, Electrochim. Acta 54 (2009) 7236.

[108] R. Jamard, A. Latour, J. Salomon, P. Capron, A. Martinent-Beaumont, J. Power Sources 176 (2008) 287.

[109] K. Ke, K. Hiroshima, Y. Kamitaka, T. Hatanaka, Y. Morimoto, Electrochim. Acta 72 (2012) 120.

[110] P. Krishnan, T.-H. Yang, S.G. Advani, A.K. Prasad, J. Power Sources 182 (2008) 106.

[111] Z.P. Li, B.H. Liu, J.K. Zhu, S. Suda, J. Power Sources 163 (2006) 555.

[112] F.H.B. Lima, A.M. Pasqualeti, M.B. Molina Concha, M. Chatenet, E.A. Ticianelli, Electrochim. Acta 84 (2012) 202.

[113] B.H. Liu, Z.P. Li, J.K. Zhu, S. Suda, J. Power Sources 183 (2008) 151.

[114] B.H. Liu, Z.P. Li, S. Suda, Electrochim. Acta 49 (2004) 3097.

[115] J.I. Martins, M.C. Nunes, J. Power Sources 175 (2008) 244.

[116] J.I. Martins, M.C. Nunes, R. Koch, L. Martins, M. Bazzaoui, Electrochim. Acta 52 (2007) 6443.

[117] I. Merino-Jimenez, M.J. Janik, C. Ponce de Leon, F.C. Walsh, J. Power Sources 269 (2014) 498.

[118] M. Mirkin, H. Yang, A. Bard, J. Electrochem. Soc. 139 (1992) 2212.

[119] J.H. Morris, H.J. Gysling, D. Reed, Chem. Rev. 85 (1985) 51.

[120] L.C. Nagle, J.F. Rohan, Int. J. Hydrogen Energy 36 (2011) 10319.

[121] C. Ponce de León, a. Kulak, S. Williams, I. Merino-Jiménez, F.C. Walsh, Catal. Today 170 (2011) 148.

[122] Y. Sahai, J. Ma, Energy Procedia 14 (2012) 358.

[123] D.M.F. Santos, P.G. Saturnino, D. Macciò, a. Saccone, C. a. C. Sequeira, Catal. Today 170 (2011) 134.

[124] D.M.F. Santos, C. a. C. Sequeira, Electrochim. Acta 55 (2010) 6775.

[125] D.M.F. Santos, P.G. Saturnino, R.F.M. Lobo, C. a. C. Sequeira, J. Power Sources 208 (2012) 131.

[126] B. Šljukić, J. Milikić, D.M.F. Santos, C.A.C. Sequeira, Electrochim. Acta 107 (2013) 577.

[127] A. Tegou, S. Papadimitriou, I. Mintsouli, Catal. Today 170 (2011) 126.

[128] S. Treimer, A. Tang, D.C. Johnson, Electroanalysis 14 (2002) 165.

[129] A. Verma, A.K. Jha, S. Basu, J. Power Sources 141 (2005) 30.

[130] K. Wang, J. Lu, L. Zhuang, Catal. Today 170 (2011) 99.

[131] M. Zhiani, I. Mohammadi, N. Salehi, RSC Adv. 5 (2015) 23635.

10 PEER-REVIEWED JOURNAL ARTICLES

C. Grimmer, M. Grandi, R. Zacharias, B. Cermenek, H. Weber, C. Morais, et al., *The electrooxidation of borohydride: A mechanistic study on palladium (Pd/C) applying RRDE , 11B-NMR and FTIR*, Appl. Catal. B Environ. 180 (**2016**) 614–621

C. Grimmer, R. Zacharias, M. Grandi, B. Pichler, I. Kaltenboeck, F. Gebetsroither, J. Wagner, B. Cermenek, S. Weinberger, A. Schenk, V. Hacker, *A membrane-free and practical mixed electrolyte direct borohydride fuel cell*, J. Electrochem. Soc. 163 (3) (**2016**) F278-F283

C. Grimmer, R. Zacharias, M. Grandi, B. Cermenek, A. Schenk, S. Weinberger, et al., *Carbon Supported Ruthenium as Anode Catalyst for Alkaline Direct Borohydride Fuel Cells*, J. Phys. Chem. C. 119 (**2015**) 23839–23844

C. Grimmer, S. Nestl, J. Senn, V. Hacker*, Selective real-time quantification of hydrogen within mixtures of gases via an electrochemical method*, Int. J. Hydrogen Energy. 40 (**2015**) 2055–2061

Applied Catalysis B: Environmental 180 (2016) 614–621

Contents lists available at ScienceDirect

Applied Catalysis B: Environmental

journal homepage: www.elsevier.com/locate/apcatb

The electrooxidation of borohydride: A mechanistic study on palladium (Pd/C) applying RRDE, ^{11}B-NMR and FTIR

Christoph Grimmer[a,*], Maximilian Grandi[a], Robert Zacharias[a], Bernd Cermenek[a], Hansjörg Weber[b], Cláudia Morais[c], Têko W. Napporn[c], Stephan Weinberger[a], Alexander Schenk[a], Viktor Hacker[a]

[a] Institute of Chemical Engineering and Environmental Technology, Fuel Cell Systems Group, Graz University of Technology, NAWI Graz, Inffeldgasse 25C, 8010 Graz, Austria
[b] Institute of Organic Chemistry, Graz University of Technology, NAWI Graz, Stremayrgasse 9, 8010 Graz, Austria
[c] IC2MP, Université de Poitiers, 4, Rue Michel Brunet-B27 TSA-51106, 86073 Poitiers Cedex 09, France

ARTICLE INFO

Article history:
Received 1 June 2015
Received in revised form 9 July 2015
Accepted 18 July 2015
Available online 23 July 2015

Keywords:
Electrochemical borohydride oxidation
Palladium catalyst
NMR spectroscopy
FTIR measurements

ABSTRACT

Electrochemical borohydride oxidation reaction, intermediates and reaction products are studied by cyclic voltammetry with rotating disk electrodes, chronoamperometry coupled with ^{11}B NMR spectroscopy and in-situ FTIR measurements. Depending on the electrode potential of a Pd/C catalyst on a rotating disk electrode the number of exchanged electrons varies between four and eight. By employing chronoamperometry the boron species are analyzed during the ongoing reaction with NMR. During all experiments no boron products other than BO_2^- are detected. Incomplete borohydride consumption during the chronoamperometry studies show that the palladium surface is poisoned by an intermediate in the low potential region. In-situ FTIR measurements confirmed that there is no interaction with BH_2-species which are acting as catalyst poison.

1. Introduction

Direct borohydride fuel cells (DBFCs) are of great interest especially for portable applications due to the capability of borohydride anion BH_4^- to deliver up to 8 electrons per molecule at very low potentials of −1.24 V vs. SHE [1]. Sodium borohydride ($NaBH_4$) was first proposed as anodic fuel in 1962, pointing out the benefits of high storage density and long-term stability in alkaline solution [2]. In combination with an oxygen electrode an overall cell voltage of 1.64 V according to the cell Reaction (3) can be obtained [3].

$$BH_4^- + 8OH^- \rightarrow BO_2^- + 6H_2O + 8e^- E^0 = -1.24\,V vs.SHE \quad (1)$$

$$O_2 + 2H_2O + 4e^- \rightarrow 4OH^- E^0 = 0.40V vs.SHE \quad (2)$$

$$BH_4^- + 2O_2 \rightarrow BO_2^- + 2H_2O E^0 = 1.64\,V \quad (3)$$

Despite much effort concerning anode catalyst development the promising advantages of the fuel cannot be fully utilized so far. On the one hand this originates from the fact that the reaction potential is a theoretic thermodynamic concept which cannot be reached in practice. On the other hand the complete oxidation Reaction (1) undergoes complex reaction steps depending on the anode material and the electrode potential [1,4,5].

In general catalysts can be divided into hydrolyzing and non-hydrolyzing materials. Catalysts that show high adsorption tendency of hydrogen such as palladium or platinum belong to the first group [5]. The main side reaction, namely the borohydride hydrolysis Reaction (4), is catalyzed by this kind of materials which lowers the coulombic efficiency and can lead to mechanical stress inside the electrode. Comparing palladium with gold anode catalysts, Pd shows better electrocatalytic activity with an onset potential approx. 200 mV lower but as mentioned above exhibits activity toward the hydrolysis side reaction [4,6].

$$BH_4^- + 2H_2O \rightarrow BO_2^- + 4H_2 \quad (4)$$

There is little literature concerning the reaction mechanism on palladium but several authors assume similar reaction steps to platinum catalysts [7–9]. The hydrolysis is reported to undergo a

* Corresponding author. Fax: +43 316 873 8782.
E-mail addresses: christoph.grimmer@tugraz.at (C. Grimmer), maximilian.grandi@student.tugraz.at (M. Grandi), robert.zacharias@student.tugraz.at (R. Zacharias), bernd.cermenek@tugraz.at (B. Cermenek), hansjoerg.weber@tugraz.at (H. Weber), claudia.gomes.de.morais@univ-poitiers.fr (C. Morais), teko.napporn@univ-poitiers.fr (T.W. Napporn), stephan.weinberger@tugraz.at (S. Weinberger), alexander.schenk@tugraz.at (A. Schenk), viktor.hacker@tugraz.at (V. Hacker).

http://dx.doi.org/10.1016/j.apcatb.2015.07.028
0926-3373/

stepwise reaction on platinum and compete with the electrooxidation. Such a CE mechanism (chemical reaction followed by electrochemical reaction) is reported by Gyenge (Reactions 5 and 6) while the product can further undergo electrooxidation yielding 6 electrons (7), hydrolysis reaction (8) or a combination of both (see Reactions 9 and 10) [1,7,10]:

$$BH_4^- + H_2O \rightarrow BH_3(OH)^- + H_2(C) \quad (5)$$

$$(E)H_2 + 2OH^- \rightarrow 2H_2O + 2e^- \quad (6)$$

$$(E)BH_3(OH)^- + 6OH^- \rightarrow B(OH)_4^- + 3H_2O + 6e^- \quad (7)$$

$$BH_3(OH)^- + 3H_2O \rightarrow B(OH)_4^- + 3H_2(C) \quad (8)$$

$$BH_3OH^- + 3OH^- \rightarrow B(OH)_4^- + 3/2H_2 + 2H_2O + 3e^- \quad (9)$$

$$BH_4^- + xOH^- \rightarrow BO_2^- + (x\text{-}2)H_2O + (4\text{-}1/2x)H_2 + xe^- \quad (10)$$

Yang et al. assume a 4 electron pathway on palladium based on their electrochemical experiments combined with the quantification of gaseous hydrogen (see Reactions 11–13) [9]. The resulting adsorbed hydrogen atoms (reaction 11) can either react electrochemically forming water or chemically forming hydrogen.

$$BH_4^- + 4OH^- \rightarrow BO_2^- + 2H_2O + 4H_{ad} + 4e^- \quad (11)$$

$$H_{ad} + OH^- \rightarrow H_2O + e^- \quad (12)$$

$$H_{ad} + H_{ad} \rightarrow H_2 \quad (13)$$

One of the most widely investigated catalysts is platinum in form of nanodispersed Pt/C as well as in bulk form. Based on electrochemical and kinetic studies Elder and Hickling proposed the following reaction mechanism on platinum with the rate determining step being Reaction (16) [11]:

$$BH_4^- + Pt \leftrightarrow Pt\cdots BH_3 + H^+ + 2e^- \quad (14)$$

$$Pt\cdots BH_3 + OH^- \rightarrow Pt\cdots BH_3OH^- \quad (15)$$

$$Pt\cdots BH_3OH^- \rightarrow Pt\cdots BH_2OH + H^+ + 2e^- \quad (16)$$

$$Pt\cdots BH_2OH + H_2O \rightarrow Pt + BH_2(OH)_2^- + H^+ \quad (17)$$

$$Pt\cdots BH_3OH^- + H_2O \rightarrow Pt + BH_{22}^- + H_2(OH) \quad (18)$$

$$BH_{22}^- + H_2O \rightarrow BH(OH)_3^- + H_2(OH) \quad (19)$$

$$(20)BH_3^- \rightarrow H_2BO_3^- + H_2(OH)$$

According to this reaction sequence there should be at least two reaction intermediates present in the bulk electrolyte, namely $BH_2(OH)_2^-$ and $BH(OH)_3^-$.

Concha et al. investigated the reaction mechanism on bulk platinum employing FTIR techniques [12].

They concluded that the potential range can be divided in four regions; first close to ocp – mainly heterogeneous hydrolysis; second 180–700 mV vs. RHE – formation of BH_3 and BH_2-species; third 700–1100 mV vs. RHE – BO_2 final product is detected; fourth above 1100 mV vs. RHE– BH_2-species decrease. In general they found the rate limiting step to be related to the consumption of BH_2-species contradicting the proposition of Elder and Hickling [11–13]. According to their proposed mechanistic steps similar intermediates namely $BH_2(OH)_2^-$ and BH_2OH should be found in the bulk electrolyte.

Employing Levich and Koutecky-Levich analyses the number of exchanged electrons was investigated with results ranging from 2 to 8 electrons for platinum [4,5,14–17]. Based on these electron counts various mechanisms and intermediates were reported. Furthermore, influences on the mechanisms of electrode morphology and concentration ratios are reported [14,18]. The anodic reactions observed during measurements are even more complicated due to electrooxidation of hydrogen that is evolved by parallel hydrolysis. While reaction intermediates are widely investigated for platinum catalysts utilizing online electrochemical mass spectrometry [19] and FTIR [20,21] there is little comparable data for Pd/C available.

Freitas et al. reported a strong effect of the thickness of the active layer on the electron count. Complete 8 electron oxidation is obtained for 3 μm thick layers while only three electrons are released at layers as thin as 0.38 μm. A smooth platinum surface only yields 2 electrons. Comparable to oxygen reduction reaction it is considered that in thicker layers the intermediates including hydrogen from hydrolysis are trapped and undergo further electrooxidation [14].

As reported by several researchers and can be seen intuitively from the Reaction Eq. (1) the reaction mechanism also strongly depends on the hydroxide concentration or more precisely the concentration ratio $[OH^-]/[BH_4^-]$ [9,18,22]. Liu et al. found a ratio of 5 or higher to be necessary for a complete 8 electron oxidation on gold Au/C and silver Ag/C catalysts and only a 3 electron exchanging mechanism for a ratio of 1 [18].

As can be seen from the short overview above the reaction mechanism is quite complex and still not completely resolved. For further development of anode materials a better understanding of the electrochemical pathway and its influences is necessary. One major aspect that is still not resolved is the aspect of reaction products that are yielded during non-optimal electrooxidation with less than 8 electrons.

To the authors' knowledge there is little information about reaction intermediates in the bulk electrolyte published in literature. One main question remains: is metaborate (BO_2^-) the only product while hydrogen is lost or are there intermediates that can undergo further electrooxidation? Following proposed mechanisms there can be at least two intermediates expected, namely $BH_2(OH)_2^-$ and $BH(OH)_3^-$.

In this paper we present electrochemical experiments on palladium catalysts with subsequent analysis of the reaction products and/or intermediates by ^{11}B nuclear magnetic resonance (NMR) spectroscopy and mechanism studies by in-situ FTIR spectroelectrochemical measurements.

2. Experimental

2.1. Catalyst preparation

Carbon supported palladium nanoparticles (40 wt.% Pd) were synthesized using the instant reduction method [23,24]. For this purpose the proper amount of $PdCl_2$ was dissolved in 20 ml of 0.5 M HCl. In a round bottom flask the appropriate amount of Vulcan XC72R (CABOT) was suspended in a 50/50 mixture of water/2-propanol via ultrasonification for 30 min. To the homogeneous dispersion, the $PdCl_2$ solution was added. The pH was adjusted to 9–10 by adding 1 M NaOH drop wise under vigorous stirring. After heating to 60 °C the mixture was stirred for 5 h before the suspension was saturated with hydrogen. The temperature and the H_2 atmosphere were maintained for another 6 h. The resulting dispersion was filtered and the remaining catalyst was washed several times with ultrapure water and dried overnight at 90 °C.

2.2. Physical characterization

Transition electron microscope experiments are performed using a TF20 TEM (FEI), Schottky cathode, operated at 200 kV equipped with an EDAX Si(Li) detector for EDX acquisition. An aliquot of the Pd/C catalyst was dispersed in an appropriate amount of isopropanol and mounted on standard Cu grids which are covered with perforated carbon film. TEM imaging experiments are conducted at room temperature.

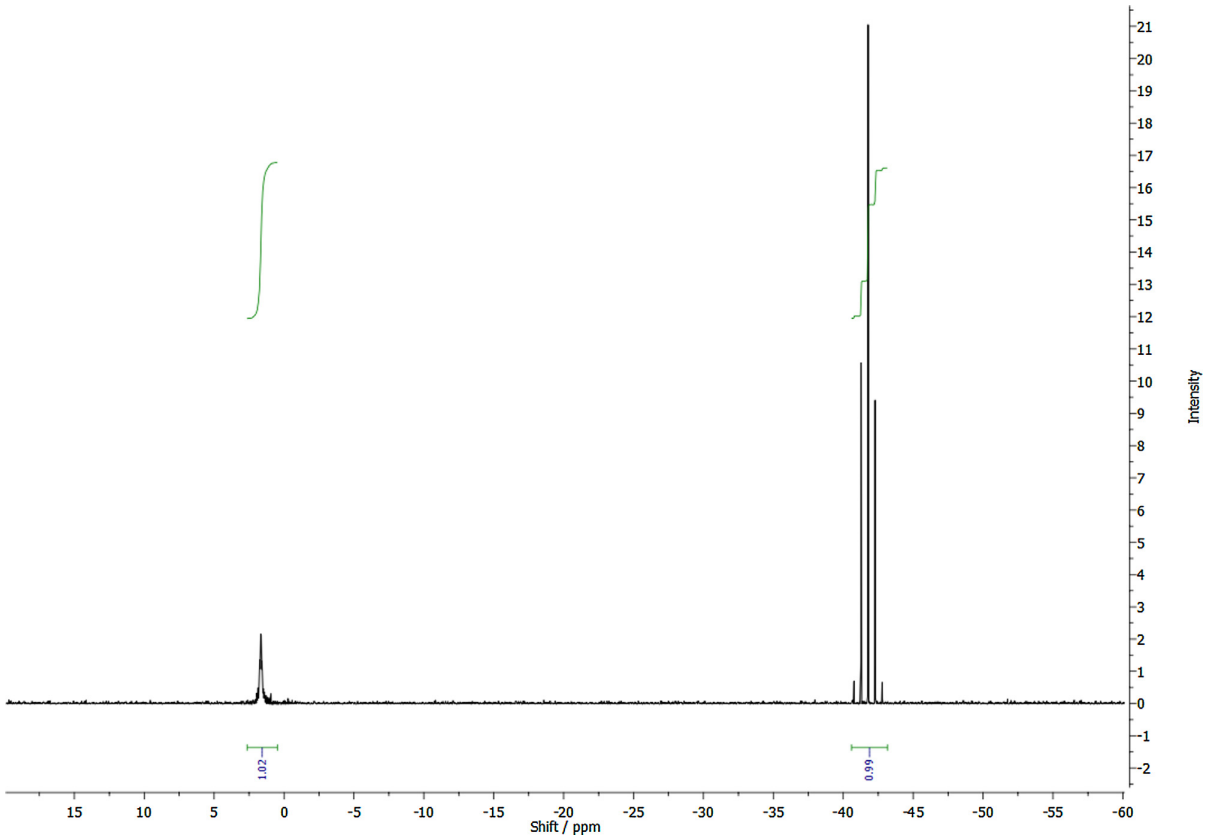

Fig. 1. ^{11}B NMR experiment of an equimolar solution of $NaBH_4$ and $NaBO_2$ in 1 M NaOH with 20%vol. D_2O.

2.3. Electrochemical measurements

The electrochemical measurements were performed with a Gamry Instruments Reference 600 potentiostat (supplied by C3 Analysentechnik, Germany) employing a glassy carbon (GC) rotating disk electrode (RDE) from Pine Industries with a geometric surface area of 0.196 cm^2 in a three electrode configuration. The rotating ring disk electrode (RRDE) consisted of a GC disk (0.247 cm^2) and a Pt ring (collection efficiency 37%, E7R9 series from Pine Industries). The measurement cell temperature was kept at 30 °C. The glassy carbon RDE was polished prior to each measurement to a mirror finish with alumina microsuspension (0.05 μm). A reversible hydrogen electrode (RHE) (gaskatel) and a glassy carbon rod (Metrohm) were used as reference electrode and counter electrode, respectively.

In order to prepare a homogeneous catalyst film the catalyst sample was dispersed in a mixture of 2-propanol/water (7:3), ultrasonificated for 30 min and an aliquot of 10 μl was dispensed on the RDE resulting in a metal loading of 28 μg cm^{-2}. The RDE was rotated at 700 rpm during dry off ensuring a homogeneous and reproducible catalyst layer [25].

The electrolyte consisted of 1 M NaOH (Fixanal, Fluka Analytical) prepared of ultrapure water (18.2 MΩ cm) that was purged with nitrogen for 30 min prior to each measurement.

The catalyst was cycled between 0.05 V to 1.20 V vs. RHE at a scan rate of 50 mV s^{-1} until stable cycles were obtained. Cyclic voltammograms of the Pd/C (40 wt.%) catalysts were recorded between 0.05 V and 1.30 V at a scan rate of 10 mV s^{-1} to determine the electrochemically active surface area (ECSA) by integrating the Pd-O reduction peak considering 405 μC cm^{-2} as conversion factor [26]. RDE and RRDE measurements were carried out after adding $NaBH_4$ with a total concentration of 5 mM at various rotation rates in the potential range of −0.05–1.60 V vs. RHE. The number of exchanged electrons was determined by Levich and Koutecky-Levich analyses [27]. RRDE experiments are conducted at 1600 rpm with fixed ring potentials and cyclic voltammetry on the disk with a scan rate of 10 mV s^{-1}.

At this point we want to stretch out that RDE experiments allow proper insight into catalytic properties of a material. However, the influences of the electrode structure and morphology etc. are not addressed by this technique [28,29].

2.4. Chronoamperometry and NMR measurements

In order to follow the change of the concentration of boron species chronoamperometric measurements were carried out in the same setup at fixed potentials of 0.40 V and 0.80 V vs. RHE with a rotation rate of 1600 rpm. The electrolyte consisted of 1 M NaOH with a starting concentration of $NaBH_4$ of 5 mM. During the measurement samples of 0.40 ml were taken from the electrolyte, 0.10 ml D_2O were added and the NMR measurement was performed instantly.

^{11}B NMR spectra were acquired on a Varian/Agilent 500 MHz Spectrometer tuned to ^{11}B at 160.38 MHz. 64 Scans were accumulated for both 1H-decoupled (Waltz Decoupling 499.87 MHz) and coupled spectra. A 45 degree pulse was used with a relaxation delay of 1 s and 1.022 s acquisition time. Data processing consisted of cutting the first 8 data points, Fourier transform, an automated baseline correction and phase correction by square of the magnitude.

The boron shifts of BH_4^- and BO_2^- and the corresponding integrals of both peaks are verified by measuring an equimolar solution

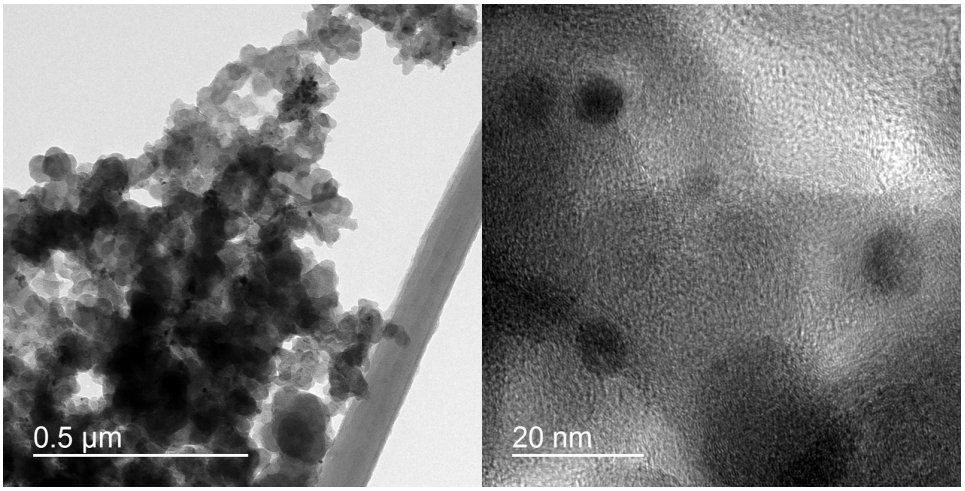

Fig. 2. TEM images of of Pd/C electrocatalyst; left: overview, right: detail view of single particles.

(2.5 mM each, see Fig. 1). We observed matching literature shifts for BO_2^- at 1.65 ppm as singlet and for BH_4^- at −41.8 ppm as quintet [30]. The coulombic efficiency is determined as a ratio of the electric charge of the corresponding experiment to the amount of borohydride considering complete 8 electron oxidation.

2.5. In-situ FTIR measurements

In-situ FTIR measurements were carried out using a Bruker IFS 66 v spectrometer which was modified for beam reflection on the electrode surface at a 65° incidence angle. A 10^{-6} bar vacuum was maintained in order to avoid interferences from atmospheric water and CO_2. The detector was a liquid nitrogen cooled MCT (HgCdTe) type. The spectral resolution was 8 cm^{-1} and the spectra were recorded in the region of 800–4000 cm^{-1}. A three-electrode spectroelectrochemical cell, fitted at the bottom with a mid-infrared (MIR) transparent window (CaF_2) was used. The counter electrode was a glassy carbon electrode, the working electrode was a glassy carbon disk (8 mm diameter) and a RHE was used as reference electrode. To minimize the absorption of the infrared beam by the solution, the working electrode was pressed against the window, resulting in a thin layer of electrolytic solution. A Chronoamperometry/FTIRS study at 0.20, 0.40, 0.60 and 0.80 V vs. RHE, each 40 min, with acquisition of spectra every 5 min, was performed. IR spectra were calculated in terms of changes in the reflectivity (R) relative to a reference single-beam spectrum (R_{ref}) as follows: $(\Delta R/R)_i = (R_i - R_{ref})/R_{ref}$. Positive and negative bands represent the decrease and increase of species, respectively. The deposition of catalyst on the glassy carbon disk, previously polished to a mirror finish, was performed by pipetting 5 µL of a catalyst ink containing 1.68 mg ml^{-1} of Pd. All measurements were performed in 0.1 M NaOH + 50 mM $NaBH_4$ electrolyte.

3. Results and discussion

3.1. TEM images

Transition electron microscopy images show homogeneous dispersed nanoparticles of Pd on carbon substrate material (see Fig. 2). The determined mean particle size is 7.3 ± 1.4 nm which is within the expected scope compared to the electrochemically determined ECSA. EDX analysis confirmed the elemental composition within the inaccuracies especially concerning the quantification of carbon.

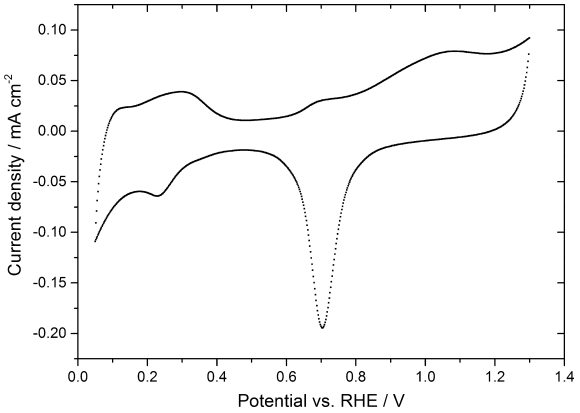

Fig. 3. Cyclic voltammograms of Pd/C in deaerated 1 M NaOH at a scan rate of 10 mV s^{-1}.

3.2. Electrochemical measurements

3.2.1. Cyclic voltammetry

Fig. 3 shows a typical result of cyclic voltammetry experiments of Pd/C in deaerated electrolyte. A well-defined reduction peak of Pd-O is observed with a charge of 422 µC originating from an electrochemical active surface area of 190 cm^2 mg^{-1} Pd. In Fig. 4 a typical cyclic voltammogram with 5 mM $NaBH_4$ in the electrolyte is shown. The anodic sweep exhibits three peaks which can be ascribed to hydrogen oxidation (around 5 mV), direct oxidation of BH_3OH^- which is generated by hydrolysis at 300 mV and direct 8-electron oxidation of borohydride with a broad shoulder starting at 0.80 V [31]. The cathodic sweep shows also three oxidation peaks which can be ascribed to the oxidation of intermediates, which are formed during ongoing hydrolysis and that are adsorbed on the catalyst surface [1].

3.2.2. RDE and RRDE experiments

RDE experiments were conducted at rotations rates up to 2000 rpm. Anodic sweeps of a typical experiment are shown in Fig. 5. As confirmed by Levich analysis (insert) two diffusion limited oxidation regions are observed at around 0.40 V vs. RHE and 0.80 V vs. RHE. Considering 1.67×10^{-5} cm^2 s^{-1} as diffusion coefficient and 0.0114 cm^2 s^{-1} as kinematic viscosity Levich analysis gives a 4-electron oxidation at 0.40 V vs. RHE and an 8-electron oxidation

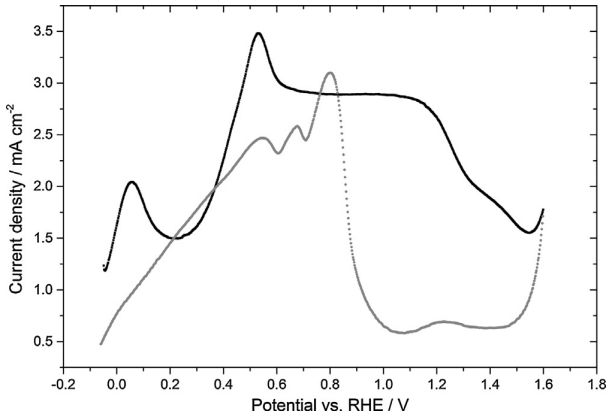

Fig. 4. Cyclic voltammograms of Pd/C in 1 M NaOH containing 5 mM borohydride (black: anodic sweep, gray: cathodic sweep).

at 0.80 V vs. RHE [4,32]. We observed a complete electrooxidation at 0.80 V vs. RHE while at 0.40 V vs. RHE there are two possible pathways: first a complete reaction to BO_2^- releasing 2 hydrogen molecules (see reaction 21) or second a 4-electron electrooxidation resulting in BH_2-species (see Reaction 22). The Levich plot at 0.80 V vs. RHE intercepts at almost zero while the linearization at 0.40 V vs. RHE has a positive value of approx. 3 mA cm^{-2}. The positive intercept indicates also a kinetic limitation at low potentials suggesting adsorbed intermediates.

If the BH_2-species is present either adsorbed on the catalyst surface or in solution is part of the discussion in section 3.3 and 3.4.

$$BH_4^- + 4OH^- \rightarrow BO_2^- + 2H_2O + 2H_2 + 4e^- \quad (21)$$

$$BH_4^- + 4OH^- \rightarrow BH_2(OH)_2^- + 2H_2O + 4e^- \quad (22)$$

For further investigations of the catalytic behavior RRDE experiments were conducted. The reaction mechanism following proposed Reaction (21) would show a hydrogen oxidation at the ring above 0.00 V vs. RHE while Reaction (22) should show oxidation currents only at higher ring potentials. In case of Reaction (21) the evolved hydrogen could be further oxidized in an intelligent three dimensional electrode architecture [14,28]. At thin films on RDEs hydrogen bubbles are swiped away and lost.

The ring current at 0.30 V vs. RHE is below 1.0 mA cm^{-2} and shows the oxidation of hydrogen that evolves during the measurement. At a potential of 0.55 V vs. RHE borohydride is completely oxidized on the metallic platinum ring. The maximum ring current density is about 13 mA cm^{-2} and corresponds the expected value for the given collection efficiency of 37%. The observed current between 0.20 V and 0.80 V vs. RHE and the low current from hydrogen evolution suggest Reaction (22) with adsorbed BH_2-species in the low potential range Fig. 6.

3.3. Chronoamperometry coupled with ^{11}B NMR

Based on the results of RDE and RRDE experiments chronoamperometry measurements were carried out at 0.40 V (4 electron oxidation) and 0.80 V (8 electron oxidation). The experiments were done employing RDEs at a rotation rate of 1600 rpm with subsequent analysis of boron species in the electrolyte by ^{11}B NMR. Based on previous published mechanisms (see discussion above) a reaction intermediate, most likely $BH_2(OH)_2^-$, or the reaction product BO_2^- is expected during oxidation at 0.40 V vs. RHE (see Reactions 21 and 22). A signal for BH_2-species in the NMR spectra would confirm Reaction 22.

Fig. 7 shows the results from chronoamperometry measurements including NMR results. No intermediate could be observed throughout the whole measurement. The current decreases to zero after only three hours although borohydride is still available in the electrolyte (concentration 4.6 mM according to NMR integrals). We conclude that reaction 16 is indeed rate-limiting at 0.40 V vs. RHE but reaction 17 does not occur on Pd at this potential. Most likely Reaction 22 is taking place without desorption of the product $BH_2(OH)_2^-$.

We assume that BH_2^--species adsorb on the surface blocking it for further electrooxidation. By integration of the current an electrical charge of 6.98 C is obtained giving a coulombic efficiency of 97.9% compared with borohydride concentration from NMR (see Table 1).

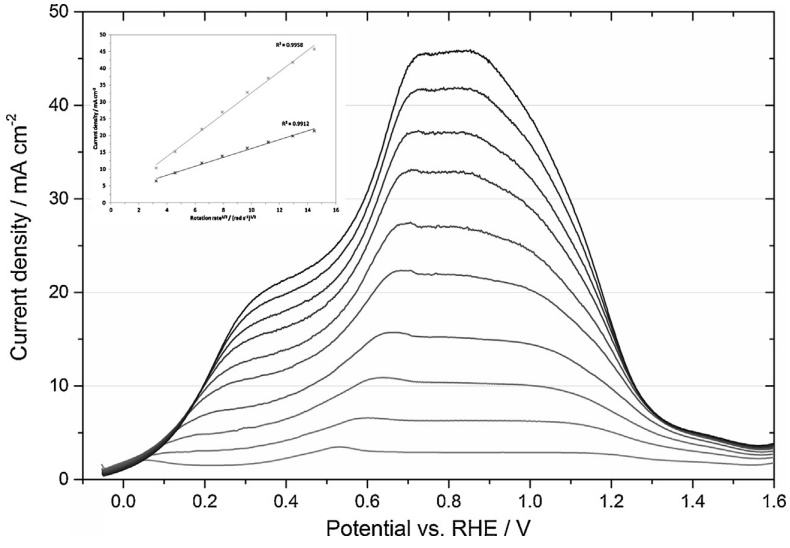

Fig. 5. Anodic sweeps of RDE experiments at 0, 50, 100, 200, 400, 600, 900, 1200, 1600 and 2000 rpm with a scan rate of 10 mV s^{-1} (5 mM $NaBH_4$); insert: according Levich plot at 0.40 V and 0.80 V.

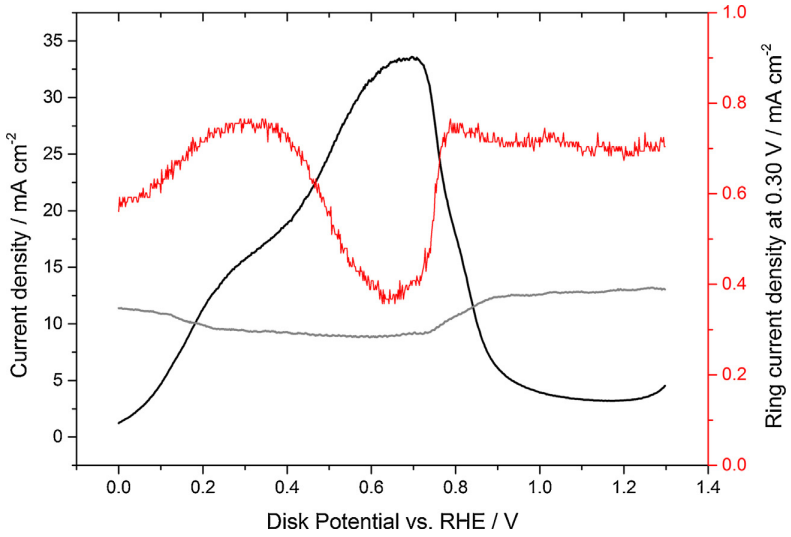

Fig. 6. RRDE experiments at 1600 rpm with a scan rate of 10 mV s^{-1} at the disk and two ring potentials: disk current density (black), ring current density at 0.55 V vs. RHE (gray) and ring current density at 0.30 V vs. RHE (red, secondary axis). (For interpretation of the references to colour in this figure legend, the reader is referred to the web version of this article.)

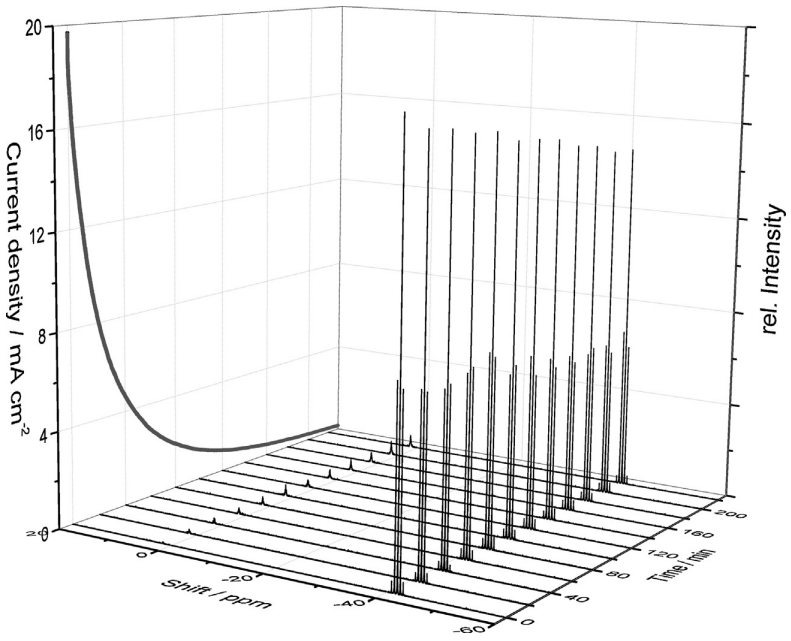

Fig. 7. Chronoamperometry at 0.40 V coupled with subsequent NMR measurements; left *z*-axis: current density of electrochemical measurement; *x*-axis: shift of ^{11}B NMR; *y*-axis: time; right *z*-axis: intensity of NMR signals.

Table 1
Borohydride concentrations before and after chronoamperometric study (by NMR integrals), electric charge obtained by chronoamperometry and coulombic efficiency.

	Start concentration [BH_4^-]	End concentration [BH_4^-]	Charge (Chronoamperometry)	Coulombic efficiency
Low potential	5.0 mM	4.6 mM	6.98 C	97.9%
High potential	5.0 mM	0.0 mM	52.17 C	54.1%

At high potentials the chronoamperometric investigation shows a complete conversion of BH_4^- to BO_2^- (see Fig. 8). Samples for NMR analysis are taken after the current declined 25, 50, 75 and 100%. The decrease of the current with ongoing reaction fits the decreasing concentration of BH_4^- in the electrolyte very well. After the reaction time of 11 h a coulombic efficiency of only 54.1% is observed. As reported for platinum based catalysts the activity toward hydrolysis is increasing with increasing potentials [33]. The adsorbed species seems to poison both reactions, the electrochemical oxidation and the heterogeneous hydrolysis reaction at 0.40 V vs. RHE.

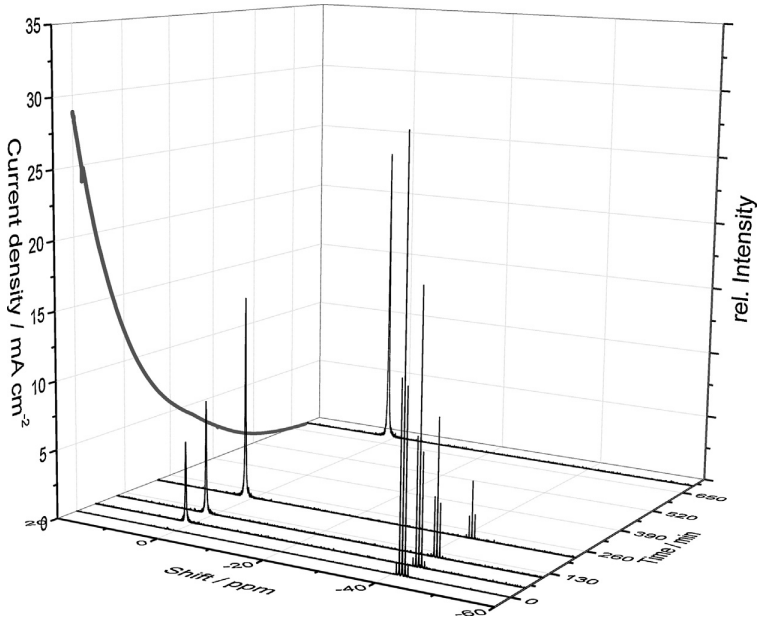

Fig. 8. Chronoamperometry at 0.80 V coupled with subsequent NMR measurements; left *z*-axis: current density of electrochemical measurement; *x*-axis: shift of ^{11}B NMR; *y*-axis: time; right *z*-axis: intensity of NMR signals.

Table 2
IR bands of boron species associated with electrochemical borohydride oxidation [12,20,21].

Bandcm^{-1}	Species
973	BH_2
1102	BH_4
1175	BH_3
1650	H_2O deformation
2268	BH_4

3.4. In-situ FTIR measurements

In Table 2 the corresponding IR bands which are used for the interpretation of the results are summarized [12,20,21]. At this point we want to draw attention to the fact that IR bands from electrochemical in-situ IR measurements are influenced by the catalysts' surface [12]. However, the obtained results can be referred to previous published results for platinum based catalysts.

Fig. 9 shows the results of in-situ FTIR measurements from chronoamperometry measurements at various potentials. The absorption bands at the potentials above 0.40 V vs. RHE show similar patterns with the only difference being the intensities. The band at 973 cm^{-1} has been assigned to electrochemical interactions of BH_2 species with the catalysts' surface and is observed at potentials above 0.40 V vs. RHE. A strong adsorption of a species shifts the IR signal and is therefore not observed at these wavenumbers. Since this band cannot be found at 0.20 V vs. RHE these species cannot be further oxidized on palladium at this potential which is also confirmed by RDE measurements. Positive bands at 1102 cm^{-1} and 2268 cm^{-1} correspond to borohydride and indicate its trans-

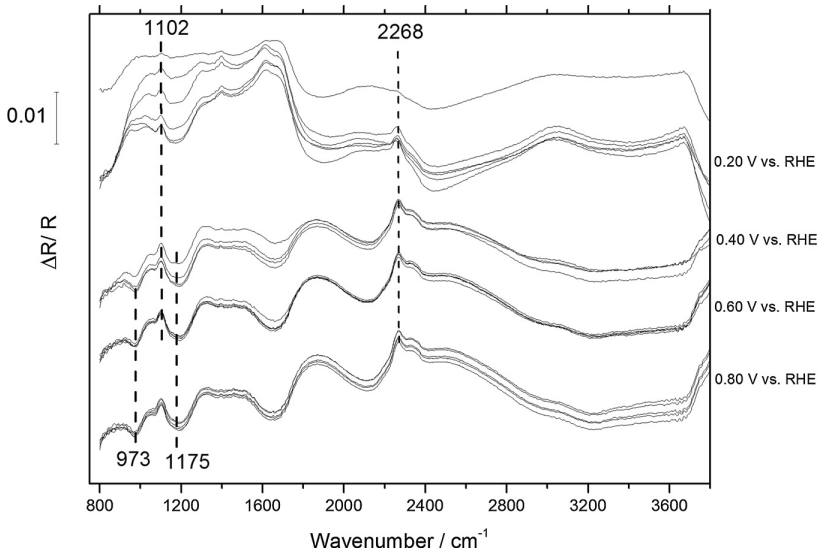

Fig. 9. In-situ FTIR measurement of chronoamperometry at various potentials at Pd/C catalyst, several measurements for each potential taken every 5 min.

formation which starts at very low potential values. At 1175 cm^{-1} a raising negative peak is found at 0.20 V vs. RHE indicating interactions with BH_3-species, which is also present in high potential measurements. In the low potential regime palladium interacts with BH_4^-- and BH_3-species (according Reactions (14) and (16)) resulting in a four electron transfer. In the higher potential regime also BH_2-interactions are detected giving a complete eight electron transfer. The broad negative band at 1650 cm^{-1} is assigned to water deformation indicating the catalytic activity of the hydrolysis reaction especially at elevated potentials, which is also observed by bubble formation during all electrochemical measurements.

Although the potential regimes do not fit perfectly we found a rate-determining step associated with BH_2-species comparable to platinum based catalysts [11]. The shift in potential is attributed to changed electrolyte concentrations which are necessary for the various measurement techniques we employed for our investigations.

4. Conclusion

By the so-called "instant method" palladium nanoparticles with a mean diameter of 7.3 nm were synthesized on carbon support material. RDE measurements and corresponding Levich and Koutecky-Levich analysis show unexpected behavior in low as well as in high potential regimes. In the low potential regime (up to 0.40 V vs. RHE) a maximum of four electrons is obtained while a complete eight electron transfer is obtained at higher potentials. By employing a RRDE we assume the main product $BH_2(OH)_2^-$ to be formed in the low potential regime (reaction 22). Using ^{11}B NMR measurements we traced the borohydride species in bulk solution during chronoamperometry measurements at 0.40 V and 0.80 V vs. RHE. In the low potential region the electrochemical oxidation stops although more than 90% of the origin borohydride is left in the bulk electrolyte. An intermediate which cannot be found in the electrolyte seems to poison the catalytic surface at this potential. By in-situ FTIR measurements we followed the BOR on palladium showing that there is no interaction of BH_2-species with palladium at 0.20 V vs. RHE.

Based on our results we conclude that the intermediate Pd · · · BH_2OH is blocking the active sites for further electrooxidation in the low potential region (compare Reaction 16). At elevated potentials this intermediate is further oxidized and a complete eight electron transfer is observed. Considering a DBFC application the intermediate could be removed by stopping the borohydride supply inducing an increase of the anode potential.

Acknowledgements

Financial support by the Austrian Federal Ministry of Science, Research and Economics (BMWFW), the Austrian Research Promotion Agency (FFG, project nr. 840476), the IEA research cooperation and our industry partners VTU engineering and proionic GmbH is gratefully acknowledged.

References

[1] E. Gyenge, Electrochim. Acta 49 (2004) 965.
[2] M. Indig, R. Snyder, J. Electrochem. Soc. 109 (1962) 1104.
[3] L.C. Nagle, J.F. Rohan, Int. J. Hydrogen Energy 36 (2011) 10319.
[4] D. Finkelstein, N. Mota, J. Phys. Chem. C 113 (2009) 19700.
[5] A. Tegou, S. Papadimitriou, I. Mintsouli, Catal. Today 170 (2011) 126.
[6] S.S. Muir, X. Yao, Int. J. Hydrogen Energy 36 (2011) 5983.
[7] B.H. Liu, Z.P. Li, S. Suda, Electrochim. Acta 49 (2004) 3097.
[8] I. Merino-Jimenez, M.J. Janik, C. Ponce de Leon, F.C. Walsh, J. Power Sources 269 (2014) 498.
[9] J.Q. Yang, B.H. Liu, S. Wu, J. Power Sources 194 (2009) 824.
[10] J.I. Martins, M.C. Nunes, J. Power Sources 175 (2008) 244.
[11] J.P. Elder, A. Hickling, Trans. Faraday Soc. 58 (1962) 1852.
[12] B.M. Concha, M. Chatenet, E.A. Ticianelli, F.H.B. Lima, J. Phys. Chem. C 115 (2011) 12439.
[13] F.H.B. Lima, A.M. Pasqualeti, M.B. Molina Concha, M. Chatenet, E.A. Ticianelli, Electrochim. Acta 84 (2012) 202.
[14] K.S. Freitas, B.M. Concha, E.A. Ticianelli, M. Chatenet, Catal. Today 170 (2011) 110.
[15] B.M. Concha, M. Chatenet, Electrochim. Acta 54 (2009) 6119.
[16] B.M. Concha, M. Chatenet, Electrochim. Acta 54 (2009) 6130.
[17] B. Šljukić, J. Milikić, D.M.F. Santos, C.A.C. Sequeira, Electrochim. Acta 107 (2013) 577.
[18] B.H. Liu, J.Q. Yang, Z.P. Li, Int. J. Hydrogen Energy 34 (2009) 9436.
[19] M. Chatenet, F.H.B. Lima, E.A. Ticianelli, J. Electrochem. Soc. 157 (2010) B697.
[20] B.M. Concha, M. Chatenet, C. Coutanceau, F. Hahn, Electrochem. Commun. 11 (2009) 223.
[21] B.M. Concha, M. Chatenet, F. Maillard, E.A. Ticianelli, F.H.B. Lima, R.B. de Lima, Phys. Chem. Chem. Phys. 12 (2010) 11507.
[22] M. Mirkin, H. Yang, A. Bard, J. Electrochem. Soc. 139 (1992) 2212.
[23] M.T. Reetz, M. Lopez, Method for in Situ Immobilization of Water-Soluble Nanodispersed Metal Oxide Colloids, WO2003078056, 2003.
[24] R.M. Piasentin, E.V. Spinacé, M.M. Tusi, A.O. Neto, Int. J. Electrochem. Sci. 6 (2011) 2255.
[25] Y. Garsany, I.L. Singer, K.E. Swider-Lyons, J. Electroanal. Chem. 662 (2011) 396.
[26] J. Datta, A. Dutta, S. Mukherjee, J. Phys. Chem. C 115 (2011) 15324.
[27] S. Treimer, A. Tang, D.C. Johnson, Electroanalysis 14 (2002) 165.
[28] C. Ponce de León, S. Kulak, I. Merino-Jiménez, F.C. Walsh, Catal. Today 170 (2011) 148.
[29] I. Merino-Jiménez, C. Ponce de León, A.A. Shah, F.C. Walsh, J. Power Sources 219 (2012) 339.
[30] A.C. Dunbar, J.E. Gozum, G.S. Girolami, J. Organomet. Chem. 695 (2010) 2804.
[31] G. Behmenyar, A.N. Akın, J. Power Sources 249 (2014) 239.
[32] M. Chatenet, M.B. Molina-Concha, N. El-Kissi, G. Parrour, J.-P. Diard, Electrochim. Acta 54 (2009) 4426.
[33] R. Jamard, A. Latour, J. Salomon, P. Capron, A. Martinent-Beaumont, J. Power Sources 176 (2008) 287.

Journal of The Electrochemical Society, **163** (3) F278-F283 (2016)
0013-4651/2016/163(3)/F278/6/$33.00 © The Electrochemical Society

A Membrane-Free and Practical Mixed Electrolyte Direct Borohydride Fuel Cell

Christoph Grimmer,[a,z] Robert Zacharias,[a] Maximilian Grandi,[a] Birgit Pichler,[a] Ilena Kaltenboeck,[a] Florian Gebetsroither,[a] Julian Wagner,[b] Bernd Cermenek,[a] Stephan Weinberger,[a] Alexander Schenk,[a] and Viktor Hacker[a]

[a]*Institute of Chemical Engineering and Environmental Technology, Fuel Cell Systems Group, NAWI Graz, Graz University of Technology, 8010 Graz, Austria*
[b]*Institute for Electron Microscopy and Nanoanalysis, Graz University of Technology, 8010 Graz, Austria*

A membrane-free direct borohydride fuel cell that is operated with a borohydride containing electrolyte is designed and constructed. Main focus of this study is the cathode catalyst that has to show high tolerance against borohydride. Both catalysts, Ag-Mn_3O_4/C as cathode catalyst and commercial Pt/C as anode catalyst, are characterized electrochemically using a rotating disk electrode. The number of exchanged electrons is calculated employing Levich and Koutecky-Levich analysis. Cathodes are fabricated using a cross rolling method with an in-house made gas diffusion layer. A cell with an implemented Luggin capillary is designed in order to follow the electrode potentials. The BH_4^-/O_2 fuel cell shows a power density of 17 mW cm^{-2} using a 1 M $NaBH_4$/1 M NaOH/5 mM thiourea electrolyte.

Manuscript submitted November 4, 2015; revised manuscript received December 29, 2015. Published January 7, 2016.

In recent years direct liquid fuel cells are gaining more and more interest, due to their big advantage of an easy, save and long-term fuel storage. Another benefit of liquid fuels is the possibility of using existing storage and distribution infrastructure. Besides commercial available direct methanol fuel cells, ethanol and borohydride are potential and promising candidates for future applications.

Borohydride as anodic fuel was first proposed by Indig and Snyder in the 1960s and first catalytic studies with platinum were published by Elder and Hickling.[1,2] The number of publications concerning the direct borohydride fuel cell (DBFC) is strongly increasing since the early 2000s.[3] The main advantages of sodium borohydride as fuel are long-term stability (half-life 426 days at pH 14), high energy density (9.3 Wh g^{-1}), release of up to eight electrons at a potential as low as −1.24 V vs. SHE and the potential usage at ambient condition.[3–6] Reaction 1 gives the borohydride oxidation reaction (BOR) with an electron release of a maximum of eight electrons. In combination with an oxygen electrode the theoretical cell voltage is 1.64 V (see Reaction 2). However, the catalyst material, electrode potential, local pH and the availability of hydroxide and borohydride at the electrode surface (more precisely the ratio of $[OH^-]/[BH_4^-]$) influence the completeness of the oxidation reaction. The general reaction can be formulated as shown in Reaction 3.[7,8]

$$BH_4^- + 8OH^- \rightarrow BO_2^- + 6H_2O + 8e^- \quad E^0 = -1.24V \text{ vs. SHE} \qquad [1]$$

$$BH_4^- + 2O_2 \rightarrow BO_2^- + 4H_2O \quad E^0 = 1.64\ V \qquad [2]$$

$$BH_4^- + xOH^- \rightarrow BO_2^- + (x-2)\,H_2O + (4-1/2x)\,H_2 + xe^- \qquad [3]$$

Most widely investigated DBFC systems consist of anode catalysts based on platinum, gold and nickel in combination with cation or anion exchange membranes.[9] Employing a cation exchange membrane, sodium cations are transported from the anode to the cathode resulting in NaOH at the cathode side. There are two major drawbacks of this approach. First, the concentration ratio of $[OH^-]/[BH_4^-]$ in the fuel has to be at least eight resulting in an unpractical diluted fuel. Second, salt formation occurs at the cathode side that is usually fueled with air, thus clogging the porous structure of the electrode.

Catalysts based on platinum nanoparticles dispersed on high surface area carbon (Pt/C) with highest catalytic activities have the disadvantage of also catalyzing the main side reaction, namely the hydrolysis of $NaBH_4$ releasing gaseous hydrogen (see Reaction 4). By adding thiourea (TU) to the aqueous borohydride fuel the hydrolysis reaction is poisoned on platinum.[10] However, the catalyst poison also influences the electrocatalytic properties toward BH_4^--oxidation of Pt/C.[11]

$$NaBH_4 + 2H_2O \rightarrow NaBO_2 + 4H_2 \qquad [4]$$

Another type of DBFCs is a mixed reactant type fuel cell without membrane.[11] For this type of fuel cell highly selective anode and cathode catalysts are necessary. Power densities of 137 mW cm^{-2} are published for this type of DBFCs.[12,13]

In this paper we present an approach that is known from direct hydrazine fuel cells employing the fuel in a mixture with the electrolyte.[14] Oxygen is supplied via a flow field and a gas diffusion layer, similar to conventional polymer electrolyte fuel cells while borohydride, that is anyway stored in alkaline solution, is supplied as mixed electrolyte. For this kind of fuel cell the cathode needs to show highly selective catalytic properties toward oxygen reduction reaction. This approach overcomes major drawbacks of cation membrane based systems, namely the formation of NaOH at the cathode and the required excess of NaOH in the fuel.

Experimental

Catalyst synthesis and electrode fabrication.—*Anode fabrication.*—Anodes are fabricated with a fixed catalyst loading of 1.0 mg Pt cm^{-2} with a commercial Pt/C catalyst (50 wt% from Alfa Aesar). A homogenous dispersion of catalyst powder and binder (FAA3 ionomer from FumaTech) in 1-propanol is prepared by ultrasonification. Using the drop coating method the appropriate amount of catalyst suspension is coated on a carbon cloth substrate material with a binder content of 20 wt% (based on active material). In an additional step an aqueous solution of ammonium carbonate is drop coated on the electrodes acting as pore former (15 wt% of active material). The as-prepared electrodes are soaked 3 times in 1 M NaOH in order to ensure complete alkalization.

Cathode catalyst and electrode fabrication.—Ag-Mn_3O_4/C cathode catalyst is synthesized employing an impregnation-pyrolysis method with $AgMnO_4$ as precursor.[15,16] The precursor is prepared by mixing equimolar aqueous solutions of $AgNO_3$ and $KMnO_4$ acidified with nitric acid at 80°C. After cooling the solution to 0°C the precipitation (dark blue needles) is filtered and washed with ice water.

An appropriate amount of $AgMnO_4$ is dissolved in a suspension of carbon support (mixture of Cabot Vulcan XC72R and Black Pearls 2000) in ultrapure water at 40–50°C. The suspension is uniformly dispersed using an ultrasonic probe. After slow evaporation of the

[z]E-mail: christoph.grimmer@tugraz.at

solvent at 60°C the dry impregnated carbon is ground and tempered for 2 hours at 400°C in inert atmosphere with a temperature ramp of 5°C min^{-1}.

Cathodes are manufactured by a cross rolling, hot pressing method using PTFE powder (3 M Dyneon, TF 2021Z) as binder. First, gas diffusion layers (GDL) are prepared with acetylene black (Alfa Aesar), PTFE and a nickel mesh as current collector. A slurry containing carbon supported catalyst, PTFE and a mixture of water and 2-propanol as solvent is cross-rolled on the GDL. The electrodes are hot-pressed at 300°C with a pressure of 120 kg cm^{-2} to a final thickness of 0.80 mm and a catalyst loading of 11 mg cm^{-1}.

Structural analysis.—Structural analysis of the cathode is conducted by scanning electron microscopy (SEM) employing a Zeiss Ultra 55. A topographical overview is taken with an Everhart-Thornley-detector (secondary electron detector) at an acceleration voltage of 5 kV. More detailed images at higher magnifications are taken with an in-lens detector (SI) at 15 kV to ensure higher lateral resolution. Additionally backscatter electron images are taken in order to resolve different materials with the so-called AsB (angle selective backscattered) detector from Zeiss. Energy dispersive X-ray spectroscopy (EDS) is conducted to quantify the elemental distribution of silver and manganese.

Ex-situ characterization.—Both electrocatalysts are further investigated by means of cyclic voltammetry employing a rotating disk electrode (RDE). The electrochemical experiments are carried out using a Reference 600 (bi-)potentiostat (Gamry, supplied by C3 Analysentechnik) and a RDE set-up from Pine Instruments Company (AFE5T050GC). The working electrode is a glassy carbon disc electrode of 5 mm fixed diameter, giving an area of 0.196 cm^2. Prior to electrode preparation, the glassy carbon disc is polished to a mirror finish using a 0.05 μm alumina suspension (MasterPrep, Buehler). The glassware is cleaned in sulfuric acid solution, followed by heating and rinsing with ultrapure water to remove sulfate residues.

In order to prepare homogeneous thin films on the RDE suspensions of the catalyst samples in a mixture of water and 2-propanol (ratio 3:7) are prepared and treated with an ultrasonic probe. 10 μl of the suspension are transferred to the electrode while it is rotated at a speed of 700 rpm during dry off.[17] The catalyst loading is set to 28 μg Pt cm^{-2} and 56 μg Ag-Mn_3O_4 cm^{-2} according to the suggested criteria by Mayrhofer et al.[18] All ex-situ experiments are conducted in temperature controlled glassware at 30°C.

The electrolytes, 1 M NaOH and 0.1 M KOH (both Fixanal, Fluka Analytical), are prepared with ultrapure water. The electrolyte is saturated with ultrapure nitrogen or oxygen during all electrochemical experiments. A glassy carbon rod was used as counter electrode and the reference electrode was a reversible hydrogen electrode (RHE, Hydroflex, Gaskatel). Hence, all potentials reported here are quoted with respect to RHE and are corrected for ohmic losses unless otherwise stated.

The internal resistance drop is determined by carrying out an impedance measurement at 30 kHz.

The number of electrons and the heterogeneous rate constant k_h are calculated with the Levich (L) and Koutecky – Levich (KL) equations (shown in Eq. 5 and Eq. 6). Calculations of KL analysis is done graphically considering the slope being proportional to the number of exchanged electrons and the intercept to the heterogeneous rate constant.[19]

$$i_l = 0.62 * n * F * A * D_r^{2/3} * \omega^{1/2} * \nu^{-1/6} * C_r \quad [5]$$

$$\frac{1}{i_{kl}} = \frac{1}{0.62 * n * F * A * D_r^{2/3} * \omega^{1/2} * \nu^{-1/6} * C_r} + \frac{1}{n * F * A * k_h * C_r} \quad [6]$$

Table I. Parameter for Levich and Koutecky-Levich analysis.[4,19,20]

	Parameter	Unit	ORR measurements	BOR measurements
F	Faraday constant	C mol^{-1}	96485	96485
A	Area of electrode	cm^2	0.196	0.196
D_r	Diffusion coefficient	cm^2 s^{-1}	$1.9*10^{-5}$	$1.67*10^{-5}$
ω	Rotation rate	rad s^{-1}	-	-
ν	Kinematic viscosity	cm^2 s^{-1}	0.01	0.0114
C_r	Bulk concentration	mol cm^{-3}	$1.10*10^{-6}$	$5.0*10^{-6}$

Potential regions for calculations are confirmed for compatibility by linearity of Levich and Koutecky-Levich plots, respectively. All parameters used for the calculations are given in Table I.[5,20,21]

Anode catalyst.—Prior to the measurements cleaning cycles are performed from 0.05 to 1.30 V vs. RHE at a scan rate of 25 mV s^{-1} until stable cyclic voltammograms (CV) are obtained. A CV of the catalyst is performed under stationary conditions from 0.05 to 1.2 V vs. RHE at a scan rate of 10 mV s^{-1} in order to obtain a CV associated with platinum surface phenomena and to determine the electrochemical active surface area (ECSA). CV scans at rotation rates of 200, 400, 600, 900, 1200, 1600 and 2000 rpm are performed in 1 M NaOH and 5 mM $NaBH_4$ from −0.05 to 1.5 V vs. RHE at scan rate of 10 mV s^{-1}. The number of electrons exchanged and the heterogeneous rate constant are calculated via the L and KL equation as described above.

Cathode catalyst.—Ag-Mn_3O_4/C is characterized as described above using potassium hydroxide (0.1 M) as electrolyte. The electrolyte is saturated with ultrapure oxygen for 20 minutes and oxygen supply is maintained during all measurements to ensure constant oxygen concentration. In order to eliminate all currents not associated to the ORR, the obtained ORR curves are corrected with the CV result measured in N_2 saturated electrolyte. L and KL analysis is applied according to Equations 5 and 6 with the parameters given in Table I.

In-situ cathode characterization.—The as-prepared cathode is installed in an electrode holder with an active area of 2 × 2 cm^2. A Luggin capillary is mounted at a distance of 2 mm to the electrode surface using a RHE. Half-cell measurements are performed with a multichannel BaSyTec CTS (Cell Test System). Synthetic air is supplied at a flow rate of 55 mL min^{-1} and 6 M KOH is used as electrolyte. All measurements are corrected for uncompensated resistances. According to the Pourbaix diagram of manganese Mn_3O_4 is reduced to soluble $Mn(OH)_3^-$ at pH 14 at potentials below approx. 0.70 V vs. RHE. Therefore all electrochemical measurements are conducted above 0.75 V vs. RHE.

After recording the OCP, the electrode is activated by increasing the current until a potential of 0.75 V vs. RHE is reached. Polarization curves are measured potentiostatically from OCP to 0.75 V vs. RHE in 10 mV steps until a stable signal is reached. Additionally long-term operation experiments are conducted for 100 hours at 0.75 V vs. RHE at room temperature.

Single cell tests.—Both electrodes with an active area of 2 × 2 cm^2 are mounted in electron holders which are closed with an EPDM sealing. In order to insert a Luggin capillary the distance between the electrodes is about 5 mm and cannot be reduced for these experiments. Hence, the reported polarization curve is corrected for internal resistance. Stationary polarization curves are recorded galvanostatically using a Zahner IM6 potentiostat recording each current step for

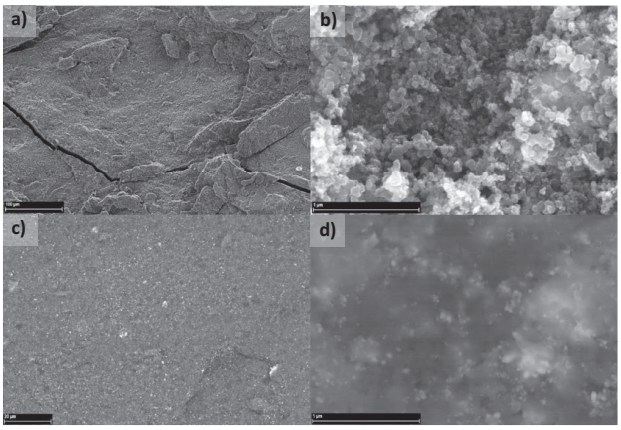

Figure 1. SEM images of a Ag-Mn_3O_4/C cathode: a) surface morphology taken with an Everhart-Thornley-detector; b) detailed view taken with an in-lens detector; c)+d) elemental contrast images taken with an AsB detector.

3 minutes. The mixed electrolyte/fuel was supplied with a flow of 10 ml min^{-1} and consisted of 1 M NaOH, 1 M $NaBH_4$ and 5 mM thiourea. Synthetic air is supplied at the cathode with a flow of 50 ml min^{-1}. The cell was temperature controlled by adjusting the temperature of the electrolyte at 30°C. A RHE is used as reference electrode and all potentials are given with respect to RHE.

Results and Discussion

Structural analysis.—Fig. 1 shows the images of the active layer based on the Ag-Mn_3O_4/C catalyst. The surface morphology consists of a dense structure without any agglomeration. Microcracks are observed in all cathodes originating from the hot pressing step. Although these cracks are omnipresent the mechanical stability of the electrodes is not affected. The top right image of Fig. 1 gives a detailed view of the electrode surface revealing the spherical shape of the carbon support material. The catalyst material is integrated into the carbon support with comparable size distribution.

The images at the bottom of Fig. 1 show back scattered electron images taken with the AsB detector giving information concerning the material distribution. The cathode shows equal distribution of the metals silver and manganese with no obvious agglomeration in the sub µm range. According to the AsB images the size of the catalyst particles is in the range of 30 to 120 nm. The overall metal composition Ag:Mn is 52:48 atomic percent measured by EDX (not shown). As expected carbon, oxygen and fluorine are detected in the cathode.

Ex-situ characterization.—*Anode catalyst.*—A typical CV of a platinum based catalyst in alkaline media is shown in Fig. 2. The

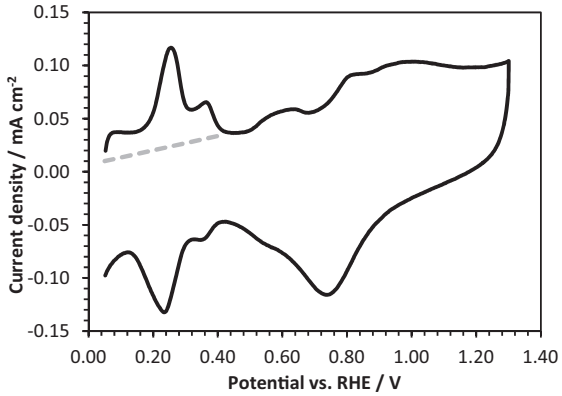

Figure 2. Cyclic voltammogram of commercial Pt/C in alkaline electrolyte (charging current from CO stripping experiments shown as gray dashed line).

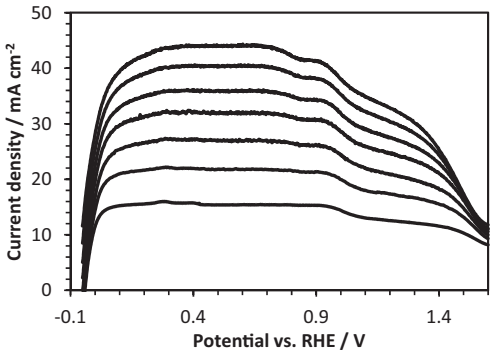

Figure 3. RDE experiments of commercial Pt/C in alkaline electrolyte consisting 5 mM $NaBH_4$ at 200, 400, 600, 900, 1200, 1600 and 2000 rpm.

ECSA from integrating the anodic H_{upd} area is 199 cm^2 mg^{-1} Pt. For proper integration the baseline is selected following the proposed method of Mayrhofer et al. considering the capacitance of the high surface area support.[18] CO stripping measurements reveal the shape of the capacitive current in the H_{upd} region. In general the baseline is not horizontal; it shows a small slope parallel to the capacitive current in the region 0.40 to 0.50 V vs. RHE. The baseline that is used for integration is shown in Fig. 2 as gray dashed line.

The recorded RDE scans and the corresponding L and KL plot are shown in Fig. 3 and Fig. 4. The catalyst shows high activity toward borohydride oxidation reaction at low onset potentials close to the hydrogen evolution potential of 0.00 V vs. RHE. Although the theoretic BOR potential is −0.41 V vs. RHE (at pH 14) anode

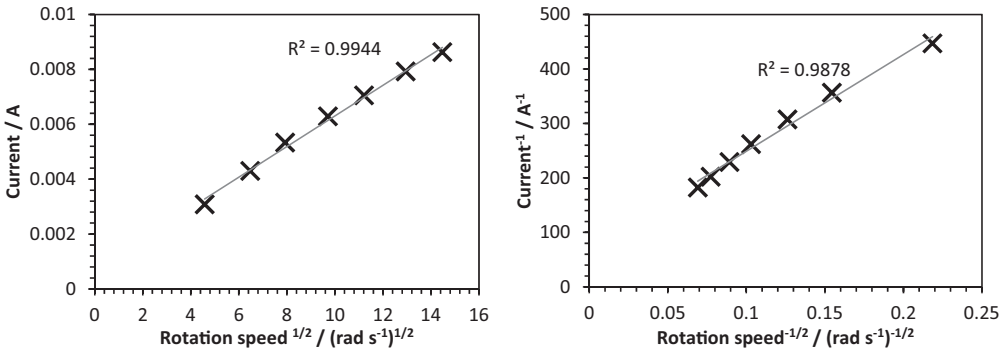

Figure 4. Levich plot of RDE results shown in Fig. 2 at 0.40 V vs. RHE; right: Koutecky-Levich plot at 0.00 V vs. RHE.

Table II. Results from Levich and Koutecky-Levich analysis of anode and cathode catalysts.

Catalyst	Potential V vs. RHE	Levich n	Koutecky-Levich N	Rate constant k_h
Ag-Mn_3O_4/C	0.30	3.91	-	-
	0.72	-	4.22	0.025
	0.74	-	4.30	0.020
	0.76	-	4.51	0.014
Pt/C	0.00	-	6.98	0.021
	0.01	-	7.91	0.020
	0.20	7.74	-	-
	0.40	7.95	-	-

potentials below the hydrogen evolution are not feasible in aqueous solutions.

At elevated potentials platinum surface oxidation is observed and lowers the activity toward BOR until it almost stops at 1.60 V vs. RHE. The low onset potential can be attributed to the hydrolysis of BH_4^- yielding BH_3OH^- and hydrogen. The onset potential of BH_3OH^- oxidation is reported to be more negative than direct BH_4^- oxidation and hydrogen evolution.[10,22] In contradiction to this, Dong et al. attributed the negative onset potential to direct oxidation of BH_4^-.[23] Further mechanistic aspects and details are not discussed at this point. Diffusion limitation and validity of L and KL equations is given by the linearity of the corresponding plots (see Fig. 4). All results from the evaluation are summarized in Table II.

The results of L and KL analysis are listed in Table II. The platinum catalyst shows a complete eight electron oxidation over a broad potential range. Even in the kinetic controlled region of 0.00 V vs. RHE the number of exchanged electrons is as high as seven and establishes almost 8 at 0.01 V vs. RHE. Therefore the anode catalyst is able to perform a complete BOR in the corresponding potential region. The high electron count and the low onset potential make it a suitable anode catalyst for our mixed electrolyte fuel cell approach.

Cathode catalyst.—The cyclic voltammogram in N_2 flushed electrolyte (Fig. 5) shows the distinctive peaks for manganese and silver oxidation and reduction. In anodic direction two weak oxidation peaks between 0.5 V and 1.0 V vs. RHE are visible. The peak at 0.62 V vs. RHE can be attributed to the formation of MnOOH from Mn(II), which is then further oxidized to MnO_2 at 0.93 V vs. RHE. The distinguished oxidation peak at 1.3 V vs. RHE can be assigned to the formation of Ag_2O, which is reduced again to pure Ag at 1.04 V vs. RHE on the cathodic sweep.[15,24] Potential cycling up to 1.40 V vs. RHE led to constant degradation of the catalyst. Therefore the thin film on the RDE is renewed before ORR experiments and CVs are conducted between 0.20 and 1.00 V vs. RHE.

Levich and Koutecky-Levich analysis (see Fig. 6) show that Ag-Mn_3O_4/C is capable of performing a complete 4 electron reduction of oxygen in the relevant potential range (results are summarized in Table II). The onset potential is approx. 850 mV vs. RHE and is approx. 50 mV below state-of-the-art platinum based catalysts (see gray line Fig. 5). The oxygen reduction reaction (ORR) performance of Ag-Mn_3O_4/C is comparable to previously published results.[15,24] However, due to high tolerance against borohydride Ag-Mn_3O_4/C outperforms platinum in the presence of borohydride. Although manganese oxide based catalysts exhibit stability issues at lower potentials (reduction to soluble $Mn(OH)_3^-$) this issue is not a concern for DBFCs due to lower current densities.

In-situ cathode characterization.—Typical in-situ electrode test results with and without correction for iR losses are show in Fig. 7. The characterization is started with a long-term operation in potentiostatic mode at 750 mV vs. RHE for 100 hours (see right diagram of Fig. 7). The polarization curve shows a high OCP of 945 mV vs. RHE which is even higher than expected from ex-situ results (onset potential of approx. 880 mV vs. RHE).[14] The cathode exhibits good behavior in the region up to 75 mA cm^{-2} with a potential of 750 mV vs. RHE. Pure manganese oxide is reported with a potential of 671 mV vs. RHE at 75 mA cm^{-2}.[25] The as-prepared gas diffusion layer shows no diffusion limitations in the corresponding current region. As mentioned before, due to limited stability of the catalyst below 700 mV vs. RHE experiments are conducted with a potential limit of 750 mV vs. RHE.

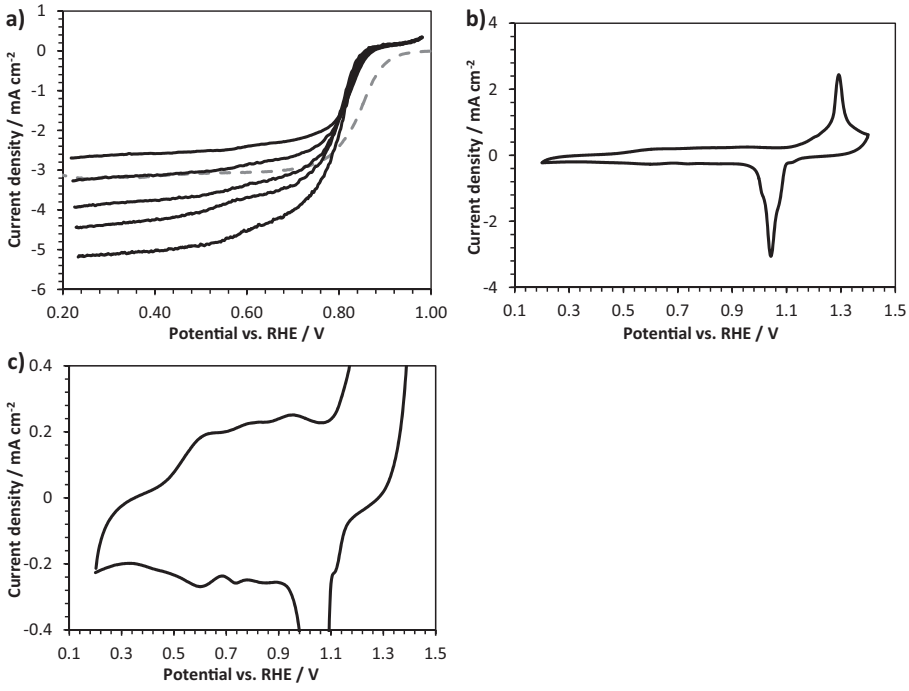

Figure 5. RDEs experiments of Ag-Mn_3O_4/C catalyst in 0.1 M KOH, 10 mV s^{-1}, 400–1600 rpm with a commercial Pt/C for comparison (without borohydride), b)+c) cyclic voltammogram in deaerated electrolyte.

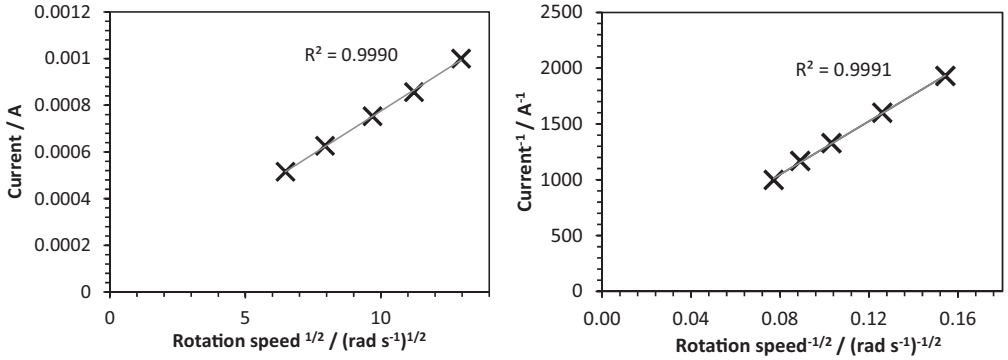

Figure 6. Levich plot of Ag-Mn_3O_4/C catalyst at 0.30 V vs. RHE, right: Koutecky-Levich plot at 0.74 V vs. RHE.

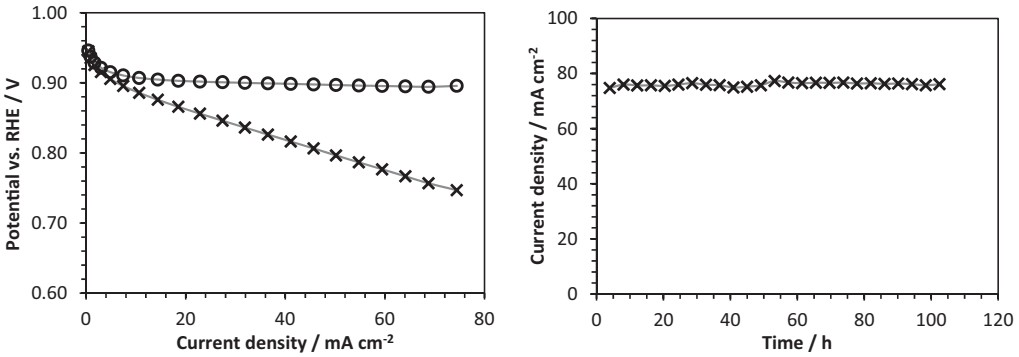

Figure 7. Polarization curve of Ag-Mn_3O_4/C based electrode with (circles) and without (crosses) R_u compensation after 100 h potentiostatic operation at 0.75 V vs. RHE (shown right).

Single cell tests.—The iR-corrected polarization curve of the mixed electrolyte BH_4^-/O_2 cell is show in Fig. 8. The open circuit voltage is 0.70 V which is compared to ex-situ and in-situ onset potentials lower than expected. Anode potentials are followed during all measurements and the corresponding cathode potentials are calculated from the cell voltage. OCP at the cathode is 0.678 V vs. RHE which is approx. 270 mV below the measured potential during in-situ electrode experiments (comparison also given in Fig. 9). The difference can be ascribed to the formation of a mixed potential in the presence of BH_4^- at the cathode. The results suggest that although Mn_3O_4 as well as Ag/C catalysts are highly selective toward ORR the electrodes do show catalytic activity toward BOR.

Since the maximum current from the cathode is 75 mA cm^{-2} the polarization curve has its maximum at this point. A power density of 17 mW cm^{-2} is observed. The anode potential starts with an OCP of −24 mV vs. RHE with a sharp increase in the region between 10 and 25 mA cm^{-2}. During all measurements the cathode revealed excellent stability and durability properties.

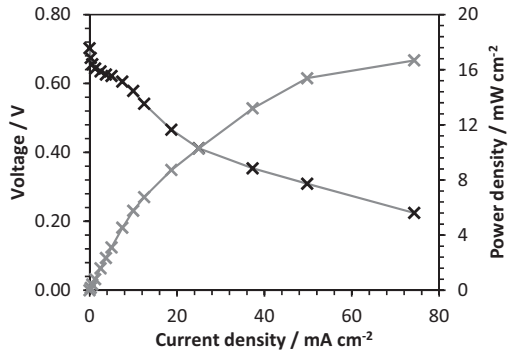

Figure 8. Polarization curve mixed electrolyte DBFC at 30°C and corresponding power densities (gray).

Conclusions and Outlook

Direct borohydride fuel cells (DBFCs) are an interesting and promising technology for low power applications. Hitherto the usage of cation exchange membranes (which is necessary to avoid borohydride crossover to the cathode) limits the practicability due to insufficient fuel concentration and salt formation at the cathode. With the approach of fueling the DBFC with a mixed electrolyte these major drawbacks can be addressed effectively.

A commercial anode catalyst (Pt/C) and a previously published cathode catalyst (Ag-Mn_3O_4/C) are characterized electrochemically employing a RDE. Both catalytic systems show good ex-situ behavior toward the desired electrode reactions. Although platinum exhibits activity toward the hydrolysis reaction it is still the anode catalyst of choice. Therefore the addition of thiourea to the electrolyte is necessary. A BH_4^-/O_2 fuel cell consisting of the catalysts mentioned above is constructed showing a power density of 17 mW cm^{-2} at room temperature. In order to increase the cell performance the tolerance of the cathode toward borohydride is crucial and has to be improved.

On the roadmap toward a DBFC based application the catalysts' performance has to be increased in terms of selectivity. The anode catalyst needs to be inactive toward hydrolysis and the cathode catalyst needs to show high tolerance for borohydride.

Acknowledgments

Financial support by the Austrian Federal Ministry of Science, Research and Economics (BMWFW), the Austrian Research Promotion

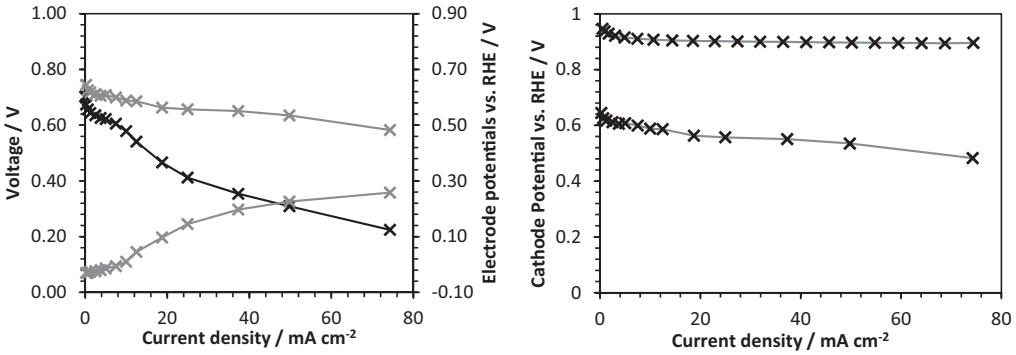

Figure 9. Cell voltage (black) and electrode potentials (gray) of mixed electrolyte DBFC at 30°C and comparison of cathode potentials with and without borohydride (right).

Agency (FFG, project nr. 840476), the IEA research cooperation and our industry partners VTU engineering and proionic GmbH is gratefully acknowledged. Additionally we want to thank Apollo Energy Systems for providing cathode materials.

References

1. J. P. Elder and A. Hickling, *Trans. Faraday Soc.*, **58**, 1852 (1962).
2. M. Indig and R. Snyder, *J. Electrochem. Soc.*, **109**, 1104 (1962).
3. I. Merino-Jiménez, C. Ponce de León, A. A. Shah, and F. C. Walsh, *J. Power Sources*, **219**, 339 (2012).
4. B. M. Concha and M. Chatenet, *Electrochim. Acta*, **54**, 6119 (2009).
5. B. M. Concha and M. Chatenet, *Electrochim. Acta*, **54**, 6130 (2009).
6. E. H. Jensen, *A Study on Sodium Borohydride*, NYT Nordisk Forlag Arnold Busck, Copenhagen, (1954).
7. B. H. Liu, Z. P. Li, and S. Suda, *Electrochim. Acta*, **49**, 3097 (2004).
8. B. H. Liu, J. Q. Yang, and Z. P. Li, *Int. J. Hydrogen Energy*, **34**, 9436 (2009).
9. J. Ma, N. A. Choudhury, and Y. Sahai, *Renew. Sustain. Energy Rev.*, **14**, 183 (2010).
10. E. Gyenge, *Electrochim. Acta*, **49**, 965 (2004).
11. Ü. B. Demirci, *Electrochim. Acta*, **52**, 5119 (2007).
12. A. Aziznia, C. W. Oloman, and E. L. Gyenge, *J. Power Sources*, **212**, 154 (2012).
13. A. Serov et al., *J. Mater. Chem. A*, **1**, 14384 (2013).
14. K. V. Kordesch, U.S. Pat. No. US3595698 (1971).
15. Q. Tang et al., *Appl. Catal. B Environ.*, **104**, 337 (2011).
16. G. Brauer, *Handbook of Preparative Inorganic Chemistry*, (1963).
17. Y. Garsany, I. L. Singer, and K. E. Swider-Lyons, *J. Electroanal. Chem.*, **662**, 396 (2011).
18. K. J. J. Mayrhofer, D. Strmcnik, B. B. Blizanac, V. Stamenkovic, M. Arenz, and N. M. Markovic, *Electrochim. Acta*, **53**, 3181 (2008).
19. B. Šljukić, J. Milikić, D. M. F. Santos, and C. A. C. Sequeira, *Electrochim. Acta*, **107**, 577 (2013).
20. J. Qiao L. Xu, P. Shi, L. Zhang, R. Baker, and J. Zhang, *Int. J. Electrochem. Sci.*, **8**, 1189 (2013).
21. G. Denuault, M. V. Mirkin, and A. J. Bard, *J. Electroanal. Chem.*, **308**, 27 (1991).
22. D. A. Finkelstein, N. D. Mota, J. L. Cohen, and H. D. Abruna, *J. Phys. Chem. C*, **113**, 19700 (2009).
23. H. Dong, R. Feng, X. Ai, Y. Cao, H. Yang, and C. Cha, *J. Phys. Chem. B*, **109**, 10896 (2005).
24. Q. Wu, L. Jiang, L. Qi, L. Yuan, E. Wang, and G. Sun, *Electrochim. Acta*, **123**, 167 (2014).
25. Y. Wang, L. Cheng, F. Li, H. Xiong, and Y. Xia, *Chem. Mater*, **19**, 2095 (2007).

THE JOURNAL OF PHYSICAL CHEMISTRY C

Article

pubs.acs.org/JPCC

Carbon Supported Ruthenium as Anode Catalyst for Alkaline Direct Borohydride Fuel Cells

Christoph Grimmer,* Robert Zacharias, Maximilian Grandi, Bernd Cermenek, Alexander Schenk, Stephan Weinberger, Franz-Andreas Mautner, Brigitte Bitschnau, and Viktor Hacker

Institute of Chemical Engineering and Environmental Technology, Fuel Cell Systems Group, Graz University of Technology, NAWI Graz, Inffeldgasse 25C, 8010 Graz, Austria

ABSTRACT: Electrochemical borohydride oxidation on nanodispersed ruthenium supported on high surface area carbon (Ru/C) is investigated by means of cyclic voltammetry, CO-stripping, rotating disk electrode experiments and chronoamperometry as well as direct borohydride fuel cell tests in a mixed electrolyte approach. All experimental results of Ru/C are compared to a commercially available Pt/C catalyst. Ru/C shows high Coulombic efficiency with a complete eight electron transfer at low anodic potentials. The electrochemical active potential window is −0.05−0.30 V vs RHE with higher activity compared to Pt/C in diffusion limited regions. In situ fuel cell tests show superior behavior in current density areas below 20 mA cm^{-2}.

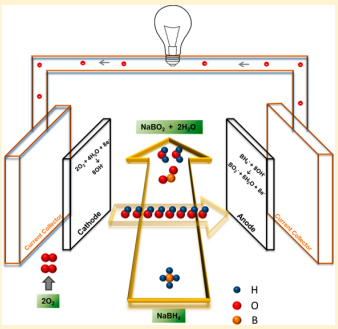

1. INTRODUCTION

Fuel cells which are capable of utilizing liquid fuels directly receive great attention for portable and mobile applications due to convenient, safe, and easy fuel storage.[1] Methanol is the only direct liquid fuel that has been commercialized among various direct liquid alcohols or fuels containing borohydride anions. The absence of a C−C bond cleavage simplifies the fuel oxidation considerably. All other direct liquid fuel cell (DLFC) systems, which are suggested in the literature, are still far from market launch mainly due to poor anode performance.

The direct borohydride fuel cell (DBFC), though being in an early stage of development, is one of the most promising candidates.[2] The DBFC utilizes the chemical stored energy in the BH_4^- anion, which is provided in the form of sodium borohydride ($NaBH_4$). $NaBH_4$ is a white crystalline solid (fcc) with a high-energy density (9.3 Wh g^{-1}), making it a promising energy as well as hydrogen storage compound.[2−4] $NaBH_4$ exhibits high solubility in water (55.0 g in 100 g H_2O), and its stability corresponds strongly to the pH (see half-life in Table 1).[5,6]

$NaBH_4$ is readily oxidized by various electrocatalyst materials, releasing up to 8 electrons at a theoretical potential of −1.24 V vs SHE (see reaction 1).[7] Combined with a regular air electrode, the DBFC exhibits a theoretical voltage of 1.64 V (reactions 2 and 3).[8]

Most widely investigated catalysts are Pt/C, Au/C, Pd/C, and alloys thereof.[9−12] Platinum-based catalysts show good Coulombic efficiencies at low potentials close to hydrogen evolution. However, platinum exhibits also high catalytic activity toward the main side reaction, namely the borohydride hydrolysis (see reaction 4).[13]

Table 1. Half-Life of Sodium Borohydride at Various pH Values of the Solution.[5,6]

pH	half-life of $NaBH_4$	
4.0	0.0037	sec
5.0	0.037	sec
6.0	0.37	sec
7.0	3.7	sec
8.0	36.8	sec
9.0	6.1	min
10.0	61.4	min
11.0	10.2	h
12.0	4.3	d
13.0	42.6	d
14.0	426.2	d

$$BH_4^- + 8OH^- \rightarrow BO_2^- + 6H_2O + 8e^- \quad E^0 = -1.24\ \text{V vs SHE} \tag{1}$$

$$O_2 + 2H_2O + 4e^- \rightarrow 4OH^- \quad E^0 = 0.40\ \text{V vs SHE} \tag{2}$$

$$BH_4^- + 2O_2 \rightarrow BO_2^- + 2H_2O \quad E^0 = 1.64\ \text{V} \tag{3}$$

$$BH_4^- + 2H_2O \rightarrow BO_2^- + 4H_2 \tag{4}$$

Since $NaBH_4$ is also considered a hydrogen carrier compound, hydrolysis results of ruthenium- and platinum-based catalysts are available in literature. Comparing the activity

Received: July 16, 2015
Revised: October 2, 2015
Published: October 3, 2015

DOI: 10.1021/acs.jpcc.5b06862
J. Phys. Chem. C 2015, 119, 23839−23844

toward hydrolysis on Ru (12900 mL H_2 min^{-1} g_{metal}^{-1}) and on Pt (175570 mL H_2 min^{-1} g_{metal}^{-1}), it is obvious that ruthenium possesses superior properties for application in DBFCs.[14,15]

Ruthenium-based catalysts are employed for hydrogenation, ammonia synthesis, or in combination with platinum as electrocatalysts.[16] Pure Ru electrocatalysts are not investigated extensively due to poor activity for central electrode reactions like the oxygen reduction reaction.[17]

Considering today's price of ruthenium (1.6 US$ g^{-1}, May 2015) and platinum (35.2 US$ g^{-1}, May 2015), the cost of raw materials for DBFCs is decreased drastically with this DBFC approach that employs a nonexpensive perovskite ($La_{0.6}Ca_{0.4}CoO_3$) at the cathode and ruthenium at the anode.

Herein, we present a nanodispersed ruthenium catalyst supported on high surface area carbon (Ru/C), which was synthesized by the so-called instant method.[18,19] The ruthenium-based catalyst shows promising results toward the borohydride oxidation reaction (BOR).

2. EXPERIMENTAL SECTION

2.1. Preparation of Ru/C. Carbon-supported ruthenium nanoparticles were synthesized using the instant reduction method. Vulcan XC72R (72 mg) was suspended in a mixture of 2-propanol (3 mL) and ultrapure water (17 mL) in a round-bottom flask with an ultrasonic homogenizer for 20 min. After the suspension was well-dispersed, $RuCl_3 \cdot 3H_2O$ (124.0 mg) in a mixture of 2 mL 2-propanol and 8 mL of ultrapure water was added, resulting in a metal loading of 40 wt %. The pH of the mixture was adjusted to 9−10 with NaOH and kept at 60 °C under continuous stirring overnight. The suspension was saturated with hydrogen for 15 min by bubbling and stirred under a hydrogen atmosphere for another 6 h. The solid product was filtered, washed repeatedly with ultrapure water, and dried overnight at 80 °C.

2.2. Structural and Chemical Analysis. X-ray powder diffraction data were obtained on a Bruker AXS D8 Advance powder diffractometer in Bragg−Brentano geometry, operated at 40 kV and 40 mA, using Cu Kα radiation (λ = 1.54178 Å). Diffraction angles were measured from 10 to 100°2θ, having a step size of 0.025°2θ. Rietveld refinement was performed using PANalytical X'Pert High Score Plus software, starting with the crystal structure data of hexagonal metallic Ru.[20] The average primary crystallite sizes of the samples (d_{XRD}) were estimated according to the broadening of the diffraction peaks using the Scherrer relationship ($d_{XRD} = (K\lambda)/\Delta(2\theta)\cos\theta$) where d is the mean crystallite dimension, K is the shape factor (0.9), λ is the X-ray wavelength in nm, $\Delta(2\theta)$ is the peak broadening compared to LaB_6 standard peaks at full width at half-maximum in radians, and θ is the Bragg angle.[21]

2.3. Electrochemical Characterization. All electrochemical measurements were carried out with a Reference600 potentiostat from Gamry instruments (supplied by C3 Analysentechnik, Germany). A reversible hydrogen electrode (RHE) was used as a reference electrode; hence, all herein reported potentials are given with respect to RHE. Ex situ measurements were conducted in a temperature-controlled electrochemical cell at 30 °C and results are not corrected for uncompensated resistances unless otherwise stated. A glassy carbon rod acted as a counter electrode.

An appropriate amount of Ru/C was well-dispersed in a mixture of 2-propanol and water (7:3) by ultrasonication. Ten microliters of this suspension was pipetted on a rotating disk electrode (RDE) equipped with a glassy carbon (GC) disk (diameter 5 mm, Pine Research Instrumentation E5 series), resulting in a ruthenium loading of 56 μg cm^{-2}. The metal loading was optimized according to the criteria suggested by Mayrhofer et al.[22] To ensure homogeneous and reproducible thin films, the catalyst was dried at room temperature during rotation of 700 rpm.[23] Prior to each measurement, the GC electrode was polished to a mirror finish using an alumina suspension (0.05 μm).

The electrolyte consisted of 1 M sodium hydroxide (NaOH) made of ultrapure water (18.2 MΩ), giving an uncompensated resistance of 4−5 Ω. The concentration of sodium borohydride was kept at 5 mM. For CO-stripping measurements, the potential of the working electrode was kept at 0.10 V for 15 min while bubbling CO through the electrolyte, assuming complete surface coverage. The electrolyte was inertized with nitrogen for another 10 min before the CV was recorded.[24] Conversion factors of 210 and 484 μC cm^{-2} were used for calculating the electrochemical active surface area (ECSA) from the H_{UPD} area and CO-oxidation peak area, respectively.[25,26]

Levich and Koutecky−Levich (KL) analyses was performed as suggested by Treimer et al.[27,28], The calculations of KL results are based on the slope and the intercept of the corresponding KL plots, where the slope and the intercept are proportional to $1/n$ and $1/k_h$ (heterogeneous rate constant), respectively.

Kinetic limited currents (i_k) are calculated, considering Koutecky−Levich theory at a rotation speed of 1600 rpm and further employed to calculate mass-specific activities (MA) and area-specific activities (SA).[29] The calculation was done at various potentials, considering the region $0.1 \times i_d < i < 0.8 \times i_d$ as proposed by Mayrhofer et al.[22] (i, measured current at given potential; i_d, diffusion-limited current).

Chronoamperometry was conducted for Ru/C and Pt/C catalysts with a rotation rate of 1600 rpm during all measurements. After keeping the working electrode potential at 0.00 V vs RHE for 30 s, the electrode potential was increased to the corresponding step for 60 s.

2.4. Fuel Cell Tests. *Anode Fabrication.* Anodes were prepared by a drop-coating method using carbon cloth as electrode substrate with a fixed platinum loading of 1 mg cm^{-2} and a ruthenium loading of 2 mg cm^{-2}. The catalyst powder was suspended in an appropriate amount of 1-propanol and FAA3 ionomer (FumaTech) as the binder. In order to replace carbonate anions from the ionomer with hydroxide anions, the electrodes were treated with 0.5 HCl and three times with 1 M NaOH.

Cathode Fabrication. Cathodes were fabricated with a borohydride tolerant perovskite structured catalyst with the composition $La_{0.6}Ca_{0.4}CoO_3$. The perovskite was synthesized with the so-called amorphous-citrate-precursor method.[30] In short, the precursor salts $La(NO_3)_3$, $Ca(NO_3)_2$ and $Co(NO_3)_2$ were dissolved in a solution of citric acid (1M). After complete evaporation of the solvent, the solid is ground and calcined at 650 °C for 2 h.

The cathodes were fabricated employing a cross rolling, hot pressing method with carbon as the conducting agent and PTFE as the binder.[31] Gas diffusion layers (GDL) were prepared using 55 wt % acetylene black (Alfa Aesar), 45 wt % PTFE, and a nickel mesh as the current collector. The catalyst containing slurry (70 wt % catalyst, 15 wt % PTFE, 15 wt % Vulcan XC72R) in a mixture of water and 2-propanol was cross rolled on the GDL with a catalyst loading of approximately 80 mg cm^{-2}. The GDLs and the active layers were pressed at room

DOI: 10.1021/acs.jpcc.5b06862
J. Phys. Chem. C 2015, 119, 23839−23844

temperature with a pressure of 330 kg cm^{-2} to a final thickness of 1.30 mm.

Fuel Cell Testing. The anode catalysts were characterized in situ in a mixed electrolyte fuel cell with a perovskite type cathode catalyst. The cell design consisted of a fuel inlet below the electrodes and the outlet above. The distance between anode and cathode was 3 mm, and a Luggin capillary was mounted toward the anode employing a RHE. The cathode was not replaced during all measurements presented here. One molar $NaBH_4$ in 1 M NaOH and 5 mM thiourea is used as fuel and cycled with a flow rate of 10 mL min^{-1}. Thiourea is added to the fuel in order to poison the borohydride hydrolysis reaction on the catalyst surface.[10] The cathode was supplied with pure oxygen at a flow rate of 50 mL min^{-1}. All measurements were conducted at room temperature.

Voltage current characteristics were measured in galvanostatic operation with constant current for 30 s. Additionally chronoamperometry measurements were conducted at 0.75 and 0.50 V.

3. RESULTS AND DISCUSSION

3.1. Structural and Chemical Analysis. The Ru/C catalysts were analyzed using the X-ray diffraction technique.

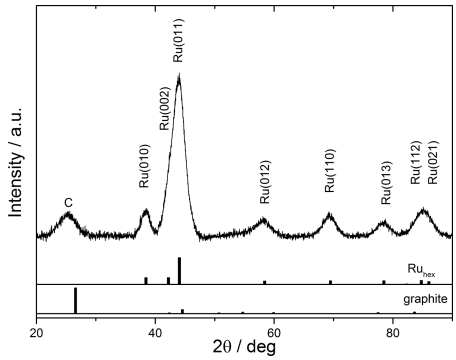

Figure 1. XRD pattern of the as-prepared Ru/C electrocatalyst.

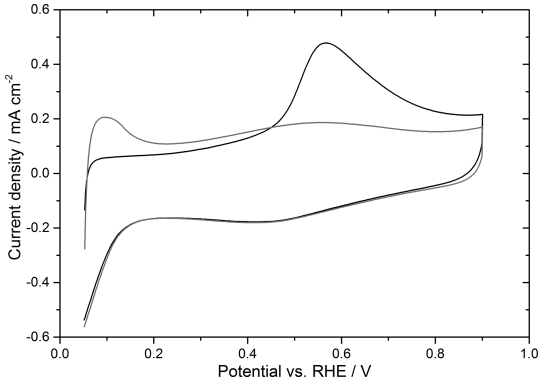

Figure 2. CO stripping experiment of Ru/C (56 μg Ru cm^{-2}). Black, first CV cycle with CO-oxidation; gray, second CV cycle.

The final observed diffraction patterns of the as-prepared Ru/C sample after Rietveld Refinement are shown in Figure 1. The 2θ Bragg peaks at ca. 25.6°, 38.6°, 42.4°, 44.0°, 58.1°, 69.2°, 78.5°, 84.5°, and 85.6° correspond to the hexagonal (hex) reflections of C(002), Ru(010), Ru(002), Ru(011), Ru(012), Ru(110), Ru(013), Ru(112), and Ru(021), respectively.[20]

The average particle size of the as-prepared Ru/C catalysts was determined by using the Scherrer relationship.[21] The obtained crystallite sizes of the Ru/C catalysts are within the range of 3.0 nm. The quantification of the diffraction pattern via profile fitting gives a ruthenium content of approximately 38 wt %.

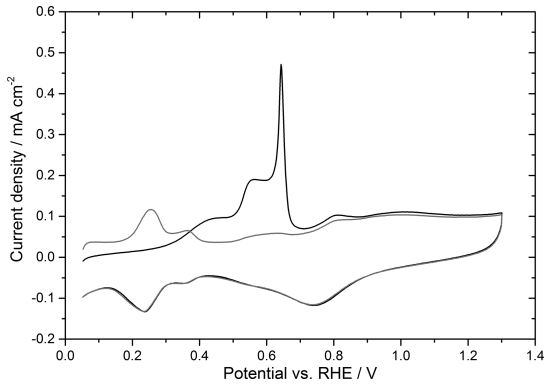

Figure 3. CO stripping of Pt/C (28 μg Pt cm^{-2}). Black, first CV cycle with CO-oxidation; gray, second CV cycle.

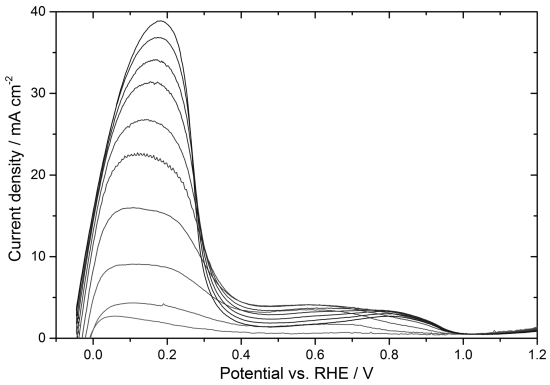

Figure 4. Anodic sweeps of RDE experiments of Ru/C at rotation rates of 0−2000 rpm, 5 mM $NaBH_4$.

Table 2. Summarized Levich and Koutecky-Levich Results for BH_4^--Oxidation

	potential V vs RHE	n (Levich)	n (Koutecky−Levich)	k_h 10^{-2} cm s^{-1}
Ru/C	0.00	–	8.36	0.6
	0.18	8.28	10.11	2.5
Pt/C	0.01	–	7.91	1.9
	0.20	7.74	8.92	5.4
	0.40	7.95	8.88	7.0

3.2. Electrochemical Characterization. All electrochemical and catalytical results of Ru/C are compared to a commercial Pt/C catalyst (Pt/C 50 wt % from Alfa Aesar).

3.2.1. Cyclic Voltammetry, CO-Stripping. In Figure 2, we present CO-stripping results of Ru/C in alkaline electrolyte with a scan rate of 10 mV s^{-1}. Electrooxidation of carbon monoxide on ruthenium occurs at potentials above approximately 450 mV vs RHE with a broad peak.[32] The ECSA was

DOI: 10.1021/acs.jpcc.5b06862
J. Phys. Chem. C 2015, 119, 23839−23844

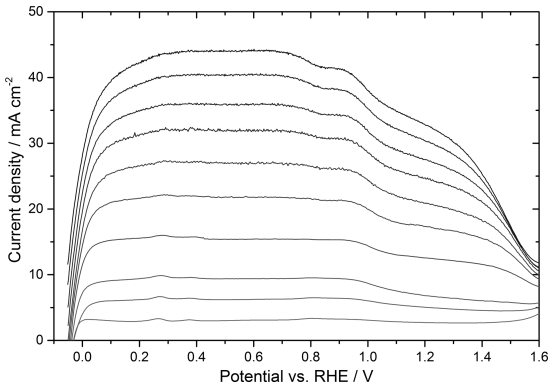

Figure 5. Anodic sweeps of RDE experiments of Pt/C at rotation rates of 0−2000 rpm, 5 mM $NaBH_4$.

determined by integrating the CO oxidation peak and using the second CV cycle as baseline in the potential region of 460−800 mV vs RHE. The ECSA of as-prepared Ru/C is 20.9 $m^2\ g^{-1}$ Ru, which is comparable to previously published results.[17] The commercially available Pt/C catalyst was also characterized by CO-stripping (see Figure 3). As discussed by Urchaga et al., the three peaks of CO electrooxidation can be ascribed to platinum surface sites: peak 1 (around 430 mV vs RHE) shows surface defects of Pt(100) and Pt(111) sites, peak 2 (around 550 mV vs RHE) represents two peaks that cannot be separated for Pt(111) and low coordinated Pt, and peak 3 (around 640 mV vs RHE) shows the CO oxidation on Pt(100).[33] The ECSA of Pt/C is 19.9 $m^2\ g^{-1}$ Pt by the integration of the H_{UPD} region and 23.3 $m^2\ g^{-1}$ Pt by integrating the CO-electrooxidation peak.

3.2.2. RDE Experiments. An appropriate amount of $NaBH_4$ was added to the electrolyte, and CVs were recorded at rotation rates of 0−2000 rpm. Anodic sweeps of RDE experiments of Ru/C and the corresponding Levich plot are shown in Figure 4 and Figure 6. BH_4^- oxidation on Ru/C starts at the lowest potential that can be measured, −0.05 V vs RHE, in order to avoid reducing currents from hydrogen evolution in aqueous electrolytes. Therefore, the real onset potential of the BOR cannot be measured. Ru/C shows further a complete eight electron reaction at low potentials. The electrocatalytic window of Ru/C toward electrooxidation of borohydride is −0.05−0.30 V vs RHE. Unexpectedly, no considerable oxidation peaks were observed at higher potentials. The CV in inertized electrolyte shows no obvious surface oxidation peak in this area, although the formation of RuO in the potential range of 0.2−0.5 V vs SHE is reported in acidic electrolyte.[34] According to the Pourbaix diagram published by Piela et al., we assume the formation of $Ru(OH)_3$ and passivation for direct borohydride oxidation in this potential range.[35]

Results from Levich and Koutecky−Levich analyses are summarized in Table 2. BH_4^- oxidation on Ru/C gives 8 electrons in the complete active potential range. Pt/C shows similar behavior in the low potential region (see Figure 5) but exhibits BOR activity in the complete potential range. The theoretical maximum of eight electrons is observed as well. The corresponding Levich as well as the Koutecky−Levich plots are

Table 3. Kinetic Limited Currents at Various Potentials

	potential	i_k	MA	SA
	V vs RHE	mA	mA $(mg\ M)^{-1}$	mA cm^{-2}
Ru/C	−0.05	0.31	5.57	0.14
	−0.04	1.04	18.62	0.46
	0.00	5.19	92.71	2.27
Pt/C	−0.05	2.40	85.54	1.87
	−0.04	4.22	150.58	3.29
	0.00	17.36	619.92	13.56

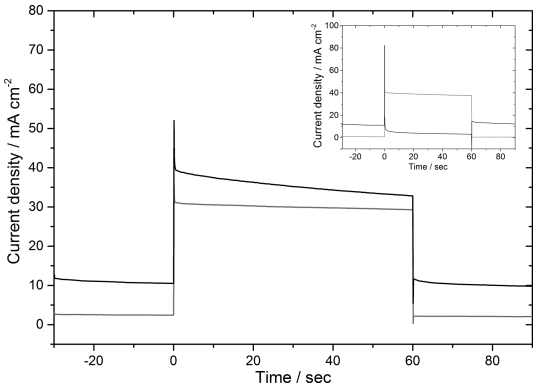

Figure 7. Chronoamperometry of Ru/C (black) compared to Pt/C (gray) at 0.10 V vs RHE; inlet, chronoamperometry at 0.30 V vs RHE.

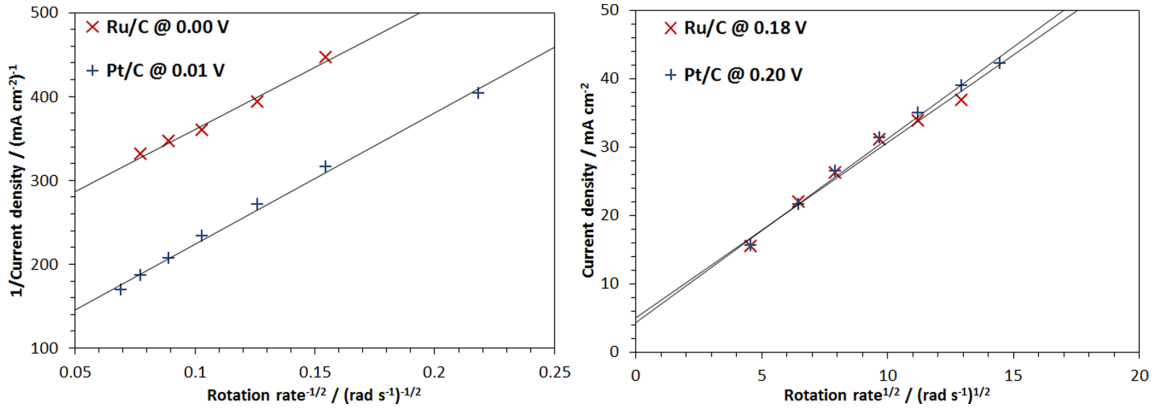

Figure 6. Koutecky−Levich (left) and Levich plot of the Ru/C and Pt/C catalyst (right).

DOI: 10.1021/acs.jpcc.5b06862
J. Phys. Chem. C 2015, 119, 23839−23844

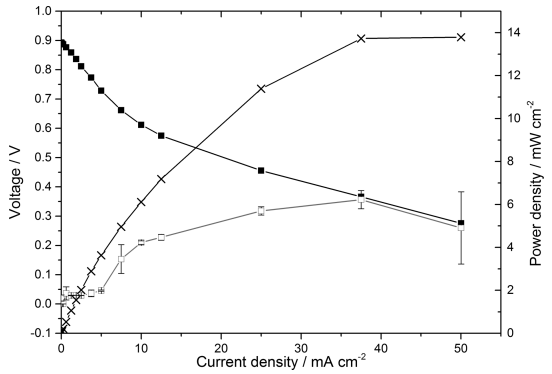

Figure 8. Voltage current characteristic and power density of mixed electrolyte DBFC with Ru/C-based anode, anode potential shown in gray hollow quadrats with black error bars (corrected for internal resistances).

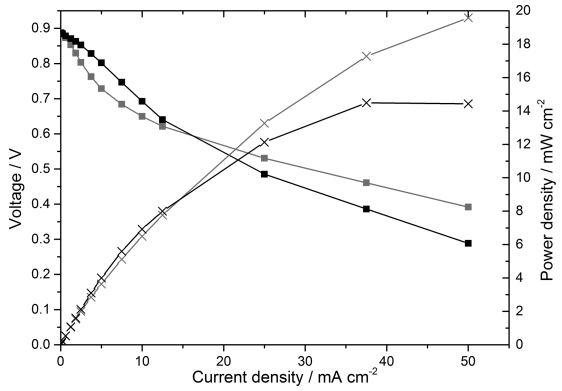

Figure 9. Voltage current characteristics of Ru/C- (black) and Pt/C (gray)-based electrodes.

given in Figure 6 (panels a (left) and b (right), respectively). The Levich plot confirms that both catalysts exploit the diffusion-limited maximum of eight electrons at low potentials. Koutecky–Levich analysis indicates that Pt/C shows higher catalytic activity with a heterogeneous rate constant three times higher compared to Ru/C. Area-specific and mass-specific currents are summarized in Table 3 showing also superior catalytic activity of Pt/C in the kinetic-controlled region.

3.2.3. Ex Situ Chronoamperometry. At potentials above the kinetic-controlled region, chronoamperometric studies show that Ru/C exhibits higher activity toward borohydride electrooxidation. In this potential window, Ru/C outperforms Pt/C significantly. In Figure 7, a typical result at an electrode potential of 0.10 V vs RHE with a borohydride concentration of 5 mM is shown. The inset of Figure 7 shows a chronoamperometry at 0.30 V vs RHE, confirming that Ru/C shows no activity toward BOR anymore. At this point, we want to highlight that steady-state measurements, like chronoamperometry, cannot be compared directly to potential sweep techniques. The main reason can be found in the influence of the support material resulting in different concentration gradients in the near surface region. However, there is extensive agreement among researchers that in situ experiments are inevitable for appropriate comparison.

3.2.4. Direct Borohydride Fuel Cell Tests. Figure 8 shows the voltage current characteristic of the mixed electrolyte DBFC with a Ru/C-based anode and the corresponding power density considering correction for internal resistance losses. The anode potential is shown in gray hollow quadrats with corresponding error bars. As expected from ex situ measurements, the ruthenium-based electrode performs excellent at low current densities with almost no overpotential losses. At current densities above approximately 5 mA cm^{-2}, anode overpotentials increase significantly. At high current densities the potential measurement underlays strong deviations that can be ascribed to hydrogen formation at the electrode. The potential can only be measured at one spot via a Luggin capillary. Due to gaseous hydrogen the potential changes locally very strong. Although a decreased anode potential is the resulting mean value of the measurement, a slight increase is assumed at 50 mA cm^{-2}.

In Figure 9, the comparison of Ru/C (2 mg cm^{-2})- and Pt/C (1 mg cm^{-2})-based anodes is presented. Ruthenium-based DBFC performs better in the low current density region with a cross of the voltage current characteristic at approximately 16 mA cm^{-2}.

4. CONCLUSION

Ruthenium nanoparticles on Vulcan XC72R prepared by the instant method show high electrocatalytic activity toward direct borohydride oxidation. The catalytic active window starts at −0.05 V vs RHE and ends at around 0.30 V vs RHE with no further activity in the more oxidizing potential regime. CO-stripping and RDE experiments show comparable ECSA values and good Coulombic efficiency with complete 8-electron transfer per borohydride anion. However, Levich and Koutecky–Levich analysis show superior catalytic activity of Pt/C compared to Ru/C in mixed kinetic and diffusion-controlled regions. Chronoamperometric studies at 0.10 V vs RHE on the other hand show enhanced activity of Ru/C.

DBFCs measurements in a mixed electrolyte approach show superior properties of ruthenium at low current densities with stable anode potentials in this region. Ru/C represents an interesting and inexpensive alternative to Pt/C for direct borohydride fuel cells.

AUTHOR INFORMATION

Corresponding Author

*E-mail: christoph.grimmer@tugraz.at. Tel: +43 316 873 8784. Fax: +43 316 873 8782.

Notes

The authors declare no competing financial interest.

ACKNOWLEDGMENTS

Financial support by the Austrian Federal Ministry of Transport, Innovation and Technology (BMVIT), the Austrian Research Promotion Agency (FFG, project number 840476) through the program a3plus, and the IEA research cooperation and our industry partners VTU engineering and proionic GmbH are gratefully acknowledged.

ABBREVIATIONS

BOR	borohydride oxidation reaction
DLFC	direct liquid fuel cell
DBFC	direct borohydride fuel cell
ECSA	electrochemical active surface area
fcc	face-centered cubic

DOI: 10.1021/acs.jpcc.5b06862
J. Phys. Chem. C 2015, 119, 23839−23844

GC	glassy carbon
GDL	gas diffusion layer
hex	hexagonal
MA	mass activity
RHE	reversible hydrogen electrode
RDE	rotating disk electrode
SA	specific activity
SHE	standard hydrogen electrode

REFERENCES

(1) Molina Concha, B.; Chatenet, M. Direct Oxidation of Sodium Borohydride on Pt, Ag and Alloyed Pt−Ag Electrodes in Basic Media. Part I: Bulk Electrodes. *Electrochim. Acta* **2009**, *54*, 6119−6129.

(2) Molina Concha, B.; Chatenet, M. Direct Oxidation of Sodium Borohydride on Pt, Ag and Alloyed Pt−Ag Electrodes in Basic Media: Part II. Carbon-Supported Nanoparticles. *Electrochim. Acta* **2009**, *54*, 6130−6139.

(3) Grimmer, C.; Friedrich, T.; Woisetschläger, D.; Mayer, N.; Kalb, R.; Hacker, V. Novel Borohydride-Based Ionic Liquids as Hydrogen Carrier. *Chem. Ing. Tech.* **2014**, *86*, 1443−1443.

(4) Grimmer, C.; Nestl, S.; Senn, J.; Hacker, V. Selective Real-time Quantification of Hydrogen within Mixtures of Gases via an Electrochemical Method. *Int. J. Hydrogen Energy* **2015**, *40*, 2055−2061.

(5) Jensen, E. H. *A Study on Sodium Borohydride*; NYT Nordisk Forlag Arnold Busck: Copenhagen, 1954.

(6) Prokopcikas, A.; Salkauskiene, J. *Zh. Fiz. Khuim.* **1970**, *44*, 2941.

(7) Finkelstein, D. A.; Mota, N. D.; Cohen, J. L.; Abruna, H. D. Rotating Disk Electrode (RDE) Investigation of BH4− and BH3OH− Electro-Oxidation at Pt and Au: Implications for BH4− Fuel Cells. *J. Phys. Chem. C* **2009**, *113*, 19700−19712.

(8) Ponce de León, C.; Kulak, a.; Williams, S.; Merino-Jiménez, I.; Walsh, F. C. Improvements in Direct Borohydride Fuel Cells Using Three-Dimensional Electrodes. *Catal. Today* **2011**, *170*, 148−154.

(9) Ma, J.; Choudhury, N. A.; Sahai, Y. A Comprehensive Review of Direct Borohydride Fuel Cells. *Renewable Sustainable Energy Rev.* **2010**, *14*, 183−199.

(10) Gyenge, E. Electrooxidation of Borohydride on Platinum and Gold Electrodes: Implications for Direct Borohydride Fuel Cells. *Electrochim. Acta* **2004**, *49*, 965−978.

(11) Chatenet, M.; Lima, F. H. B.; Ticianelli, E. A. Gold is not a Faradaic-Efficient Borohydride Oxidation Electrocatalyst: An Online Electrochemical Mass Spectrometry Study. *J. Electrochem. Soc.* **2010**, *157*, B697.

(12) Yang, J. Q.; Liu, B. H.; Wu, S. Carbon-Supported Pd Catalysts: Influences of Nanostructure on their Catalytic Performances for Borohydride Electrochemical Oxidation. *J. Power Sources* **2009**, *194*, 824−829.

(13) Jamard, R.; Latour, A.; Salomon, J.; Capron, P.; Martinent-Beaumont, A. Study of Fuel Efficiency in a Direct Borohydride Fuel Cell. *J. Power Sources* **2008**, *176*, 287−292.

(14) Bai, Y.; Wu, C.; Wu, F.; Yi, B. Carbon-Supported Platinum Catalysts for on-site Hydrogen Generation from NaBH4 Solution. *Mater. Lett.* **2006**, *60*, 2236−2239.

(15) Zhang, J. S.; Delgass, W. N.; Fisher, T. S.; Gore, J. P. Kinetics of Ru-Catalyzed Sodium Borohydride Hydrolysis. *J. Power Sources* **2007**, *164*, 772−781.

(16) Vigier, F.; Coutanceau, C.; Hahn, F.; Belgsir, E. M.; Lamy, C. On the Mechanism of Ethanol Electro-Oxidation on Pt and PtSn Catalysts: Electrochemical and In Situ IR Reflectance Spectroscopy Studies. *J. Electroanal. Chem.* **2004**, *563*, 81−89.

(17) Johnston, C. M.; Cao, D.; Choi, J.-H.; Babu, P. K.; Garzon, F.; Zelenay, P. Se-Modified Ru Nanoparticles as ORR Catalysts − Part 1: Synthesis and Analysis by RRDE and in PEFCs. *J. Electroanal. Chem.* **2011**, *662*, 257−266.

(18) Reetz, M. T.; Lopez, M. Method for In Situ Immobilization of Water-Soluble Nanodispersed Metal Oxide Colloids. WO2003078056, 2003.

(19) Piasentin, R. M.; Spinacé, E. V.; Tusi, M. M.; Neto, A. O. Preparation of PdPtSn/C-Sb2O5.SnO2 electrocatalysts by Borohydride Reduction for Ethanol Electro-Oxidation in Alkaline Medium. *Int. J. Electrochem. Sci.* **2011**, *6*, 2255−2263.

(20) Swanson, H. E.; Fuyat, R. K.; Ugrinic, G. M. Standard X-Ray Diffraction Powder Patterns IV. *Natl. Bur. Stand. Circ. (U.S.)* **1955**, *539*, 1−75.

(21) Scherrer, P. Bestimmung der Grösse und der Inneren Struktur von Kolloidteilchen Mittels Röntgenstrahlen. *Nachr. Ges. Wiss. Goettingen, Math.-Phys. K1.* **1918**, *26*, 98−100.

(22) Mayrhofer, K. J. J.; Strmcnik, D.; Blizanac, B. B.; Stamenkovic, V.; Arenz, M.; Markovic, N. M. Measurement of Oxygen Reduction Activities via the Rotating Disc Electrode Method: From Pt Model Surfaces to Carbon-Supported High Surface Area Catalysts. *Electrochim. Acta* **2008**, *53*, 3181−3188.

(23) Garsany, Y.; Singer, I. L.; Swider-Lyons, K. E. Impact of Film Drying Procedures on RDE Characterization of Pt/VC Electrocatalysts. *J. Electroanal. Chem.* **2011**, *662*, 396−406.

(24) Mayrhofer, K. J. J.; Arenz, M.; Blizanac, B. B.; Stamenkovic, V.; Ross, P. N.; Markovic, N. M. CO Surface Electrochemistry on Pt-Nanoparticles: A Selective Review. *Electrochim. Acta* **2005**, *50*, 5144−5154.

(25) Di Noto, V.; Negro, E. Pt-Fe and Pt-Ni Carbon Nitride-Based "Core-Shell" ORR Electrocatalysts for Polymer Electrolyte Membrane Fuel Cells. *Fuel Cells* **2010**, *10*, 234−244.

(26) Schenk, A.; Grimmer, C.; Perchthaler, M.; Weinberger, S.; Pichler, B.; Heinzl, C.; Scheu, C.; Mautner, F.-A.; Bitschnau, B.; Hacker, V. Platinum−Cobalt Catalysts for the Oxygen Reduction Reaction in High Temperature Proton Exchange Membrane Fuel Cells − Long Term Behavior under Ex-Situ and In-Situ Conditions. *J. Power Sources* **2014**, *266*, 313−322.

(27) Treimer, S.; Tang, A.; Johnson, D. C. A Consideration of the Application of Koutecky-Levich Plots in the Diagnoses of Charge-Transfer Mechanisms at Rotated Disk Electrodes. *Electroanalysis* **2002**, *14*, 165−171.

(28) Bard, A. J.; Faulkner, L. R. *Electrochemical Methods: Fundamentals and Applications*; John Wiley & Sons, Inc.: New York, 2001.

(29) Garsany, Y.; Baturina, O. A.; Swider-Lyons, K. E.; Kocha, S. S. Experimental Methods for Quantifying the Activity of Platinum Electrocatalysts for the Oxygen Reduction Reaction. *Anal. Chem.* **2010**, *82*, 6321−6328.

(30) Shimizu, Y.; Kenichi, U.; Matsuda, H.; Miura, N.; Yamazoe, N. Bi-Functional Oxygen Electrode Using Large Surface Area La1-xCaxCoO3 for Rechargeable Metal-Air Battery. *J. Electrochem. Soc.* **1990**, *137*, 3430−3433.

(31) Kordesch, K.; Jahangir, S.; Schautz, M. Engineering Concepts and Technical Performance of Oxygen-Reducing Electrodes for Batteries and Electrochemical Processes. *Electrochim. Acta* **1984**, *29*, 1589−1596.

(32) Ochal, P.; Gomez De La Fuente, J. L.; Tsypkin, M.; Seland, F.; Sunde, S.; Muthuswamy, N.; Rønning, M.; Chen, D.; Garcia, S.; Alayoglu, S.; et al. CO Stripping as an Electrochemical Tool for Characterization of Ru@Pt Core-Shell Catalysts. *J. Electroanal. Chem.* **2011**, *655*, 140−146.

(33) Urchaga, P.; Baranton, S.; Coutanceau, C.; Jerkiewicz, G. Electro-Oxidation of CO Chem on Pt Nanosurfaces: Solution of the Peak Multiplicity Puzzle. *Langmuir* **2012**, *28*, 3658−3663.

(34) Sugawara, Y.; Yadav, a. P.; Nishikata, a.; Tsuru, T. EQCM Study on Dissolution of Ruthenium in Sulfuric Acid. *J. Electrochem. Soc.* **2008**, *155*, B897.

(35) Piela, P.; Eickes, C.; Brosha, E.; Garzon, F.; Zelenay, P. Ruthenium Crossover in Direct Methanol Fuel Cell with Pt-Ru Black Anode. *J. Electrochem. Soc.* **2004**, *151*, A2053.

DOI: 10.1021/acs.jpcc.5b06862
J. Phys. Chem. C 2015, 119, 23839−23844

INTERNATIONAL JOURNAL OF HYDROGEN ENERGY 40 (2015) 2055–2061

Available online at www.sciencedirect.com

ScienceDirect

journal homepage: www.elsevier.com/locate/he

Selective real-time quantification of hydrogen within mixtures of gases via an electrochemical method

Christoph Grimmer[*], *Stephan Nestl*, *Jan Senn*, *Viktor Hacker*

Institute of Chemical Engineering and Environmental Technology, Fuel Cell Systems Group, Graz University of Technology, NAWI Graz, Inffeldgasse 25C, 8010 Graz, Austria

ARTICLE INFO

Article history:
Received 4 August 2014
Received in revised form
13 November 2014
Accepted 22 November 2014
Available online 18 December 2014

Keywords:
Hydrogen quantification
Highly selective
Real-time
Electrochemical method

ABSTRACT

Herein a highly selective real-time hydrogen quantification method based on electrochemical oxidation of hydrogen in a mixture of dry or humid gases is presented. This approach gives more reliable data for any area of research dealing with hydrogen with impurities or in a mixture of various gases especially for dynamic processes. The method itself is tested and verified by employing defined amounts of hydrogen to the electrochemical test cell with a mass flow controller. The limit of quantification is 0.30 ml H_2 min^{-1} and the maximal hydrogen flow investigated in the test cell is 100 ml H_2 min^{-1}. The method is applied for two processes with highly dynamic hydrogen evolution reactions: the steam iron process and the catalytic hydrolysis of borohydride as chemical hydrogen storage compound. In comparison to state-of-the-art methods it is possible to detect hydrogen selectively and in real-time.

Introduction

Hydrogen is considered to play a major role as energy carrier in a future society based on renewable resources [1–3]. Therefore, research focuses on developments in the fields of production, storage and utilization of hydrogen. For all these areas accurate, selective and reliable methods of hydrogen quantification are necessary to evaluate new technological approaches accordingly.

Most researchers in the field of chemical hydrogen storage determine hydrogen release rates by employing a mass flow meter/controller [2,4–6], by gas chromatography (GC) [7–10] or by water displacement in a graduated cylinder [11–14]. The main issue concerning the utilization of mass flow meters is the inaccuracy when it comes to impurities and/or humidity in the H_2 stream which disables a quantification in gas mixtures. GC measurements are capable of analyzing complex mixtures of gases but due to poor time resolution fluctuating hydrogen flows cannot be detected. The drawbacks of water displacement techniques are the non-selectivity, the inaccuracy caused by reading the values by hand and the poor time resolution. Therefore it is necessary that the process generates pure hydrogen or potential byproducts are removed. However, the poor time resolution and the error rate can hardly be addressed.

In this study an electrochemical approach is introduced which is capable of quantifying hydrogen selectively in real-time within any gas mixture (except oxygen) at a time

* *Corresponding author*. Tel.: +43 316 873 8784; fax: +43 316 873 8782.
E-mail addresses: christoph.grimmer@tugraz.at (C. Grimmer), stephan.nestl@tugraz.at (S. Nestl), jan.senn@student.tugraz.at (J. Senn), viktor.hacker@tugraz.at (V. Hacker).
http://dx.doi.org/10.1016/j.ijhydene.2014.11.126

resolution of one second or less. The presented method is a modified hydrogen crossover measurement which is employed in polymer electrolyte fuel cell (PEFC) science [15,16]. This technique yields more reliable data and therefore fundamental data such as kinetic reaction parameters and activation energies can be obtained more accurately (Fig. 1).

We demonstrate the benefit of this technique by using the cyclic steam iron process and the catalytic hydrolysis of sodium borohydride $NaBH_4$ as model systems. The corresponding reactions are given below (equations (1)–(6)) [17–19].

$$Fe_3O_4 + 4H_2 \rightarrow 3Fe + 4H_2O \quad (1)$$

$$Fe_3O_4 + 4CO \rightarrow 3Fe + 4CO_2 \quad (2)$$

$$3Fe + 4H_2O \rightarrow Fe_3O_4 + 4H_2 \quad (3)$$

Within this chemical looping process iron acts as an oxygen carrier that is reduced by a syngas that contains hydrogen, carbon monoxide and inert gases and re-oxidized by steam generating pure hydrogen. The combination of the steam iron process with small-scale steam reforming enables the decentralized production of pure hydrogen without additional purification steps. In addition iron can also be used for hydrogen storage. Based on equation (3) a storage density of 4.8 wt% based on the mass of iron is possible [20,21]. Reactions (1)–(3) can be further divided into single steps involving wüstite as intermediate (reduction reactions are given in equations (4) and (5)).

$$Fe_3O_4 + H_2 \rightarrow 3FeO + H_2O \quad (4)$$

$$3FeO + 3H_2 \rightarrow 3Fe + 3H_2O \quad (5)$$

For developing and optimizing this process the gas streams need to be analyzed accordingly. Due to incomplete reactions and the formation of solid carbon during reduction, mixtures of H_2, H_2O, CO and CO_2 can occur during both reactions. In general this analysis is done by mass flow controllers and/or by gas chromatography. By employing a mass flow controller the data acquisition is continuous but the quantification of hydrogen is limited for moisture and not possible for gas mixtures. Gas chromatography is able to detect complex gas mixtures but samples can only be taken in a timescale of minutes and need the addition of defined amounts of a reference species for quantification. In contrast the herein presented electrochemical method is capable of detecting the hydrogen flow continuously irrespective of gas mixtures or humidity.

Borohydride based compounds with sodium or any other cation are a potential hydrogen carrier of the group of chemical hydrides [22]. The borohydride hydrolysis reaction (see equation (6)) is an optimal candidate to emphasize the advantage of our quantification method since there are still controversies on the kinetics of this complex reaction. As reviewed by Retnamma et al. there are several proposed models assuming zero-order, first-order, second-order, power law, Langmuir–Hinshelwood, Michaelis–Menten and semi-empirical kinetics. Furthermore they conclude that volume based measurements especially at higher temperatures have to be treated with caution due to water vapor [23].

$$NaBH_4 + 2H_2O \rightarrow NaBO_2 + 4H_2 \quad (6)$$

$$\Delta H = -75 \text{ kJ mol}^{-1} H_2$$

Method

A potential of 430 mV vs. SHE which equals an overpotential of 430 mV concerning the HOR (hydrogen oxidation reaction) is applied to the test electrode where hydrogen is oxidized immediately. The electrode reaction at the test electrode is the HOR releasing 2 electrons (see equation (7)). Resulting protons are transported through the membrane to the counter electrode where the back reaction takes place and the released electrons are analyzed according to Faraday's Law (conversion factor: 1 A ≡ 7.05 ml min^{-1}). The counter electrode of the fuel cell like electrochemical cell is fed with hydrogen in order to be useable as pseudo reference electrode.

$$H_2 \rightarrow 2H^+ + 2e^- \quad (7)$$

$$E^0 = 0.00 \text{ V vs. SHE}$$

The electrochemical cell is an in-house made and previously published fuel cell with an active area of 25 cm^2 consisting of end plates (steel), current collectors (gold bathed

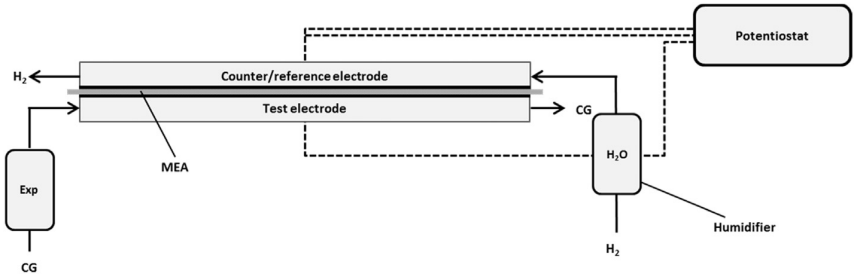

Fig. 1 – Schematic illustration of electrochemical test equipment; CG – carrier gas; MEA – membrane electrode assembly; Exp – hydrogen releasing experiment.

copper), flow fields (graphite) and a commercial fuel cell membrane electrode assembly (MEA) [24].

To provide sufficient gas transport for short response times and accurate time resolution an inert carrier gas flow is supplied to the test electrode. In dependence of the expected amount of hydrogen the carrier gas flow has to be adjusted. The hydrogen gas flow of the counter/reference electrode is humidified in order to maintain sufficient membrane humidification and ensure constant hydrogen crossover and background signal. Being aware of this phenomenon we observed constant background signals during our measurements and presume constant crossover. The maximum quantification limit of the hydrogen flow is the breakthrough of unreacted hydrogen which leaves the test electrode with the carrier gas. By changing the carrier gas flow it has to be considered that the hydrogen breakthrough changes. The method is limited to gas mixtures without oxidizable and reducible components at this potential (e.g. oxygen). Additionally it has to be considered that gases that might poison the catalyst or the membrane should be avoided or only fed in traces (e.g. ammonia).

To quantify very small amounts or traces of hydrogen this method can be adjusted to an electrochemical cell with liquid electrolyte (see Fig. 2). The test electrode (consisting of gas channels, diffusion layer and active layer) and the membrane are unchanged while the counter and the reference electrode are in liquid acidic electrolyte. This configuration has two major advantages, first no external hydrogen has to be provided to the counter/reference electrode and second the limit of quantification can be lowered significantly because hydrogen crossover is not present. The electrode reactions are the same including hydrogen evolution at the counter electrode.

Experimental

Electrochemical measurements

The electrochemical oxidation of hydrogen is conducted in a fuel cell like compartment with a commercial polymer electrolyte membrane electrode assembly (MEA) having an active area of 10 × 2.5 cm^2 (PRIMEA® MEA cleo series 58, 18 μm membrane, 0.40 μg Pt cm^{-2}). Gases are supplied to the MEA with a meander like flowfield with channel widths of 0.50 mm.

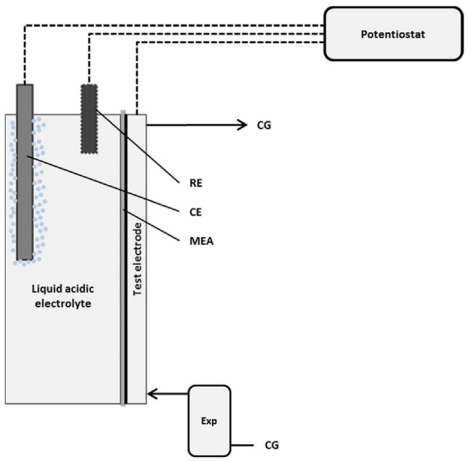

Fig. 2 – Illustration of alternative electrochemical test cell with liquid electrolyte; RE – reference electrode; CE – counter electrode.

The hydrogen containing gas mixture is transported to the test electrode while the counter electrode is supplied with hydrogen acting also as pseudo reference electrode at a gas flow of 30 ml H_2 min^{-1}. With a power potentiostat (Zahner IM6 in combination with a PP240) a potential of 430 mV vs. SHE is applied to the test electrode and the corresponding current is recorded.

The approach itself and the limitations in terms of maximum gas flow and detection limit are tested by supplying hydrogen with a mass flow controller (Bronkhorst, F-201CV-020, 20 ml_n min^{-1}) to the test electrode. All volumetric gas flows presented herein are calculated using the ideal gas law at standard conditions (273.15 K, 1 atm).

Steam iron process

The chemical looping process is conducted in a fixed bed reactor (Hastelloy® alloy, Parker Autoclave Engineers, USA) filled with a layer of silicon dioxide as preheating zone and Fe_2O_3 with 10 wt% of Al_2O_3 as stabilizer (3.57 g, 40.0 mmol Fe). The reactor is placed in an automated test stand (MICRO-ACTIVITY Reference) equipped with an electric furnace, a hot-box and mass flow controllers for gas supply (Bronkhorst). The gas analysis is performed with a micro gas chromatograph (Agilent 3000) taking a sample every three minutes before the gas mixture is analyzed electrochemically. The oxidation step is performed by applying 0.03 ml H_2O_l min^{-1} with a HPLC pump (Gilson 307 piston pump) into the evaporator section of the system. For the reduction of the oxygen carrier 25 ml H_2 min^{-1} are supplied. Both reactions are conducted at 750 °C and 10 ml N_2 min^{-1} are added as internal standard for the GC measurement.

Borohydride hydrolysis

The catalytic hydrolysis of borohydride is carried out in a temperature controlled reaction chamber with a small volume (9.4 cm^3) with an in-house prepared cobalt based catalyst on nickel foam. The chamber is loaded with the catalyst, closed up and flushed with nitrogen before the alkaline $NaBH_4$ solution is added via a septum. A continuous gas flow of nitrogen is used for this reaction as carrier gas to minimize the response time. By driving the hydrolysis reaction under various temperatures the activation energy is determined.

Cobalt on nickel foam catalysts are prepared by a previous published method by Dai et al. [11]. In short, a piece (0.5 × 0.5 cm^2) of the previous washed nickel foam (10 × 10 × 1.6 mm^3, Goodfellow, 20 pores cm^{-1}, porosity 95%) is immersed in an aqueous precursor solution, containing $CoCl_2$, $NaWO_4$, NH_4Cl and NH_3. After several minutes the same amount of a reduction solution containing $NaBH_4$ and NaOH is added. To achieve the desired metal loading this step is repeated four times. The catalyst samples are tempered in inert atmosphere for 2 h at 250 °C with a temperature ramp of 2 °C min^{-1}.

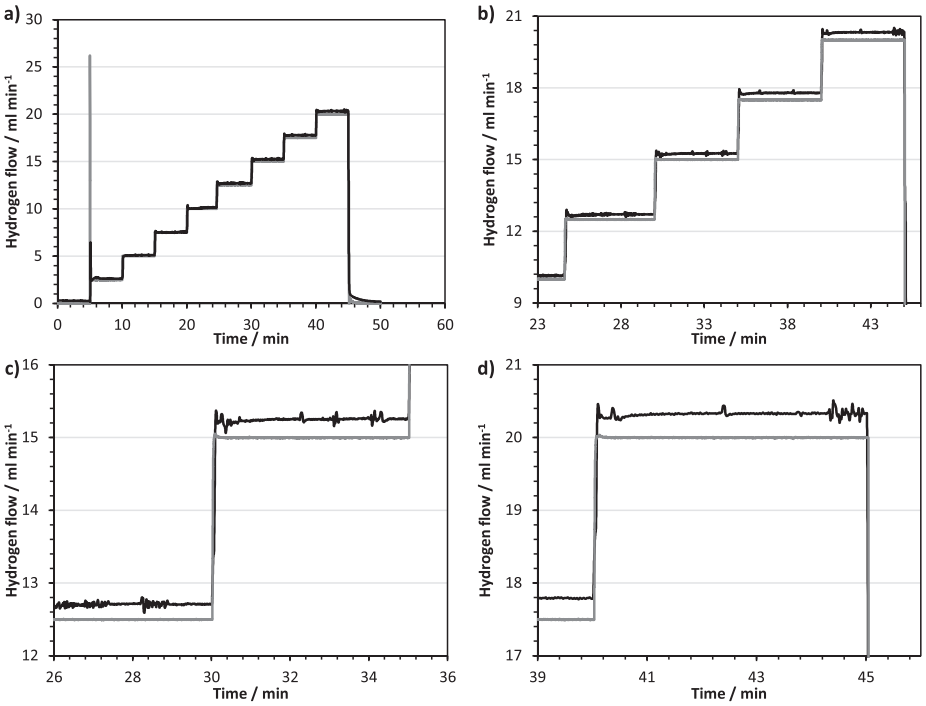

Fig. 3 – Electrochemical detection of hydrogen supplied by a MFC with a stepwise increased flow rate of 0–20 ml H_2 min^{-1}, potentiostatic at 0.430 V, black: electrochem. data; gray: data from MFC.

Results and discussion

The electrochemical cell was tested concerning the background noise from hydrogen crossover. Therefore a carrier gas flow of 30 ml N_2 min^{-1} at the test electrode and a counter electrode gas flow of 30 ml H_2 min^{-1} were supplied and an electrochemical measurement was conducted. An average background current of 27 mA (1.1 mA cm^{-2}) with a noise of approx. 5 mA was detected which is within expected values for hydrogen crossover through an intact membrane [15,16]. With an assumed signal to noise ratio of 3 the limit of quantification is therefore 0.30 ml H_2 min^{-1}. By employing a carrier gas flow of 500 ml N_2 min^{-1} a hydrogen concentration as low as 600 ppm can be quantified.

A mass flow controller from Bronkhorst was employed to supply hydrogen to the test electrode in the range of 0–20 ml_n min^{-1} (Fig. 3).

At a given flow rate of zero the MFC supplied small amounts of hydrogen as confirmed by the MFC data as well as by the electrochemical data and when starting the hydrogen supply the MFC responds with a sharp peak of oversupply (Fig. 3a). In general the gas flow given by the MFC matches the result from the electrochemical measurements very well. With increasing mass flows more hydrogen than expected was detected due to higher inaccuracies by relative deviation given by the MFC manufacturer (Fig. 3c and d). Due to the high carrier gas flow the response to changes of the hydrogen flow is very accurate as well.

Steam iron process

Fig. 4 shows the results of the oxidation process analyzed by GC and electrochemical oxidation (see equation (3)). The electrochemical data gives further insights into the highly fluctuating evolution of hydrogen which cannot be detected with the previous mentioned GC and MFC techniques. Experiments with a mass flow controller show much less sensitivity concerning this fluctuations and GC measurements are not suitable for this kind of experiment (see Fig. 4b). Due to the long sampling interval of 3 min the GC system does not provide useful data. The fluctuations are attributed to the non-perfect liquid flow supply by the HPLC pump that is amplified by the liquid-gaseous phase transition. Fig. 4c shows that the fluctuations are periodical and of similar form evidencing that the fluctuations are caused by the pump. The three GC results above the electrochemical detected flow (Fig. 4b) is considered to originate from non-homogeneous nitrogen flow due to pressure fluctuations within the system. Providing less internal standard to the GC sampler leads to incorrect evaluation of the experimental data.

Following the averaged data the reaction steps magnetite-wüstite (approx. 27 ml H_2 min^{-1}) and wüstite-metallic iron (approx. 18 ml H_2 min^{-1}) can be separated and accord to 71 and 48% steam conversion. Integrating the electrochemical data and converting the charge gives an amount of 44.9 mmol produced hydrogen. Following equation (3) this equals 83.7% conversion of the oxygen carrier. The reduction cycle was performed by supplying 25 ml H_2 min^{-1} to the fixed bed

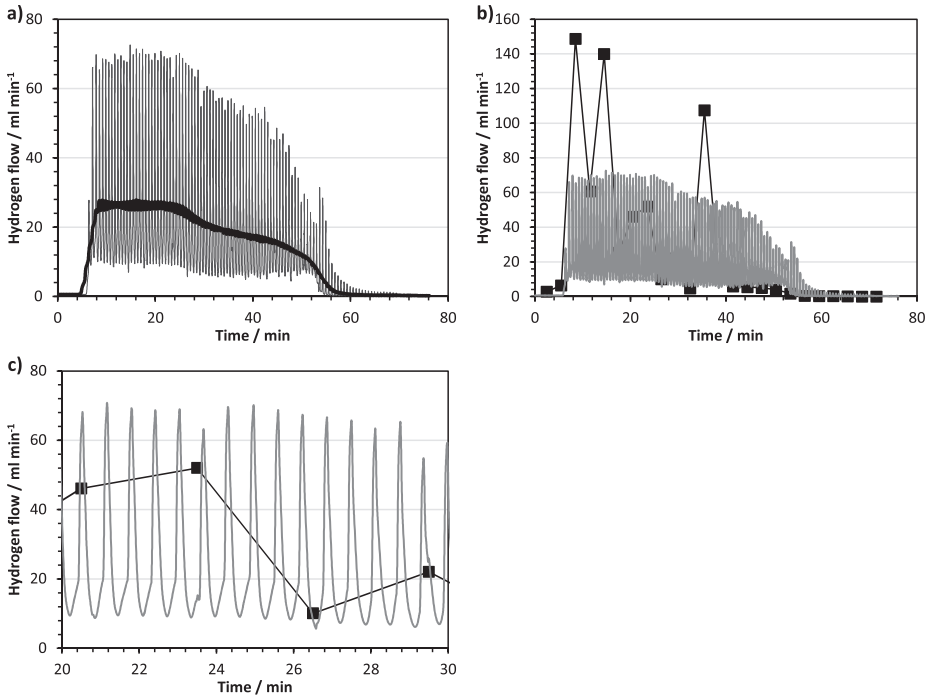

Fig. 4 – Hydrogen flow of the oxidation step of the steam iron process; a) gray: original electrochemical data, black: averaged electrochemical data; b) gray: original electrochemical data, black: results from GC measurements; c) gray: original electrochemical data, black: results from GC measurements between minute 20 and 30.

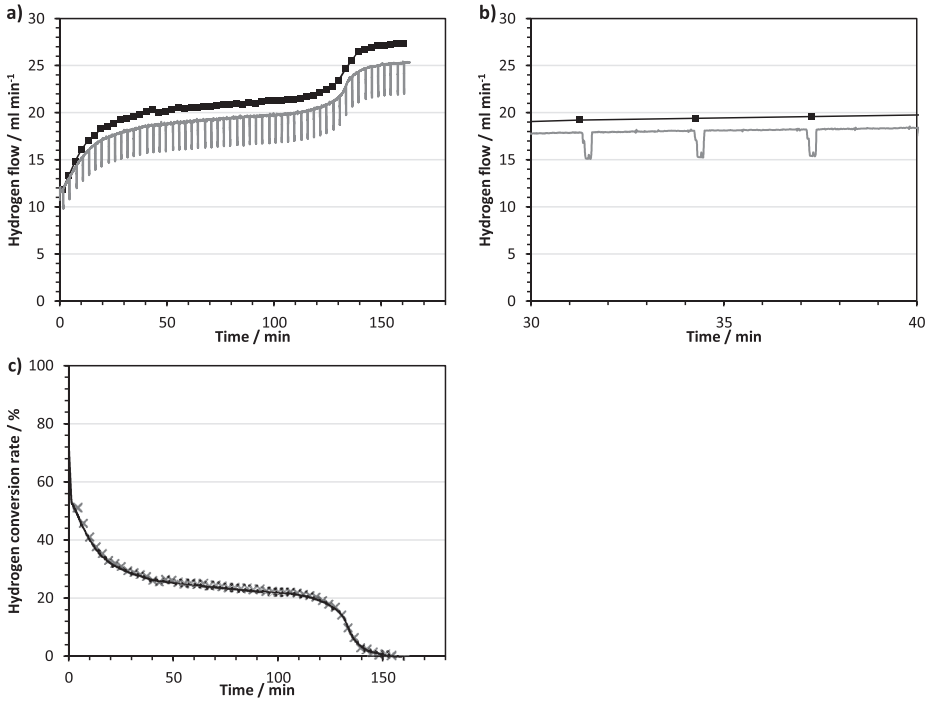

Fig. 5 – Hydrogen flow of the reduction step of the steam iron chemical looping process; a) and b) gray: original electrochemical data, black: GC results; c) hydrogen conversion rate during reduction, black: electrochemical data, gray: GC data.

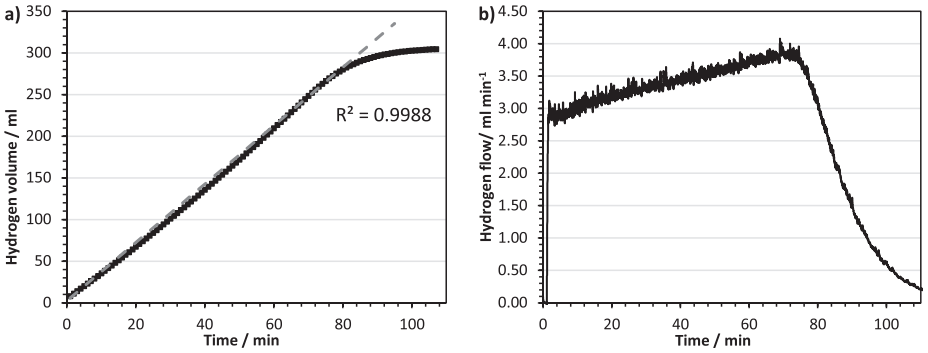

Fig. 6 – Hydrogen release by borohydride hydrolysis reaction with cobalt on nickel foam catalyst; a: cumulated volume of hydrogen with a time resolution of one minute, b: hydrogen flow detected by electrochemical oxidation; black: electrochem. data; gray dashed: linear fit.

reactor and analyzing the exhaust gas in terms of excess hydrogen (see Fig. 5).

With this configuration the GC sample that is taken every 3 min can be seen clearly (Fig. 5b). A total gas amount of 0.75 ml is sampled during approx. 14 s. The results indicate that the detected amount of hydrogen by the GC measurement is approx. 10% too high. This error most likely occurs due to inaccurate internal standard gas supply by the nitrogen MFC.

At the end of the reaction the full amount of the supplied hydrogen leaves the reactor, in our case 25 ml min^{-1} as confirmed by the electrochemical measurement. Fig. 5c gives the conversion rate of the supplied hydrogen during the reduction step. The total amount of reacted hydrogen calculated from the electrochemical measurement is 42.2 mmol (78.7% oxygen carrier conversion) which is on good accordance with the obtained values from previous oxidation.

Borohydride hydrolysis

The cobalt based catalyst (total 38.5 mg, 6.4 mg Co) is placed in the reaction chamber at 30 °C, flushed with nitrogen and 3 ml of a $NaBH_4$ solution are added (total amount of $NaBH_4$ 143.4 mg). The reaction starts immediately with a hydrogen flow of approx. 3 ml min^{-1} (approx. 500 ml min^{-1} g_{Co}^{-1}). Fig. 6 shows the same experiment plotted in different diagrams. Usually water displacement experiments are presented as given in Fig. 6a [11–13,25]. The accumulated hydrogen flow with a time resolution of one minute seems to rise linearly ($R^2 = 0.9988$) with time. By comparing the same results from our experiment an obvious deviation can be observed. The gas flow increases from 3 ml min^{-1} at the beginning to almost 4 ml min^{-1} which can be explained by a raise of the temperature due to the ongoing exothermic reaction even though the temperature was control by a Julabo ME. The temperature was measured employing a type-K thermocouple and was raising from 30.0 °C to 31.8 °C during the reaction. As can be seen by comparing Fig. 6a and b water replacement techniques cannot resolve this effect and can lead to incorrect conclusions.

Additional hydrolysis reaction experiments at various temperatures were conducted to evaluate the activation energy by Arrhenius analysis. Fig. 7 shows the Arrhenius plot resulting in an activation energy of 59.8 kJ mol^{-1} in very good agreement with literature [26]. Comparing the fit with published literature one can observe much better linearity with our experimental approach [11,25–27].

Conclusion

The herein presented electrochemical method is capable of quantifying hydrogen within a mixture of gases in real-time irrespective of moisture and calibration. By supplying hydrogen with a mass flow controller this technique was tested and verified. The detection limits can be varied by adjusting the thickness of the membrane to suppress the hydrogen crossover from the counter electrode and the active area of the electrode to increase the maximum gas flow. Within our approach hydrogen flows of 0.3–100 ml min^{-1} are quantifiable.

By employing the steam iron process as model reaction we demonstrated the benefits of the electrochemical quanti

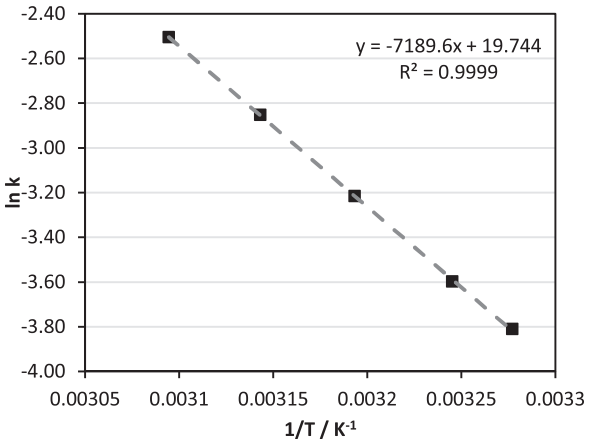

Fig. 7 – Arrhenius plot of borohydride hydrolysis with cobalt on nickel foam catalyst at 32, 35, 40, 45 and 50 °C.

fication of hydrogen for certain applications. In terms of continuous hydrogen quantification in a mixture of gases (except oxygen) our approach outperforms state-of-the-art approaches such as GC or mass flow meters. The borohydride model reaction results show that techniques with less accuracy can lead to incorrect conclusions.

Acknowledgments

Financial support by the Austrian Federal Ministry of Transport, Innovation and Technology (BMVIT), the Research Studios Austria program (832025) and the Austrian Research Promotion Agency (FFG) (840476) through the program a3plus and the IEA research cooperation is gratefully acknowledged.

REFERENCES

[1] Patel N, Fernandes R, Guella G, Kale A, Miotello A, Patton B, et al. Structured and Nanoparticle Assembled Co-B Thin Films Prepared by Pulsed Laser Deposition: A Very Efficient Catalyst for Hydrogen Production. J. Phys Chem. C 2008;112:6968–76.
[2] Krishnan P, Advani S, Prasad A. Cobalt oxides as Co2B catalyst precursors for the hydrolysis of sodium borohydride solutions to generate hydrogen for PEM fuel cells. Int. J. Hydrogen Energy 2008;33:7095–102.
[3] Schenk A, Grimmer C, Perchthaler M, Weinberger S, Pichler B, Heinzl C, et al. Platinum–cobalt catalysts for the oxygen reduction reaction in high temperature proton exchange membrane fuel cells – Long term behavior under ex-situ and in-situ conditions. J. Power Sources 2014;266:313–22.
[4] Lee J, Kong KY, Jung CR, Cho E, Yoon SP, Han J, et al. A structured Co–B catalyst for hydrogen extraction from NaBH4 solution. Catal. Today 2007;120:305–10.
[5] Jeong SU, Cho Ea, Nam SW, Oh IH, Jung UH, Kim SH. Effect of preparation method on Co–B catalytic activity for hydrogen generation from alkali NaBH4NaBH4 solution. Int. J. Hydrogen Energy 2007;32:1749–54.
[6] Cento C, Gislon P, Prosini PP. Hydrogen generation by hydrolysis of NaBH4. Int. J. Hydrogen Energy 2009;34:4551–4.
[7] Hacker V, Faleschini G, Fuchs H, Fankhauser R, Simader G, Ghaemi M, et al. Usage of biomass gas for fuel cells by the SIR process. J. Power Sources 1998;71:226–30.
[8] Rydén M, Arjmand M. Continuous hydrogen production via the steam–iron reaction by chemical looping in a circulating fluidized-bed reactor. Int. J. Hydrogen Energy 2012;37:4843–54.
[9] Jin L, Si H, Zhang J, Lin P, Hu Z, Qiu B, et al. Preparation of activated carbon supported Fe–Al2O3 catalyst and its application for hydrogen production by catalytic methane decomposition. Int. J. Hydrogen Energy 2013;38:10373–80.
[10] Takenaka S, Nomura K, Hanaizumi N, Otsuka K. Storage and formation of pure hydrogen mediated by the redox of modified iron oxides. Appl. Catal. A Gen 2005;282:333–41.
[11] Dai H, Liang Y, Wang P, Yao X, Rufford T, Lu M, et al. High-performance cobalt–tungsten–boron catalyst supported on Ni foam for hydrogen generation from alkaline sodium borohydride solution. Int. J. Hydrogen Energy 2008;33:4405–12.
[12] Ingersoll JC, Mani N, Thenmozhiyal JC, Muthaiah A. Catalytic hydrolysis of sodium borohydride by a novel nickel–cobalt–boride catalyst. J. Power Sources 2007;173:450–7.
[13] Liang J, Li Y, Huang Y, Yang J, Tang H, Wei Z, et al. Sodium borohydride hydrolysis on highly efficient Co–B/Pd catalysts. Int. J. Hydrogen Energy 2008;33:4048–54.
[14] Malvadkar N, Park S, Urquidi-MacDonald M, Wang H, Demirel MC. Catalytic activity of cobalt deposited on nanostructured poly(p-xylylene) films. J. Power Sources 2008;182:323–8.
[15] Inaba M, Kinumoto T, Kiriake M, Umebayashi R, Tasaka A, Ogumi Z. Gas crossover and membrane degradation in polymer electrolyte fuel cells. Electrochim. Acta 2006;51:5746–53.
[16] Tang H, Peikang S, Jiang SP, Wang F, Pan M. A degradation study of Nafion proton exchange membrane of PEM fuel cells. J. Power Sources 2007;170:85–92.
[17] Muir SS, Yao X. Progress in sodium borohydride as a hydrogen storage material: Development of hydrolysis catalysts and reaction systems. Int. J. Hydrogen Energy 2011;36:5983–97.
[18] Hacker V, Fankhauser R, Faleschini G, Fuchs H, Friedrich K, Muhr M, et al. Hydrogen production by steam–iron process. J. Power Sources 2000;86:531–5.
[19] Hacker V. A novel process for stationary hydrogen production: the reformer sponge iron cycle (RESC). J. Power Sources 2003;118:311–4.
[20] Thaler M, Hacker V. Storage and separation of hydrogen with the metal steam process. Int. J. Hydrogen Energy 2012;37:2800–6.
[21] Lorente E, Peña JA, Herguido J. Separation and storage of hydrogen by steam-iron process: Effect of added metals upon hydrogen release and solid stability. J. Power Sources 2009;192:224–9.
[22] Grimmer C, Friedrich T, Woisetschläger D, Mayer N, Kalb R, Hacker V. Novel Borohydride-Based Ionic Liquids as Hydrogen Carrier. Chemie Ing. Tech 2014;86. 1443–1443.
[23] Retnamma R, Novais AQ, Rangel CM. Kinetics of hydrolysis of sodium borohydride for hydrogen production in fuel cell applications: A review. Int. J. Hydrogen Energy 2011;36:9772–90.
[24] Ramschak E, Peinecke V, Prenninger P. Online stack monitoring tool for dynamically and stationary operated fuel cell systems. Fuel Cells Bull. 2006;2006:12–5.
[25] Metin Ö, Özkar S. Synthesis and characterization of poly(N-vinyl-2-pyrrolidone)-stabilized water-soluble nickel(0) nanoclusters as catalyst for hydrogen generation from the hydrolysis of sodium borohydride. J. Mol. Catal. A Chem. 2008;295:39–46.
[26] Zhao J, Ma H, Chen J. Improved hydrogen generation from alkaline NaBH4NaBH4 solution using carbon-supported Co–BCo–B as catalysts. Int. J. Hydrogen Energy 2007;32:4711–6.
[27] Tian H, Guo Q, Xu D. Hydrogen generation from catalytic hydrolysis of alkaline sodium borohydride solution using attapulgite clay-supported Co-B catalyst. J. Power Sources 2010;195:2136–42.